Applied Research Laboratory

Technical Report

COMPUTER MODELING OF ULTRASONIC
PIEZOELECTRIC TRANSDUCERS

by

W. J. Hughes
Michael J. Zipparo

PENNSTATE

DISCLAIMER NOTICE

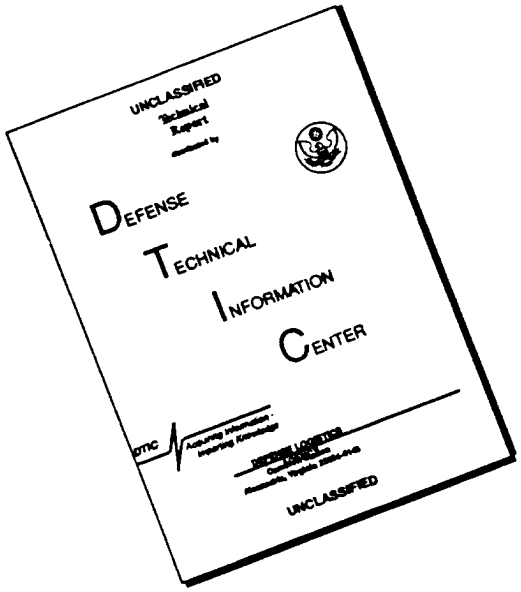

THIS DOCUMENT IS BEST QUALITY AVAILABLE. THE COPY FURNISHED TO DTIC CONTAINED A SIGNIFICANT NUMBER OF PAGES WHICH DO NOT REPRODUCE LEGIBLY.

The Pennsylvania State University
APPLIED RESEARCH LABORATORY
P.O. Box 30
State College, PA 16804

COMPUTER MODELING OF ULTRASONIC PIEZOELECTRIC TRANSDUCERS

by

W. J. Hughes
Michael J. Zipparo

Technical Report No. TR 96-007
June 1996

L.R. Hettche, Director
Applied Research Laboratory

ABSTRACT

A method is formulated to accurately and efficiently model ultrasonic piezoelectric transducers. A computer program based on the Mason model for a longitudinal resonator has been developed which is able to model the performance of a variety of different transducers, including those of widely varying types of piezoceramics constructed with and without matching layers and backing materials. Equivalent circuits for each part of the transducer are developed and then pieced together to form a complete equivalent circuit. A detailed description of how the model is implemented in software is presented. It is designed to allow easy manipulation of all material parameters and dimensions in order to examine their effects on the electrical input impedance and transient response of the transducer. Modeled results are presented and compared with measurements of actual transducers in order to test the accuracy of the model. The usefulness of the program as an engineering tool is discussed.

TABLE OF CONTENTS

LIST OF FIGURES

LIST OF TABLES

LIST OF SYMBOLS

A	area of the piezoelectric disk
Co	clamped capacitance of the piezoelectric disk
c_b	speed of sound in backing material
c_{bf}	speed of sound in front bond layer
c_{br}	speed of sound in rear bond layer
c_l	speed of sound in load medium
c_m	speed of sound in the matching layer
c_p	speed of sound in the piezoelectric disk
e_{33}	piezoelectric stress constant
F_f	force on the front face of the piezoelectric disk
F_r	force on the rear face of the piezoelectric disk
d1	diameter of the piezoelectric disk
f	frequency variable in Hz
f_{bf}	frequency where front bond layer is 1/4 λ
f_{br}	frequency where rear bond layer is 1/4 λ
f_m	frequency where matching layer is 1/4 λ
f_0	fundamental resonance frequency of the piezoelectric disk
F_f	force on the face of the transmitter
IR1	current used to calculate the receiver response
IT1	current used to calculate transmitted signal
Io	output current at receiver electrical terminals
Iin	input current at transmitter electrical terminals
K_3^T	ratio of dielectric constants

k_{33}	longitudinal electromechanical coupling factor
N1	frequency constant
p_f	pressure on the face of the transmitter
Ttr	transfer function between transmitter and receiver
t_{bf}	thickness of front bond layer
t_{br}	thickness of rear bond layer
t1	thickness of the piezoelectric disk
t_m	thickness of matching layer
UR1 to UR4	velocities used to calculate the receiver response
UT1 to UT4	velocities used to calculate transmitted signal
V_i	input voltage to the electrical terminals
Vin	frequency domain input signal
Vo	frequency domain output voltage at receiver electrical terminals
vin	time domain input signal
vo	time domain output voltage at receiver electrical terminals
Z_{L1}, Z_{L2}	circuit elements of the matching layer T-network
Z_{L3}, Z_{L4}	circuit elements of the front bond layer T-network
Z_{L5}, Z_{L6}	circuit elements of the rear bond layer T-network
Z_{P1}, Z_{P2}	circuit elements of the Mason model
Z_b	mechanical impedance of backing material
Z_{br}	mechanical impedance of rear bond layer
Z_{bf}	mechanical impedance of front bond layer
Z_p	mechanical impedance of the piezoelectric disk
ZR1 to ZR13	circuit impedances used to calculate the receiver response
ZT1 to ZT11	circuit impedances used to calculate the electrical input impedance

Za_{bf}	acoustic impedance of front bond layer
Za_{br}	acoustic impedance of rear bond layer
Za_m	acoustic impedance of matching layer
Za_p	acoustic impedance of piezoceramic
Za_b	acoustic impedance of backing material
Zal	acoustic impedance of load medium
Zein	electrical input impedance
Zl	mechanical impedance of the load medium

Greek Symbols

α_{bf}	relative frequency variable for front bond layer
α_{br}	relative frequency variable for rear bond layer
α_m	relative frequency variable for matching layer
α_p	relative frequency variable for piezoelectric disk
ε_0	permitivity of free space
ε_{33}	permitivity of the piezoelectric disk
ϕ	transformation element value of the Mason model
λ	wavelength in piezoceramic disk
λ_b	wavelength in matching layer
ρ_b	density of backing material
ρ_{bf}	density of front bond layer
ρ_{br}	density of rear bond layer
ρ_l	density of load medium
ρ_m	density of the matching layer

ρ_p density of the piezoelectric disk

ω radian frequency variable

Chapter 1

INTRODUCTION AND STATEMENT OF GOALS

1.1 Introduction

Ultrasound has been shown to be a useful tool for both medical imaging [1, 2, 3,] and nondestructive testing (NDT) [4, 5] applications. Both methods use ultrasonic acoustic waves of frequencies near one megahertz and higher to characterize impedance variations in their respective test specimens. Sound waves of ultrasonic frequency are also used in some cleaning and therapeutic applications, where higher power continuous waveform signals are used. In all cases ultrasonic transducers are used to generate and / or receive acoustic waves. This work presents a modeling program which can be used to design transducers for a particular application. The program allows easy manipulation of transducer specifications in order to optimize the response for a particular application.

Both medical imaging and NDT applications are based on a sonar approach, as depicted in Figure 1.1 where a target of acoustic impedance Zt is surrounded by a load medium of acoustic impedance Zl. The target, for example, could be a hard lump which is surrounded by fatty tissue. To image this somewhat idealized scenario, a short duration acoustic pulse is transmitted to the load medium. At the interface between target and load, a portion of the pulse will be reflected back to the receiver. With a knowledge of the 'time of flight' and of the speed of sound in the load medium, the location of the target can be determined. In order to accurately judge the location of the target, the duration of the pulse in time, referred to as pulse width, must be less than the travel time for the wave to reach the target and return. Interference between the excitation pulse and the return echo will make the pulses indistinguishable if this condition is not met. Also, if two pulses in

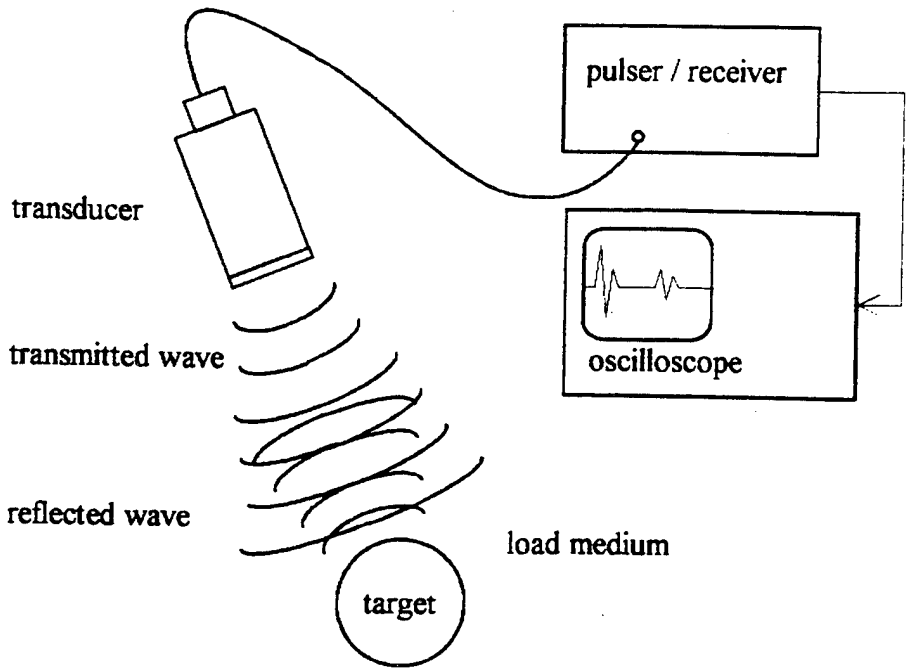

Figure 1.1 Generalized medical imaging application

close proximity are to be resolved in time, the pulse width must be less than the difference in the travel times for the two targets.

The above discussion is based on an idealized situation where the load medium is assumed lossless. In practical situations the losses of the travel medium play a critical role in determining the maximum frequency usable at a given depth. The difference in the acoustic impedance of the load and target determines how much energy is reflected back to the receiver; the shape of the target also affects the reflection factor, as does the size of the target relative to the wavelength of the transmit pulse. Materials with similar acoustic impedances, such as fat and water, will reflect less than materials with contrasting acoustic impedances, such as air and water; likewise, a flat target will reflect more energy back to the receiver than a spherical target. All of the modeled results in this work assume a lossless medium and a perfectly flat, infinitely wide target. These are realistic

approximations to a typical measurement setup which is used to test the performance of a transducer under ideal conditions.

1.2 Typical Transducer Applications

Most modern medical imaging equipment is composed of phased or linear arrays of piezoelectric elements [6]. In some simple applications, however, a single element is used to generate a response where only the amplitude of the signal is processed. This is sometimes referred to as an A-scan. Even the more advanced arrays are composed of sub-elements which are single element transducers. Therefore, it is very useful to be able to accurately predict the behavior of a simple transducer under various loading conditions.

A generalized medical imaging application was described in section 1.1. A typical NDT application, as depicted in Figure 1.2, is to image the thickness of a metal plate. An acoustic pulse is transmitted to a load medium, which can be a fluid such as water. At the water-plate interface a reflection will take place, sending a pulse back to the receiver. A portion of the original pulse is transmitted into the plate. When this reaches the back side of the plate, another reflection occurs; this sends a pulse back to the receiver, through an additional plate-load interface. Because of the additional interfaces, the amplitude of the "back wall echo" will be less than the amplitude of the "front wall echo." This can be seen in a typical amplitude transient response shown in Figure 1.3 where the first pulse in time is the front wall echo and the second pulse is the back wall echo, having a lower signal level. A short pulse width is necessary so that the two echoes can be differentiated in time for a very thin metal plate. The minimum plate thickness which can be imaged by this method is determined by the frequency of the transducer and its ring down characteristics. For the situation depicted in Figure 1.3 the plate thickness could be more than three times

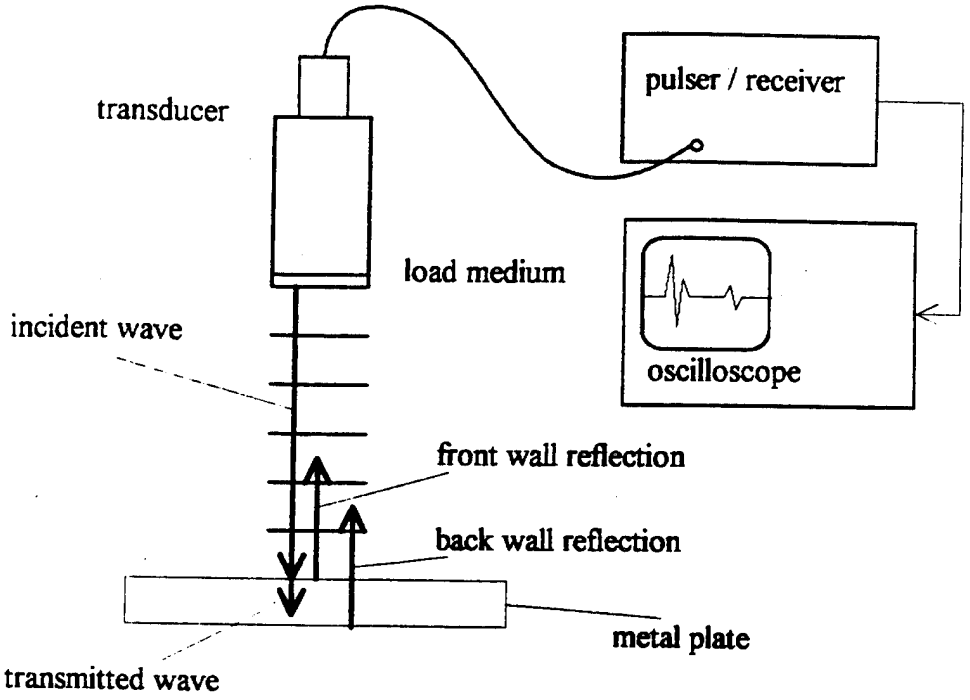

Figure 1.2 Imaging the thickness of a metal plate

as thin before the back wall echo becomes indistinguishable from the front wall ring down. A transducer with a faster ring down could achieve even better results.

Some applications process the signals in the frequency domain. This is referred to as spectral analysis [7, 8, 9]. It will be shown that the frequency response is directly related to the transient response through the Fourier transform. It has been shown by Silk [10] that the two methods are limited in resolution in an equivalent way. Moreover, the transient response seems to be used more often in basic applications, possibly due to the fact that it is easy to visualize. For these reasons the results of the modeling for this work are presented in the time domain as transient responses.

In addition to medical imaging and NDT, there exist other applications which use ultrasonic piezoelectric transducers, an ultrasonic cleaner being a good example. This

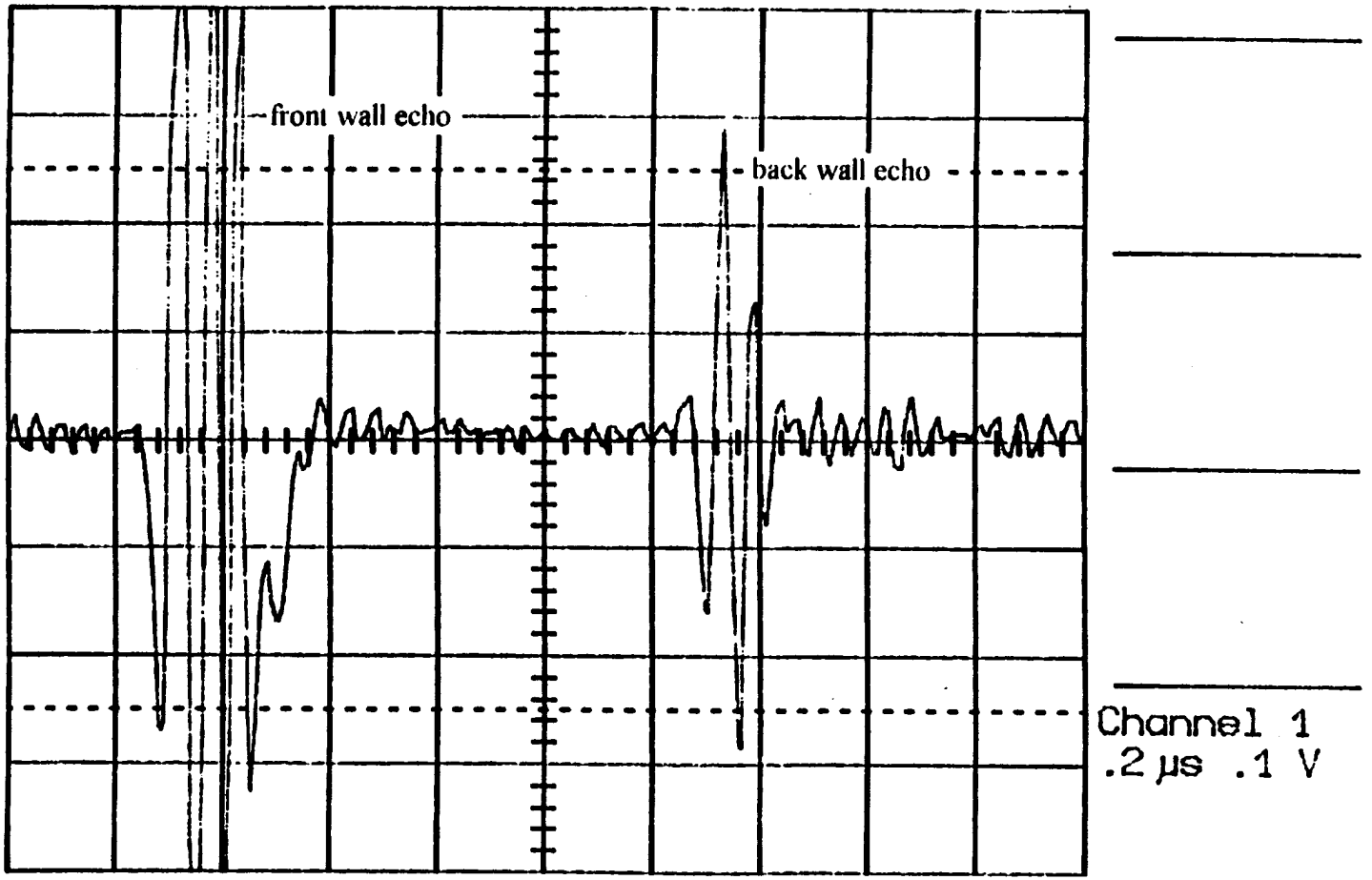

Figure 1.3 Measured front and back wall echoes from a thin metal plate

application uses a continuous signal to drive the transmitter. The action of the high frequency acoustic wave is useful for cleaning small and intricate parts which would be difficult to clean otherwise. As no signal processing is involved, the transient response is not of primary importance. What is most important is the efficiency of energy transfer from the transducer to the cleaning fluid. An inefficient transducer will dissipate more heat and needs to be driven at a higher level for a given agitation level in the fluid.

Transducers useful for both high resolution imaging and cleaning applications are presented. The specifications of each of the designs are discussed in terms of how they relate to the transducer responses. The usefulness of the program for adjusting the model parameters in order to meet all of the operating requirements is discussed.

1.3 Modeling of Ultrasonic Transducers

The computer program models transducers constructed from materials which exhibit the piezoelectric effect. An example of a natural material which displays the piezoelectric effect is quartz. Modern transducers are usually constructed of man-made materials, these being termed piezoceramics, which can be designed to exhibit various desired characteristics. Selection of the appropriate piezoceramic material is of key importance in designing a transducer.

Models for various types of ultrasonic transducers have been developed by a number of authors. Mason [11] developed a model upon which much work was based. This model provides a way to characterize the operation of a piezoceramic material under different loading conditions. As an alternative to the Mason model, Krimholtz, Leedom and Matthaei developed the KLM model [12]. It has been said that the KLM model is easier to use than the Mason model because changes in the model parameters more

realistically reflect physical changes [10]; also there is a clear distinction between the electrical and mechanical parts of the circuit, and the functioning of the mechanical domain as an acoustic transmission line is clearly evident. Both models have been used successfully as the basis of more advanced work.

Kossoff [13] used the Mason model to predict the response of transducers under different operating conditions, such as a piezoceramic material matched by a quarter-wave layer to water. His approach was to simplify the Mason model under these specific operating conditions in order to obtain a mathematical transfer function. Only under the air-backed case, however, was he able to derive the transient response from the frequency domain transfer function.

Persson and Hertz [14] also used a model based on the Mason model to investigate the pulse shape of various transducers constructed with backing material only, matching layers only, and backing and matching. Relationships between pulse shape, frequency response, and efficiency are developed.

Fox and Donnelley [15] developed a method to determine the constants for the Mason model from measurement of the electrical input impedance. Their approach also uses a simplified equivalent circuit; all of the parameters for the model can be determined from impedance measurements made around resonance and from the physical dimensions of the disk. This is quite useful, as manufacturers' data sheets are often incomplete or in error.

Wolf [16] used the Mason model to investigate the effect of matching layers on the transient response under pulsed conditions for both air backing and high impedance backing. A design method was described which minimizes ringing for each backing. A computer program was written which implements a gradient search of the adjustable parameters, including backing impedance and matching layer impedance and thickness, in

order to find a suitable parameter space which results in an improved response.

More recent developments have used the KLM model in favor of the Mason model. Desilets, Fraser and Kino [17] developed an alternative method for choosing the impedance of the matching layers. Improvements in the bandwidth of the frequency response are claimed. Measurements and theory are compared for several transducer designs. Silk [18] uses the KLM model to examine the effects of matching layers and backing materials on the transient and frequency response of probes. He also examines the effect of bond lines on the response. Collie and Player [19] use the KLM model as the basis of a more complete model which also takes into account diffraction effects.

Despite the recent trend towards the use of the KLM model, this study uses the Mason model exclusively for the basis of the program developed. Since adjustments to the model are made automatically by the program when a piezoelectric parameter is changed, this should alleviate any confusion with the model parameters. Also, the Fox and Donnelley paper provides a convenient way to measure piezoelectric constants for unknown materials for the Mason model. In any respect, the models should be equivalent.

1.4 Computer Methods for the Design and Analysis of Piezoelectric Transducers

Because of he large number of calculations necessary to predict the response of even a single element transducer, computers have long been used as a tool for analyzing equivalent circuits. One of the factors which in the past limited the complexity of the transducers which could be modeled was the lack of adequately fast computers. Kossoff [13], for example, was limited to analyzing an air backed transducer with a quarter wavelength matching layer because this was the most complex case for which he could obtain a closed form transient response transfer function.

Today, fast computers are available at a reasonable cost in the form of desktop personal computers. Many design and analysis methods have been developed which utilize desktop computers to predict the response of piezoelectric transducers, including programs written for work being done at universities and Naval labs, and programs available commercially.

Among those available include TEA [20], Transducer Element Analysis. This program allows the user to input parameters for both single element transducers and arrays of transducers. The program then computes the response for a particular combination of input parameters. Also available is TRN [21], which is designed to run on Hewlit Packard 9000 series computers. This program also analyzes the response for a particular parameter set which is input through a menu system. Both of these programs are somewhat cumbersome and are not designed with the NDT transducer designer in mind, as some of the terminology used for sonar transducers is somewhat different than that used for NDT transducers.

PiezoCAD [22] is an example of a commercially available software package which is intended as an analysis tool for a variety of different transducer configurations including single and multi-element thickness mode transducers and Tonpilz type transducers. The program is able to calculate a variety of responses including electrical input impedance and frequency, and pulse-echo transient response. This program seems to be of more use to the designer of MHz-range transducers, as these are the responses which are typically of interest.

In contrast to TEA and TRN, the program developed for this work is designed to predict the response under conditions typically used to evaluate the performance of actual NDT transducers; the input source models a standard ultrasonic pulser and the transient response is presented in a format like that which would be viewed on an oscilloscope

under actual measurement conditions. In addition, the method presented allows a user-friendly interface which is flexible in that the code can be easily adjusted to examine any aspect of the response, such as the velocity at the back acoustic port, which may be of interest but is not typically available for analysis with the other programs. Also, through additions to the code, the responses which are available with PiezoCAD, such as input admittance and transmitting voltage response, can be made available with this method, if desired.

It should be noted that the program compiled for this work is able to predict the response of a transducer for a specific set of operating parameters. It is not, however, designed to iterate a set of design parameters in order to find a suitable compromise which will satisfy the operating requirements. It therefore should be considered an interactive analysis tool that requires proper adjustment of the design parameters by the user in order to find an acceptable combination.

This is in contrast to a design program that starts with a specific transducer configuration and a set of required operating conditions and adjusts certain parameters until the operating conditions are met. This type of program has been developed by McCammon [23] to design a Tonpilz transducer. The operating parameters include operating frequency, admittance magnitude and phase, and node placement. The adjustment parameters include the length, density, cross-sectional area, bar velocity, and loss factor for each section. These parameters were adjusted using Nonlinear Goal Programming to find a combination which would meet the required operating parameters. With this technique the user is required to enter the desired operating parameters and possibly some fixed parameters which are not adjustable, such as the head mass area. The program then finds a suitable combination that will meet the required operating conditions. The technique of Wolf [16] uses a similar approach.

1.5 Goals and Outline of the Thesis

The purpose of this thesis is to implement a computer algorithm of the Mason model for a piezoelectric transducer, including additional constructional variables such as backing material, matching layers, and bond layers. In this way a useful tool for analyzing ultrasonic transducers is developed. Analysis of varying any number of parameters can be easily achieved. In addition, the structure of the program allows easy manipulation of the code to examine any aspect of the response which is not typically available, such as the amount of energy absorbed by the backing.

Chapter 2 details the model of the piezoceramic material and other parts of the transducer. Physical constants and dimensions which specify the model parameters are presented for each part. The complete model is then pieced together. Chapter 3 shows how the model is implemented in software. The model is analyzed starting with the electrical input impedance. Then the transmitted force at the transducer face is determined for a specified voltage input. Finally, this force is used to calculate the voltage at the receiver electrical terminals. Details of how the model parameters are calculated from input parameters are also presented. Specific parameters for three different transducers are described. Chapter 4 then presents the modeled electrical input impedance and transient response for these three transducers. A discussion of which parameters affect the responses is included for each design. In Chapter 5 the modeled results are compared with measurements of actual transducers. Adjustments to some of the model parameters are made in order to improve the performance or demonstrate how poorly designed probes may malfunction. Chapter 6 draws general conclusions about the validity of the model and its usefulness as an engineering tool. Recommendations for future work are also made.

Chapter 2

A MODEL FOR ULTRASONIC PIEZOELECTRIC TRANSDUCERS

2.1 Introduction

A complete model for a piezoelectric transducer includes material parameters for all parts of the transducer, including the piezoceramic material. This usually includes some material on the back of the piezoceramic disk, commonly referred to as backing material, and some sort of layer designed to match the acoustic energy transfer from the piezoceramic disk to the load medium, commonly referred to as a matching layer. Also included in this model are additional layers between the disk and backing material and the disk and matching layer; these are referred to as bond layers. A schematic of the transducer assembly which is the subject of this work is shown in Figure 2.1.

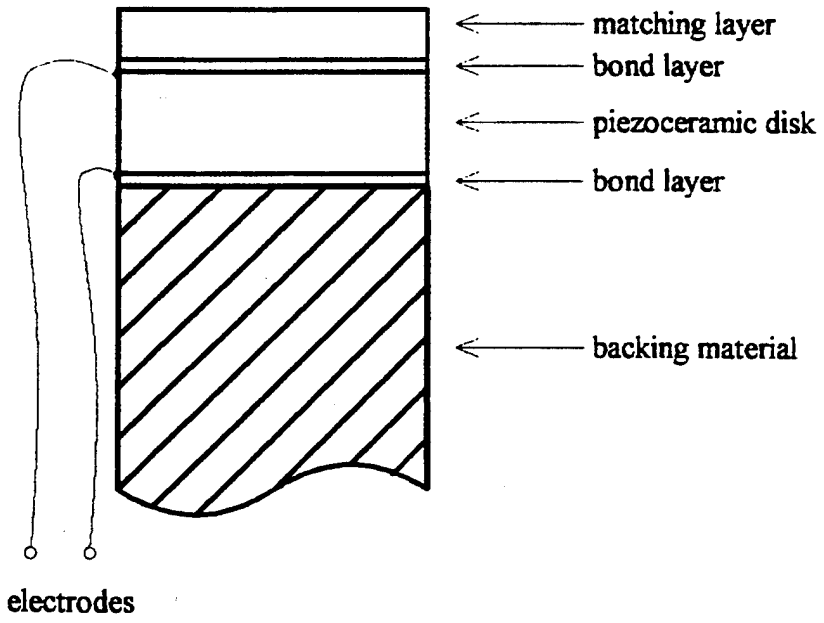

Figure 2.1 Transducer Schematic

Equivalent circuits which model each part of the transducer are presented. The complete

model which describes the entire transducer is shown at the end of this chapter.

2.2 The Mason Model for a Transducer Operating in the Thickness Mode

Several versions of the Mason model exist for modeling transducers operating in various modes; the model for a disk operating in the radial mode, i.e. expanding in the radial direction for a positive voltage input, will have slightly different parameters than the model for a disk operating in the thickness mode, i.e. expanding in the axial direction for a positive voltage input. This thesis deals entirely with transducers operating in the thickness mode.

The Mason model for a piezoceramic disk operating in the thickness mode [11] is shown in Figure 2.2. The electrical signal is measured at the terminals labeled Vi; there are two mechanical ports, one for the force on the rear face, F_r, and one for the force on the front face, F_f. For a given voltage input, Vi, the force on either face may be determined. Likewise, a given force, F, may be applied to each face and the resulting voltage may be determined. It should be noted that symbols with subscripts in the text do not have subscripts in the figures.

The impedance of the elements in the circuit are determined by the material parameters and dimensions of the disk. These properties include: ρ_p, the density of the disk (kg/m^3); c_p, the velocity of sound in the disk (m/s); e_{33}, the piezoelectric stress constant (C/m^2), defined as the stress produced in the piezoelectric material by the application of a unit electric field without strain [5, p103]; N1, the frequency constant of the disk (m/s), defined as the fundamental resonance frequency per unit thickness; and K_3^T, the ratio of free dielectric constants, given by

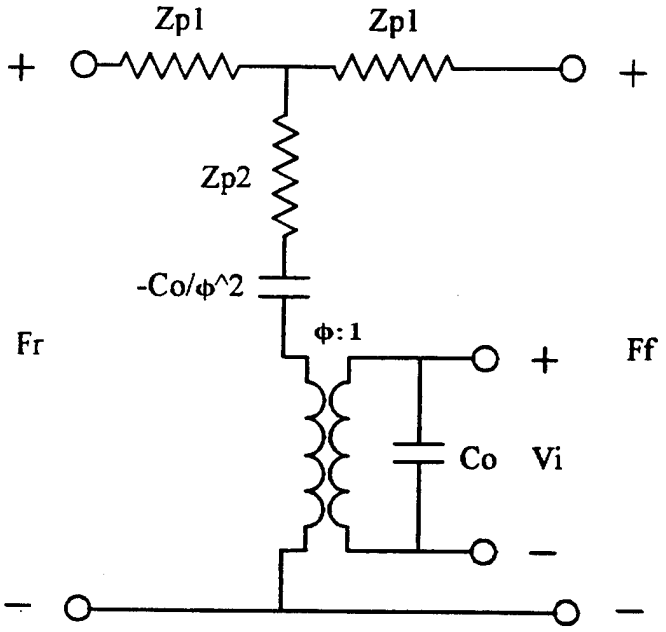

Figure 2.2 The Mason model for a piezoceramic disk operating in the thickness mode

$$K_3^T = \frac{\varepsilon_{33}}{\varepsilon_0}, \tag{2.1}$$

where ε_{33} is the dielectric constant of the disk (F/m) and ε_0 is the dielectric constant of free space (=8.85*10^{-12} F/m). The dimensions of the disk are in meters where d1 is the diameter of the disk and t1 is the thickness. The circuit elements are

$$Z_{p1} = j \cdot Z_p \cdot \tan\left(\frac{\alpha_p}{2}\right), \tag{2.2}$$

$$Z_{p2} = \frac{-j \cdot Z_p}{\sin(\alpha_p)}, \tag{2.3}$$

where Z_p is the mechanical impedance of the piezoceramic disk (kg/s), given by

$$Z_p = \rho_p \cdot c_p \cdot A, \tag{2.4}$$

with A equal to the area of the disk. The term α_p is the frequency variable and is equal to

$$\alpha_p = \frac{\pi \cdot f}{f_0}, \tag{2.5}$$

where f_0 is the fundamental resonance frequency of the disk. The fundamental resonance of the disk occurs when the total thickness of the disk is one half wavelength ($\lambda/2$) and is determined from the material frequency constant, N1, and thickness, t1,

$$f_0 = \frac{N1}{t1}, \tag{2.6}$$

The element values can be calculated from the parameters and dimensions or, in some cases, may be measured directly for a particular disk. The clamped capacitance of the disk, Co, may be measured directly or calculated. Various authors suggest different frequency ranges for this measurement; Sigelman and Caprihan [24] measured the capacitance well below resonance (1 kHz for a 5 MHz resonator); Gerber [25] measured the capacitance far above the thickness mode resonance, where the disk was essentially clamped; Fox and Donnelly [15] measured the capacitance just above or below resonance, where the impedance was mostly capacitive. The results may vary depending on what type of piezoceramic material is being measured. The calculated value for Co is [15]

$$Co = \frac{A \cdot K_3^T \cdot \varepsilon_0 \cdot (1 - k_{33}^2)}{t1}, \tag{2.7}$$

where k_{33} is the longitudinal electromechanical coupling factor. The value of ϕ (C/m) is calculated according to the equation

$$\phi = \frac{A \cdot e_{33}}{t1}. \tag{2.8}$$

These calculated parameters completely specify the Mason model for a piezoceramic resonator operating in the thickness mode.

2.3 A Model for Backing Material and Load Medium

The backing material will load the rear face of the piezoceramic disk, greatly affecting the response of the transducer. The function of the backing material is to absorb the rear wave from the disk, thereby minimizing reflection which would send energy back to the front of the disk. This serves to lessen the ring down of the signal, allowing a better time or spatial resolution for a transducer at a given frequency. The expense paid for obtaining improved resolution is a decrease in efficiency due to the loss of energy which is dissipated in the backing. Thus, a compromise in efficiency and resolution must be reached for each specific design.

The model for the backing material is a simple resistive element, Z_b (kg/s), shown in Figure 2.3. The value of Z_b is determined from the density of the backing, ρ_b, the speed

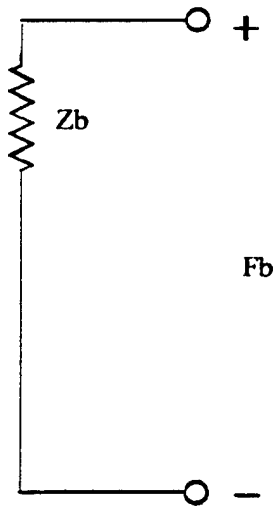

Figure 2.3 A model for backing material and load medium

of sound in the backing, c_b, and the area of the disk, A, according to the equation

$$Z_b = \rho_b \cdot c_b \cdot A. \tag{2.9}$$

This model assumes that all of the energy which enters the backing is dissipated, with no reflection at the end of a finite length termination. In practice this is usually achieved with the use of a highly absorptive material. The model also assumes that the parameters are independent of frequency. In designs where efficiency is of greater importance than resolution, a low impedance material or air is often used as the backing material. Designs with both high and low impedance backings are examined in Chapters 4 and 5.

The load medium is also represented by a resistive element of value Zl (kg/s). The value of Zl is determined by the density of the load medium, ρ_l, the speed of sound in the load medium, c_l, and the area, A, according to the equation

$$Zl = \rho_l \cdot c_l \cdot A. \tag{2.10}$$

The model assumes that the medium is semi-infinite in extent, i.e. that any energy transferred to the medium at the interface is not returned by an energy storage element. The medium is also assumed lossless, a fair approximation at the frequencies of interest in this study.

2.4 A Model for a Matching Layer

The matching layer serves to maximize the energy transfer of the acoustic wave from the piezoceramic disk to the load medium. It is usually a layer whose impedance, Z_m (kg/s), is chosen to be the geometric mean between the impedances of the disk and the load medium. The thickness of the layer, t_m, is chosen to be a quarter wavelength ($\lambda/4$) at the resonance frequency of the transducer. Transmission theory shows that the

transmission coefficient between two semi-infinite medium is thus maximized. While the finite thickness piezoceramic disk is not a semi-infinite medium, this arrangement is typically used to provide a good match between the transducer and load medium.

The equivalent circuit for a matching layer is a T-network, as shown in Figure 2.4. It consists of two mechanical terminals, one for the force at the piezoceramic disk side, F_f,

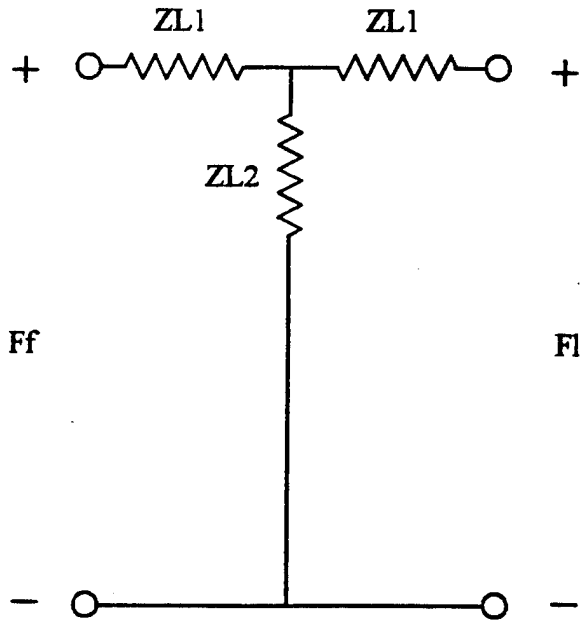

Figure 2.4 A model for a matching and bond layers

and one for the force exerted on the load medium, F_l. The impedances of the elements in the circuit are

$$Z_{L1} = j \cdot Z_m \cdot \tan\left(\frac{\alpha_m}{2}\right), \tag{2.11}$$

and

$$Z_{L2} = \frac{-j \cdot Z_m}{\sin(\alpha_m)}, \tag{2.12}$$

where Z_m is the mechanical impedance of the matching layer, determined by the material parameters, density, ρ_m, and sound velocity, c_m, and area, A,

$$Z_m = \rho_m \cdot c_m \cdot A. \tag{2.13}$$

The term α_m is again the frequency variable, equal to

$$\alpha_m = \frac{\pi \cdot f}{2 \cdot f_m}, \tag{2.14}$$

where f_m is the frequency where the layer is a quarter wavelength ($\lambda/4$); f_m is usually chosen to be equal to f_0, in which case f_m is given by

$$f_m = \frac{c_m}{4 \cdot t_m}. \tag{2.15}$$

Transducers with and without matching layers are examined in Chapters 4 and 5.

2.5 A Model for Bond Layers

This model includes the effect of finite thickness bond layers on the response of the transducer. Bond layers are construction anomalies which sometimes cannot be avoided. Their effect is to reduce the matching between the piezoceramic disk and the backing material, and the piezoceramic disk and the matching layer. This reduced matching can interfere with the energy transfer between disk and backing, causing an increased number of internal reflections in the piezoceramic material. This causes an increase in the ring down time.

The model for a bond layer is exactly the same as that for a matching layer, as seen in Figure 2.4. The material properties for a bond line are its density, ρ_b, and sound velocity, c_b. The mechanical impedance of the bond layer, Z_b, is thus

$$Z_b = \rho_b \cdot c_b \cdot A. \tag{2.16}$$

The frequency dependent term for a bond layer, α_b, is

$$\alpha_b = \frac{\pi \cdot f}{2 \cdot f_b}, \tag{2.17}$$

where f_b is the frequency where the layer is a quarter wavelength ($\lambda_b/4$). For a bond layer whose thickness is known or estimated to be t_b, f_b is calculated as

$$f_b = \frac{c_b}{4 \cdot t_b}. \tag{2.18}$$

The complete model includes two bond layers, one on each side of the piezoceramic disk. The one on the rear of the disk is noted by the subscript 'r', and the one on the front is noted by the subscript 'f'. The impedance elements in the bond layers are thus

$$Z_{L3} = j \cdot Z_{bf} \cdot \tan\left(\frac{\alpha_{bf}}{2}\right), \tag{2.19}$$

$$Z_{L4} = \frac{-j \cdot Z_{bf}}{\sin(\alpha_{bf})}, \tag{2.20}$$

$$Z_{L5} = j \cdot Z_{br} \cdot \tan\left(\frac{\alpha_{br}}{2}\right), \tag{2.21}$$

$$Z_{L6} = \frac{-j \cdot Z_{br}}{\sin(\alpha_{br})}, \tag{2.22}$$

with Z_{L3} replacing Z_{L1} and Z_{L4} replacing Z_{L2} for the front bond layer, and Z_{L5} replacing Z_{L1} and Z_{L6} replacing Z_{L2} for the rear bond layer.

2.6 The Complete Equivalent Circuit

The complete equivalent circuit for a piezoceramic transducer operating in the thickness mode is made by connecting the mechanical terminals of each of the elements according to the configuration of Figure 2.1 and is shown in Figure 2.5. This model is able to predict the force on the face of the transmit transducer resulting from a particular electrical excitation, as well as the output voltage of a receive transducer for a particular force excitation. Chapter 3 describes how this model is implemented in software to predict the transmit-receive response of a pair of transducers.

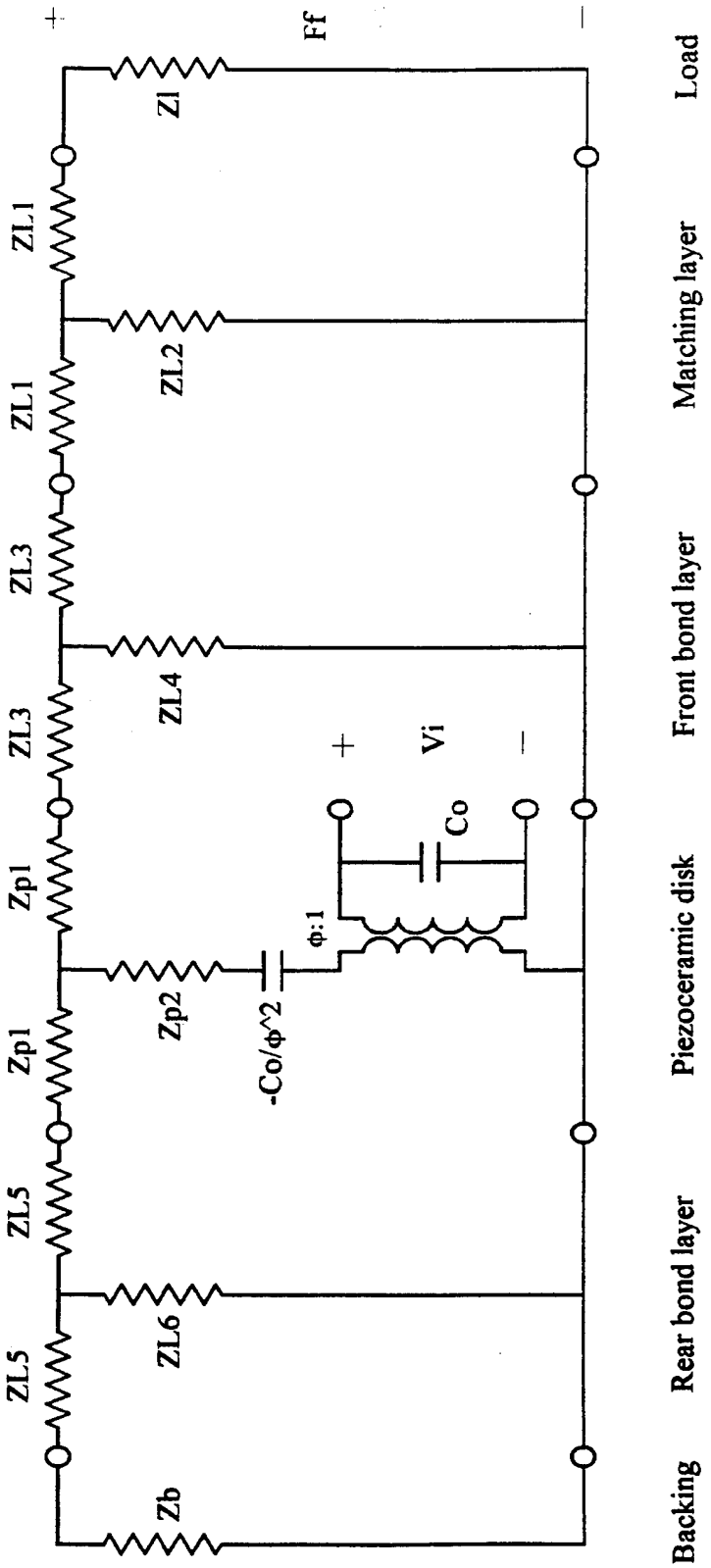

Figure 2.5 The complete equivalent circuit

Chapter 3

COMPUTER IMPLEMENTATION OF THE MASON MODEL

3.1 Introduction

A computer program has been implemented based on the equivalent circuit of Figure 2.5. Analysis of the circuit yields the complete response of a single transducer operating as pulser-receiver or a pair of transducers operating as transmitter and receiver.

The program code for the model is written in the popular mathematics processing program Mathcad. Its format allows the user a flexible interface for examining all aspects of a transducer response. An organized input section allows efficient entry of all the necessary input parameters and dimensions. A well-documented computation section performs all of the necessary calculations. Formatted output plots show electrical input impedance for a transducer, as well as both transient and frequency response for a pair of transducers. The program is structured so that a complete transducer configuration may be saved in a three-page file which can be pasted back into the main program at a later time. This allows the engineer to save promising designs for later analysis. The following sections detail the program configuration and use.

3.2 Calculation of the Electrical Input Impedance

The complete equivalent circuit of Figure 2.5, shown schematically for impedance analysis in Figure 3.1, is used to calculate the electrical input impedance under loaded conditions. The impedance of each element of the model is calculated at a number of discrete frequencies. These elements are then connected in series and parallel combinations, starting with the outer branches, Z_b and Zl, and ending at the electrical

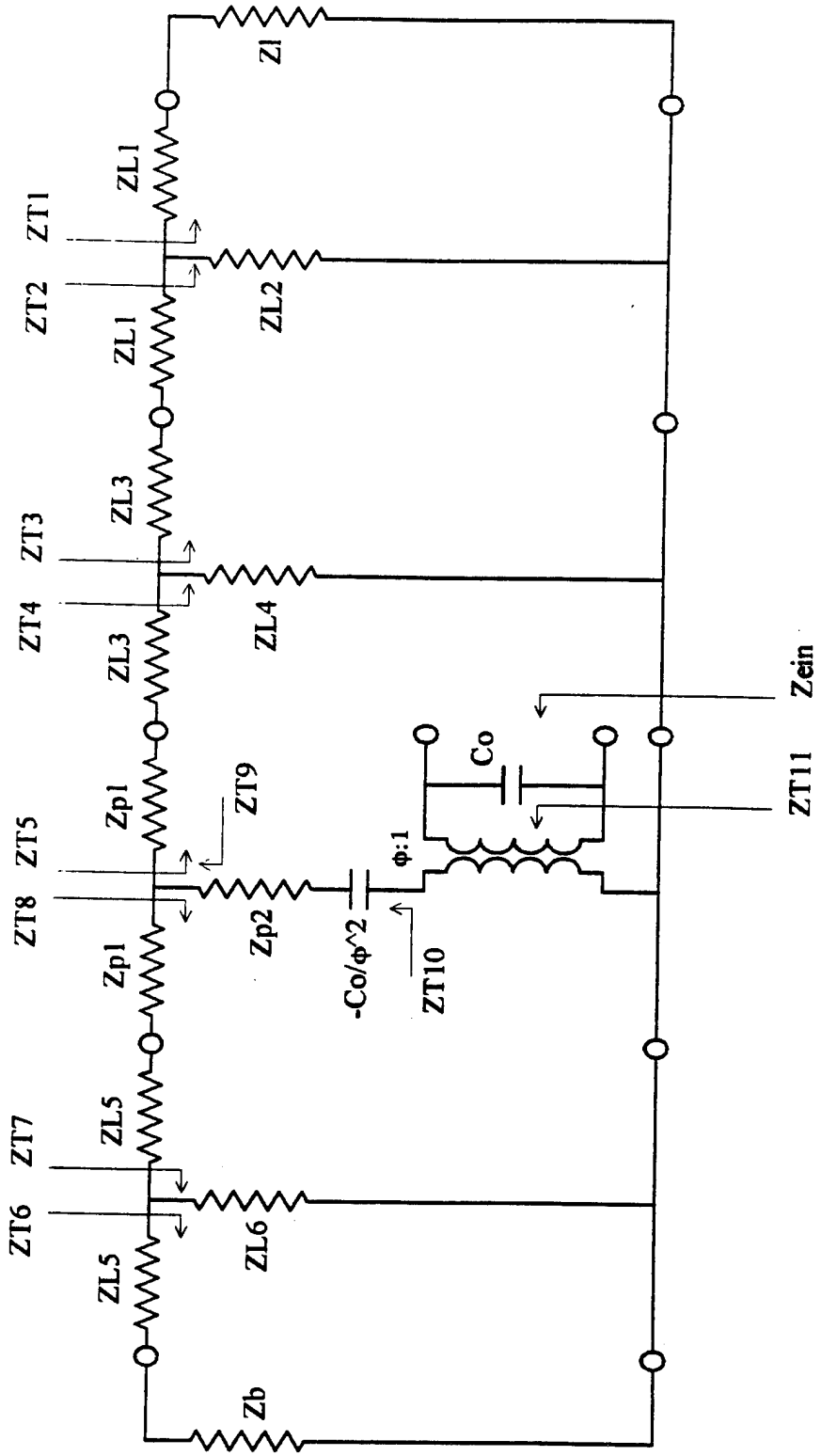

Figure 3.1 A schematic showing the impedances used to calculate the electrical input impedance, Zein

terminals, Zein. To aid in notation, the function Za || Zb defines the parallel combination of impedances Za and Zb,

$$Za||Zb = \frac{Za \cdot Zb}{Za + Zb}. \tag{3.1}$$

The analysis proceeds, first analyzing the elements at the matching layer, where ZT1 is

$$ZT1 = ZL1 + Zl, \tag{3.2}$$

and ZT2 is

$$ZT2 = ZT1 \,||\, ZL2. \tag{3.3}$$

At the front bond layer, ZT3 is

$$ZT3 = ZL3 + ZL1 + ZT2, \tag{3.4}$$

and ZT4 is

$$ZT4 = ZL4 \,||\, ZT3. \tag{3.5}$$

At the piezoceramic disk, ZT5 is

$$ZT5 = Zp1 + ZL3 + ZT4. \tag{3.6}$$

At the rear bond layer ZT6 is

$$ZT6 = ZL5 + Zb, \tag{3.7}$$

and ZT7 is

$$ZT7 = ZL6 \,||\, ZT6. \tag{3.8}$$

Again at the piezoceramic disk, ZT8 is

$$ZT8 = Zp1 + ZL5 + ZT7. \tag{3.9}$$

Continuing with the remaining piezoceramic impedance elements, ZT9 is

$$ZT9 = ZT8 \,||\, ZT5, \tag{3.10}$$

and ZT10 is

$$ZT10 = \frac{-\phi^2}{j \cdot \omega \cdot Co} + Zp2 + ZT9. \tag{3.11}$$

Transforming across the transformation element yields ZT11,

$$ZT11 = \frac{ZT10}{\phi^2}. \tag{3.12}$$

The electrical input impedance, Zein can now be written as

$$Zein = \frac{1}{j \cdot \omega \cdot Co} \parallel ZT11. \tag{3.13}$$

Thus the calculated electrical input impedance takes into account loading at the rear of the transducer by the backing, Z_b, and loading at the face of the transducer, Zl, both of which are affected by a bond layer and/or a matching layer.

3.3 Calculation of the Transmit Response to an Electrical Input

The electrical input impedance is used to calculate the frequency response to a given electrical excitation. As the input signal is often defined in the time domain, it is necessary to transform this signal to the frequency domain. This is accomplished with the use of the Fast Fourier Transform (FFT) function [26], which calculates the spectral components of the input signal at each discrete frequency where the input impedance is calculated. Thus all of the response calculations are done in the frequency domain. The frequency domain input signal, Vin, is the FFT of the time domain input, vin

$$Vin = FFT(vin). \tag{3.14}$$

With the input voltage defined at each frequency, the flow quantities are calculated or each branch of the equivalent circuit using the basic circuit theory current divider law. To aid in notation, the function Io(Iin, Zshunt, Zseries) is used to define the output current flow, Io, through the generalized impedance circuit with input current, Iin, as shown in

Figure 3.2. With knowledge of Iin and the circuit impedances, Zshunt and Zseries, the output current flow is defined as Io where

$$Io(Iin, Zshunt, Zseries) = Iin \cdot \frac{Zshunt}{Zshunt + Zseries}. \tag{3.15}$$

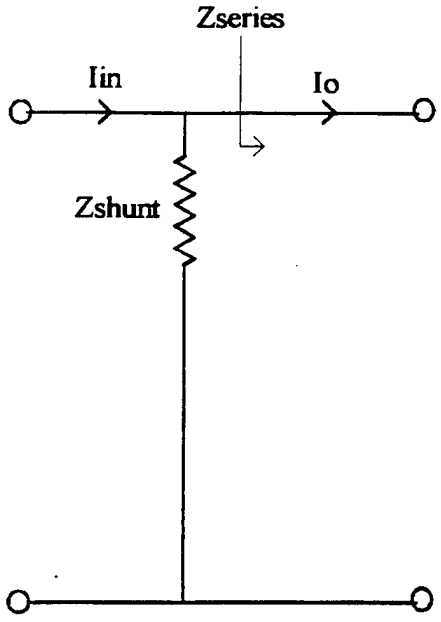

Figure 3.2 A schematic showing the current divider function

All necessary current and linear velocity flow quantities are calculated, starting at the electrical input terminals and ending at the branch representing the load medium, where the output force or pressure at the face of the transducer is calculated. This is shown schematically in Figure 3.3 where each of the current or linear velocities are labeled along with the impedances used to calculate them. When transmitting, the current flowing into the electrical terminals, Iin, is calculated as

$$Iin = \frac{Vin}{Zein}. \tag{3.16}$$

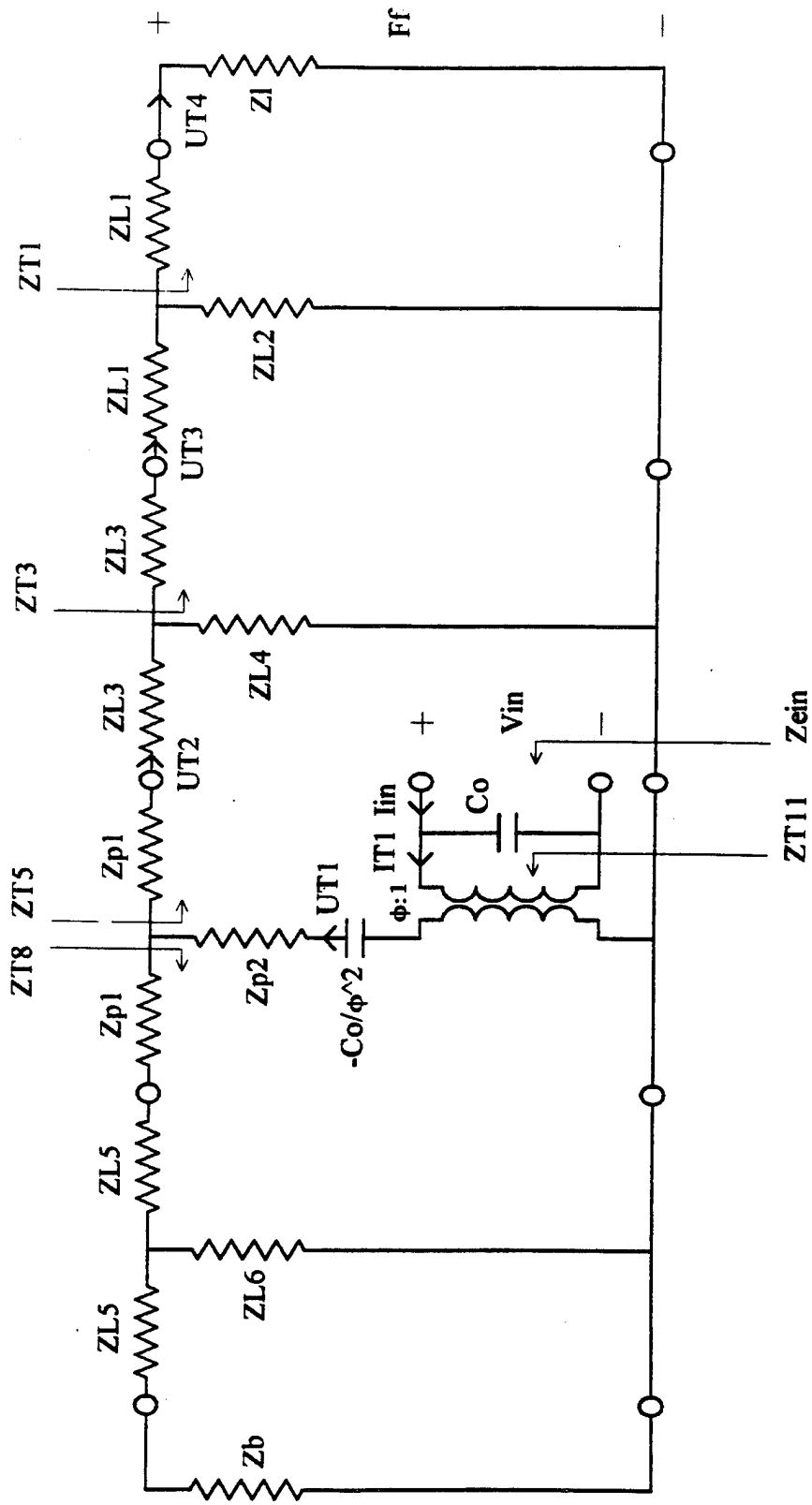

Figure 3.3 A schematic showing the calculation of the force on the face of the transducer, Ff

The analysis proceeds, calculating the current in the next branch, IT1, as

$$IT1 = Io(Iin, \frac{1}{j \cdot \omega \cdot Co}, ZT11). \quad (3.17)$$

The transformer element converts the current, IE1, to a linear velocity, UT1 (m/s),

$$UT1 = \frac{IT1}{\phi}. \quad (3.18)$$

The next divider determines the velocity at the front of the piezoceramic disk, UT2. The notation Uo(Uin, Zshunt, Zseries) replaces Io(Iin, Zshunt, Zseries) for calculations in the mechanical domain.

$$UT2 = Uo(UT1, ZT8, ZT5). \quad (3.19)$$

The velocity at the front of the front bond layer, UT3, is

$$UT3 = Uo(UT2, ZL4, ZT3). \quad (3.20)$$

The velocity at the face of the matching layer, UT4, is

$$UT4 = Uo(UT3, ZL2, ZT1). \quad (3.21)$$

This velocity will determine the force which is exerted on the load medium at the face of the transducer, F_f,

$$F_f = UM4 \cdot Zl . \quad (3.22)$$

The force may also be used to determine the power transmitted into the load medium, P_f, by the equation

$$P_f = (UM4)^2 \cdot Zl . \quad (3.23)$$

In order to calculate the resulting pressure field in front of the transducer, the directivity pattern and directivity index must be calculated. This is not necessary for the purpose of this work, since the signal of interest is the voltage read at the electrical terminals of the receive probe, Vo. To calculate Vo, the force on the face of the receive

probe is assumed to be equal to the force on the face of the transmit probe, F_f. In effect, this approach ignores the entire transmission path from the transmitter to the receiver. This approximation is valid for the high frequency transducers studied in this work, since most of the energy is transmitted through a narrow beam width due to the high directionality of the probe. Thus, with close spacing between transmitter and receiver very little energy is lost.

3.4 Calculation of the Receive Response to an Excitation Force

The force on the face of the receive probe is assumed equal to the force on the face of the transmit probe, as discussed in section 3.3. The approach used to calculate the voltage at the electrical terminals of the receiver is the same as that used to calculate the force at the face of the transmitter. In this case, however, the analysis is proceeding from the mechanical to the electrical domain. The end result is the current flowing in the receiver electrical load. This is used to calculate the output voltage of the receiver.

The receive circuit is excited by a force source in series with a load impedance equal to the mechanical impedance of the load medium, Zl. This is shown in Figure 3.4 along with the impedances used to calculate the net impedance seen by the force source, Z13. The analysis starts at the electrical terminals of the receiver where it is loaded with a 50Ω impedance.

$$ZR1 = 50\Omega. \tag{3.24}$$

The impedance ZR2 is then

$$ZR2 = \frac{1}{j\cdot\omega\cdot Co} \| ZR1 . \tag{3.25}$$

The impedance on the mechanical side of the transformer, ZR3, is

$$ZR3 = ZR2\cdot\phi^2. \tag{3.26}$$

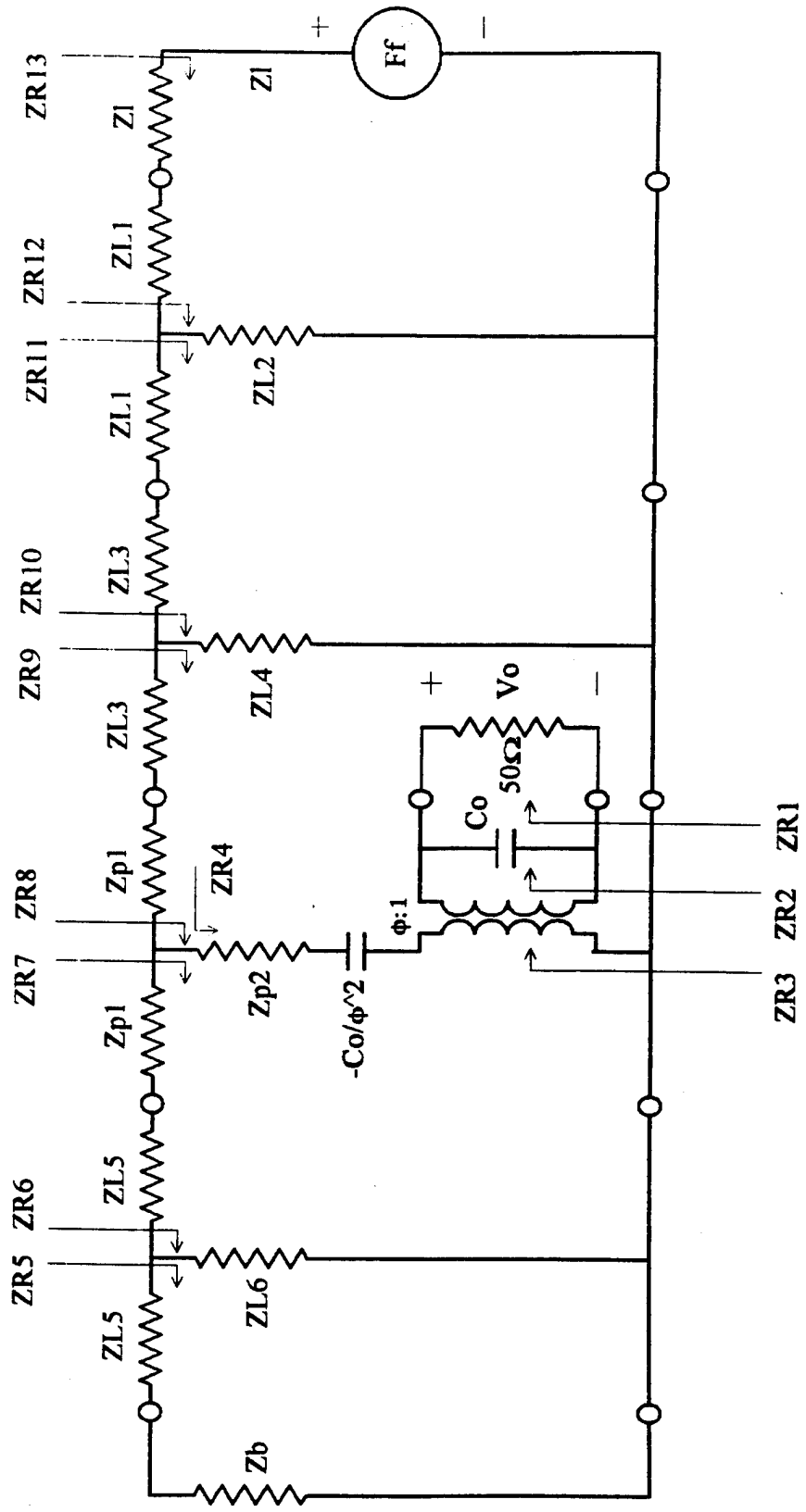

Figure 3.4 A schematic showing the impedances used to calculate the output voltage, Vo

Continuing, from the top of the piezoceramic T-network, ZR4 is

$$ZR4 = Zp2 + \frac{-\phi^2}{j \cdot \omega \cdot Co} + ZR3. \tag{3.27}$$

On the backing side of the piezoceramic, ZR5 is

$$ZR5 = ZL5 + Zb, \tag{3.28}$$

and, ZR6 is

$$ZR6 = ZL6 \parallel ZR5. \tag{3.29}$$

From the piezoceramic T-network ZR7 is

$$ZR7 = Zp1 + ZL5 + ZR6. \tag{3.30}$$

The parallel combination of ZR7 and ZR4 is ZR8,

$$ZR8 = ZR7 \parallel ZR4. \tag{3.31}$$

From the front bond layer, ZR9 is

$$ZR9 = ZL3 + Zp1 + ZR8, \tag{3.32}$$

and ZR10 is

$$ZR10 = ZL4 \parallel ZR9. \tag{3.33}$$

From the matching layer, ZR11 is

$$ZR11 = ZL1 + ZL3 + ZR10, \tag{3.34}$$

and ZR12 is

$$ZR12 = ZL2 \parallel ZR11. \tag{3.35}$$

Finally the impedance seen by the force source, ZR13, is

$$ZR13 = Zl + ZL1 + ZR12. \tag{3.36}$$

With the input impedance seen by the source, ZR13, known, the output voltage at the receiver electrical terminals is calculated. Figure 3.5 shows the linear velocities and

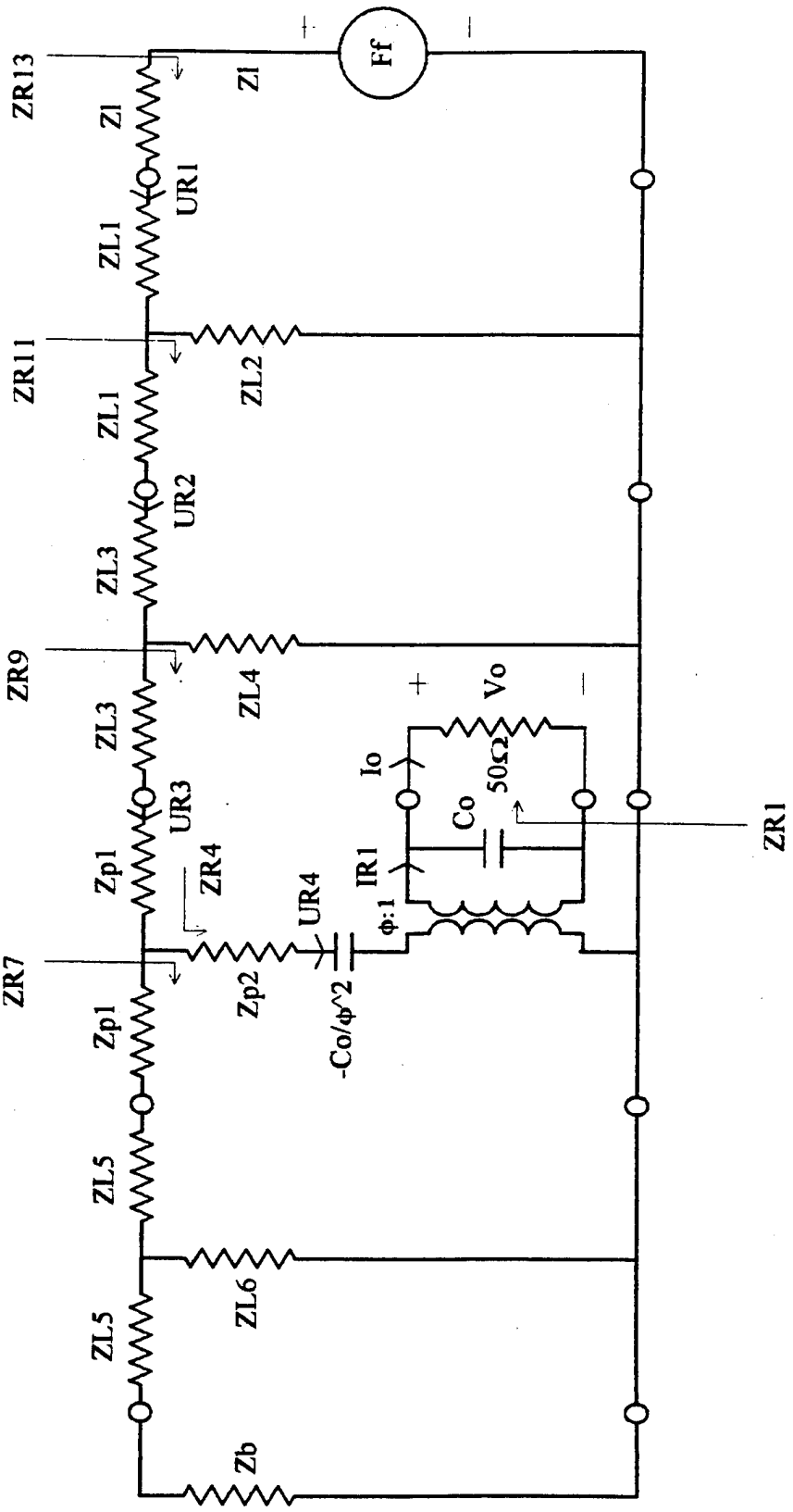

Figure 3.5 A schematic showing the calculation of the output voltage, Vo

currents flowing in each branch, leading to the current flowing in the 50Ω electrical load. The velocity at the face of the receive transducer is UR1, given by

$$UR1 = \frac{F_f}{ZR13}. \tag{3.37}$$

Using the same notation as used for the transmitter, the velocity at the front of the front bond layer, UR2, is

$$UR2 = Uo(UR1, ZL2, ZR11). \tag{3.38}$$

The velocity at the load side of the piezoceramic disk is UR3, given by

$$UR3 = Uo(UR2, ZL4, ZR9). \tag{3.39}$$

Continuing through the piezoceramic T-network, UR4 is

$$UR4 = Uo(UR3, ZR7, ZR4). \tag{3.40}$$

The transformation element converts UR4 to the current IR1 by the equation

$$IR1 = UR4 \cdot \phi . \tag{3.41}$$

The current flowing into the load termination, Io, is thus

$$Io = Io(IR1, \frac{1}{j \cdot \omega \cdot Co}, ZR1). \tag{3.42}$$

This current is used to calculate the output voltage, Vo, at the electrical terminals of the receive transducer by the equation

$$Vo = Io \cdot ZR1. \tag{3.43}$$

The voltage Vo thus represents the discrete frequency components of the signal measured at the receiver when excited by a force F_f, which is generated by a transmitter excited by an input voltage Vin. The transfer function for the complete system, Ttr, is thus

$$Ttr = \frac{Vo}{Vin}. \tag{3.44}$$

The time domain response of the received signal, vo, is also of interest; vo is derived from Vo with the Inverse Fast Fourier Transform (IFFT) [21].

$$vo = IFFT(Vo). \tag{3.45}$$

3.5 Input of Parameters for a Transducer Configuration

The program allows for a structured entry of all of the parameters necessary to completely specify the complete equivalent circuit of Figure 2.5. The parameters for the piezoceramic material are, density, ρ_p; dielectric constant, K_3^T; acoustic impedance, Za_p (rayl); and stress constant, e_{33} (C/m). These are input by selecting an index value, Nn, from a table, shown here as Table 3.1. The table includes complete specifications for

Table 3.1 Piezoceramic material values

Nn	type	ρ (10^3*kg/m^3)	K_3^T	Za_p (Mrayl)	e_{33}	reference
1	K81	6.2	300	19.0	4.7	[27]
2	K83	4.3	175	24.5	3.4	[27]
3	K85	5.7	800	18.5	7.1	[27]
4	PZT5-A	7.75	1700	33.7	15.8	[28]
5	PZT7-A	7.6	425	36.5	9.5	[28]
6	Kynar	1.78	12	2.7	.108	[29]
7	PVDF	1.47	7.6	1.2	.148	[30]
8	User defined	***	***	***	***	N/A

several commonly used piezoceramic materials, as well as a row which can be used for a piezoceramic type not included in the table. The dimensions of the disk are the diameter, d1, and thickness, t1. These are input to a separate section of the program. The program then converts these parameters and dimensions into those used in section 2.2 to define the piezoelectric disk model.

$$A = \frac{\pi \cdot d1^2}{4}, \tag{3.46}$$

$$N1 = \frac{Za_p}{2 \cdot \rho_p}, \tag{3.47}$$

$$Z_p = Za_p \cdot A. \tag{3.48}$$

All other parameters and dimensions are defined in a separate two page section labeled 'Input of Parameters'. Input parameters for the matching layer include the frequency, f_m, where the matching layer is a quarter wavelength ($\lambda/4$); the acoustic impedance of the matching layer, Za_m (rayl); and the velocity of sound in the matching layer, c_m (m/s). The program then calculates the mechanical impedance of the matching layer, Z_m (kg/s), as used in section 2.4,

$$Z_m = Za_m \cdot A. \tag{3.49}$$

Input parameters for the bond layers include the acoustic impedance of the front and rear bond layers, Za_{bf} and Za_{br}; the thickness of the front and rear bond layers, t_{bf} and t_{br}; and the velocity of sound in the front and rear bond layers, c_{bf} and c_{br}. The program then calculates the mechanical impedances of the bond layers, Z_{bf} and Z_{br}, used in section 2.5,

$$Z_{bf} = Za_{bf} \cdot A, \tag{3.50}$$

$$Z_{br} = Za_{br} \cdot A. \tag{3.51}$$

Finally, the acoustic impedance of the backing, Za_b, and the acoustic impedance of the load medium, Za_l are input. .These are used to calculate their respective mechanical impedances, Z_b and Z_l, used in section 2.3,

$$Z_b = Za_b \cdot A, \tag{3.52}$$

$$Zl = Za_l \cdot A. \tag{3.53}$$

All of the variables used in Chapter 2 to define the complete equivalent circuit are thus defined from the input parameters. The next section shows the parameter values for each of the configurations modeled in Chapter 4. The values are chosen to reflect actual transducers which are tested in Chapter 5.

3.6 Parameter Values for three Transducer Configurations

Transducers modeled include: 1) an air-backed PZT unit with a quarter wavelength matching layer ($\lambda/4$); 2) a lead metaniobate unit with a high impedance backing and a quarter wavelength matching layer; and 3) an air-backed PVDF unit with no matching layer. The values for the material parameters are chosen according to the operating specifications for each design; these include ring down time, efficiency and operating impedance. Since each of these characteristics often affects the others, a careful design tradeoff must be accomplished in order to meet all of the required operating conditions. One of the main benefits of the program is its ability to efficiently determine the appropriate tradeoff of parameters without actually constructing a transducer. The main operating specifications for each of the three designs are discussed.

3.6.1 Parameters for Air-backed PZT with a Matching Layer

Lead Zirconate Titanate (PZT) is a common piezoceramic material, often chosen for designs where efficiency is critical; this is due to its high piezoelectric stress constant (e_{33} = 15.8 C/m^2). PZT also has a higher acoustic impedance (Za_p = 33 Mrayl). The design configuration uses PZT5-A as the piezoceramic material. To increase efficiency further, a quarter wave matching layer is used to increase the coupling to the load medium; also, the unit is air-backed to increase efficiency still further, as mentioned in section 2.3.

The values for the input parameters, calculated parameters, and dimensions are shown in Figure 3.6. For each of the transducer configurations the material properties for the piezoceramic material are taken from Table 4.1, except for N1 which is calculated using equation 2.6. The resonance frequency, fo, static capacitance, Co, and dimensions, d1, t1, and A, are taken from measurements of actual transducers. The transformer coupling constant, ϕ, is calculated using equation 2.8. The material properties for the matching layer, backing material, and bond layers are taken from measurements of the materials used to construct the actual transducers. The resonance frequency of the matching layer, f_m, is equal to the resonance frequency of the piezoceramic material. The thickness of the matching layer, t_m, is calculated using equation 2.15 under the assumption that the layer is a quarter wavelength. The thicknesses of the bond layers, t_{br} and t_{bf}, are chosen to be very thin so that their effect is minimized. If bond layers are thought to be a problem for a particular design, the thicknesses can be manipulated within the program to quickly asses what effect a thicker bond layer may have.

Piezoceramic type: PZT5-A

Material properties:

$\rho = 7.75 \cdot 10^3 \cdot \frac{kg}{m^3}$

$e_{33} = 15.8 \cdot \frac{C}{m^2}$

$K_3^T = 1700$

$Za_p = 33.7 \cdot Mrayl$

$N1 = 2174 \cdot Hz \cdot m$

Dimensions:

$f_0 = 1.6 \cdot MHz$

$A = 3.45 \cdot cm^3$

$d1 = 0.825 \cdot in$

$t1 = 0.053 \cdot in$

$Co = 2100 \cdot pF$

$\phi = 4.01 \cdot \frac{C}{m}$

Matching layer material: epoxy

Material properties:

$Za_m = 3.8 \cdot Mrayl$

$c_m = 2.7 \cdot \frac{mm}{\mu s}$

Dimensions:

$f_m = 1.6 \cdot MHz$

$t_m = 16.6 \cdot mil$

Backing material: air

Material properties:

$Za_b = 415 \cdot rayl$

Dimensions:

assumed infinite

Load medium: water

Material properties:

$Zal = 1.5 \cdot Mrayl$

Dimensions:

assumed infinite

Bond layer material, rear: air

Material properties:

$Za_{br} = 3.8 \cdot Mrayl$

$c_{br} = 2.7 \cdot \frac{mm}{\mu s}$

Dimensions:

$t_{br} = 0.005 \cdot \mu m$

Bond layer material, front: epoxy

Material properties:

$Za_{bf} = 3.8 \cdot Mrayl$

$c_{bf} = 2.7 \cdot \frac{mm}{\mu s}$

Dimensions:

$t_{bf} = 0.005 \cdot \mu m$

Figure 3.6 Parameters for PZT transducer

3.6.2 Parameters for Lead Metaniobate with a High Impedance Backing and a Matching Layer

Lead metaniobate is a less commonly used piezoceramic, due to its reduced stress constant (e_{33} = 7.15 C/m^2). However, it does have advantages in certain applications. When excited with a broadband pulse it has a lower coupling to the radial mode than does PZT. Its lower acoustic impedance (Za_p = 18.5 Mrayl) matches better to a water load and to a high impedance backing. These benefits are particularly useful in designs where fast ring down is of more importance than efficiency. Certain medical and NDT applications where resolution is of primary concern require the use of lead metaniobate.

The configuration modeled uses K85, a type of lead metaniobate manufactured by Keramos, Inc (Indianapolis, IN). It includes a front matching layer to increase the efficiency, and a backing whose impedance is close to that of the piezoceramic disk. Thus, with a fast ring down this transducer is designed for resolution more than for efficiency. The values for the input and calculated parameters and dimensions are shown in Figure 3.7.

3.6.3 Input of Parameters for PVDF with Air Backing without a Matching Layer

Polyvinylidine Fluoride (PVDF) is a different type of piezoelectric material. Its characteristics are much different than either those of PZT or lead metaniobate. Its efficiency is much less, due to its very low stress constant (e_{33} = 0.148 C/m^2). The acoustic impedance of PVDF is also much less than that of other piezoceramics, having a value slightly lower than water (Za_p = 1.4 Mrayl). This enables a transducer to be built without needing a matching layer, as the coupling from PVDF to water is quite good without one. As a result of its exotic properties, PVDF may be used in different

Piezoceramic type: K85

Material properties:

$\rho = 5.7 \cdot 10^3 \cdot \frac{kg}{m^3}$

$e_{33} = 7.15 \cdot \frac{C}{m^2}$

$K_3^T = 800$

$Za_p = 18.5 \cdot Mrayl$

$Nl = 1623 \cdot Hz \cdot m$

Dimensions:

$f_0 = 5.4 \cdot MHz$

$A = 0.183 \cdot cm^3$

$dl = 0.190 \cdot in$

$tl = 0.012 \cdot in$

$Co = 300 \cdot pF$

$\phi = 0.438 \cdot \frac{C}{m}$

Matching layer material: epoxy

Material properties:

$Za_m = 3.8 \cdot Mrayl$

$c_m = 2.7 \cdot \frac{mm}{\mu s}$

Dimensions:

$f_m = 5.4 \cdot MHz$

$t_m = 4.9 \cdot mil$

Backing material: tungsten loaded epoxy

Material properties:

$Za_b = 14.5 \cdot Mrayl$

Dimensions:

assumed infinite

Load medium: water

Material properties:

$Zal = 1.5 \cdot Mrayl$

Dimensions:

assumed infinite

Bond layer material, rear: epoxy

Material properties:

$Za_{br} = 3.8 \cdot Mrayl$

$c_{br} = 2.7 \cdot \frac{mm}{\mu s}$

Dimensions:

$t_{br} = 0.005 \cdot \mu m$

Bond layer material, front: epoxy

Material properties:

$Za_{bf} = 3.8 \cdot Mrayl$

$c_{bf} = 2.7 \cdot \frac{mm}{\mu s}$

Dimensions:

$t_{bf} = 0.005 \cdot \mu m$

Figure 3.7 Parameters for lead metaniobate (K85) transducer

applications than the more conventional piezoceramics.

A transducer using PVDF is modeled without a matching layer; i.e. the disk radiates directly to the water load. The unit uses an air backing to increase efficiency, although the resulting efficiency is still quite low. The values for the input and calculated parameters and dimensions are shown in Figure 3.8.

Piezoceramic type: PVDF

Material properties:

$\rho = 1.47 \cdot 10^3 \cdot \frac{kg}{m^3}$

$e_{33} = 0.148 \cdot \frac{C}{m^2}$

$K_3^T = 7.6$

$Zal = 1.4 \cdot Mrayl$

$N1 = 408 \cdot Hz \cdot m$

Dimensions:

$f_0 = 750 \cdot kHz$

$A = 0.713 \cdot cm^3$

$d1 = 0.375 \cdot in$

$t1 = 0.022 \cdot in$

$Co = 12.3 \cdot pF$

$\phi = 0.013 \cdot \frac{C}{m}$

Matching layer material: none

Material properties:

$Za_m = N / A$

$c_m = N / A$

Dimensions:

$f_m = N / A$

$t_m = N / A$

Backing material: air

Material properties:

$Za_b = 415 \cdot rayl$

Dimensions:

assumed infinite

Load medium: water

Material properties:

$Zal = 1.5 \cdot Mrayl$

Dimensions:

assumed infinite

Bond layer material, rear: copper

Material properties:

$Za_{br} = 33.0 \cdot Mrayl$

$c_{br} = 3.7 \cdot \frac{mm}{\mu s}$

Dimensions:

$t_{br} = 1.5 \cdot mils$

Bond layer material, front: copper

Material properties:

$Za_{bf} = 33.0 \cdot Mrayl$

$c_{bf} = 3.7 \cdot \frac{mm}{\mu s}$

Dimensions:

$t_{bf} = 1.5 \cdot mils$

Figure 3.8 Parameters for PVDF transducer

Chapter 4

PREDICTED TRANSDUCER RESPONSES

4.1 Introduction

This chapter presents the computer simulated responses for each of the configurations presented in Chapter 3. Included are plots of the electrical input impedance and the transient response to a pulsed input voltage. The importance of both is discussed for each transducer configuration, along with the parameters which affect the responses the most.

4.2 Simulated Electrical Input Impedance

The electrical input impedance affects how well the transducer impedance will match the electronics used to transmit and receive the signal. Connections are usually made with a 50Ω coaxial cable. Because of the high frequency of operation, a mismatch between the transducer and cable impedance will reduce the efficiency of the system. In extreme cases a transformer must be used to match the impedances.

Figure 4.1 is the Mathcad printout showing the real and imaginary parts of the modeled impedance, Zein, for the PZT5-A transducer. The real part shows a somewhat narrow peak just above 1.5MHz, with a value of 45Ω. This peak, as well as the peak and dip in the imaginary part curve, is due to the mechanical resonance of the piezoceramic disk. The large negative reactance at very low frequencies is due to the clamped capacitance, Co. The magnitude and phase of Zein are shown in Figure 4.2. At frequencies well above and below resonance, the impedance is dominated by the capacitance of the transducer, Co. This is why the phase of the impedance is close to -90 degrees away from resonance. The effect of the mechanical resonance is to superimpose a

(a)

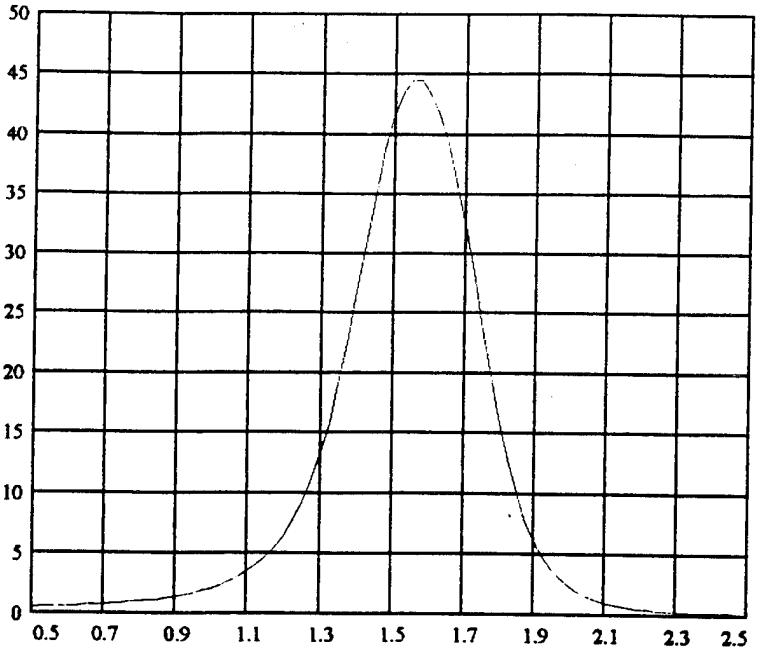

(b)

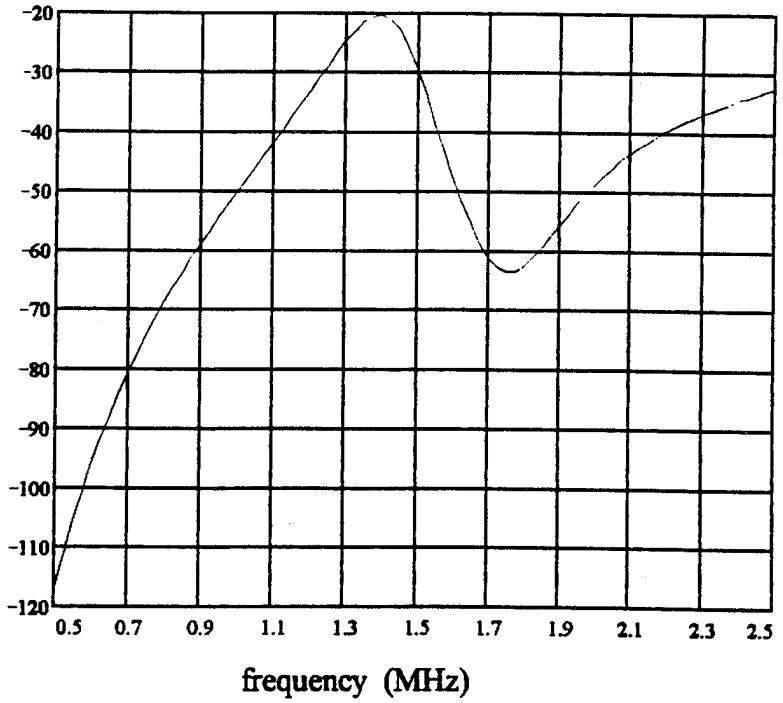

Figure 4.1 Modeled electrical input impedance for PZT5-A transducer; (a) real part; (b) imaginary part

(a)

M{Zein}
(Ω)

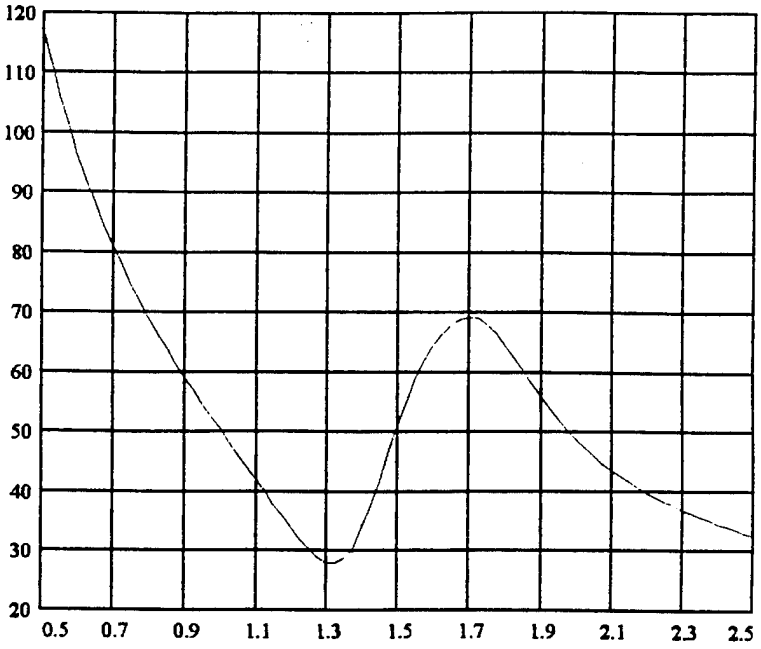

(b)

Ph{Zein}
(deg)

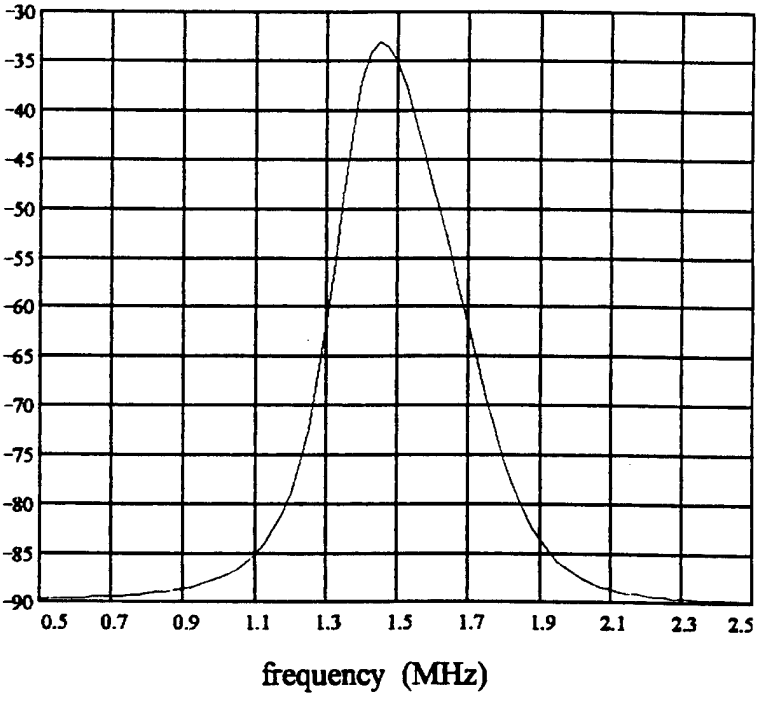

Figure 4.2 Modeled electrical input impedance for PZT5-A transducer;
(a) magnitude; (b) phase

peak and dip on the magnitude curve around the resonance frequency, fo. The change in impedance from dip to peak is predicted to be 40Ω. This is dependent on the amount of damping in the system; a highly damped system will have a smaller change, as will be seen for the lead metaniobate transducer. A piece of ceramic loaded by air on both sides with little internal loss, on the other hand, will have an even larger change in impedance from dip to peak, with the phase reaching a positive angle close to 90 degrees. This would be a high quality factor, Q, transducer.

The real and imaginary parts of Zein for the lead metaniobate transducer are shown in Figure 4.3. The real part shows a peak of about 27Ω at 4MHz, somewhat below the resonance frequency of 5.4MHz; also, the curve can be seen to be broader than the same curve for the PZT transducer. This is due to the damping of the backing material. The imaginary part again shows a large negative reactance at low frequencies. The impedance magnitude plot, shown in Figure 4.4 along with the phase, shows a response where the dip and peak around resonance is very small, being little more than a ripple at about 4.5MHz. This is again due to the higher system damping caused by the high impedance backing. For the same reason the phase response is flat, deviating from -90 degrees by less than 15 degrees. This damping will also be evident in the transient response.

The real and imaginary parts of the electrical input impedance for the PVDF transducer are shown in Figure 4.5. The real part again shows a peak. At 400kHz, however, the peak is at a frequency much lower than the fundamental resonance frequency of the disk. It is believed that this is due to the thick copper electrodes, which tend to mass load the disk causing the lower resonance frequency. At 11kΩ, the value of the peak impedance is much higher than for either of the other materials. The imaginary part again shows a large negative value at low frequencies and a peak and dip in the response around the resonance at 450kHz. The magnitude of the impedance, shown in Figure 4.6

(a)

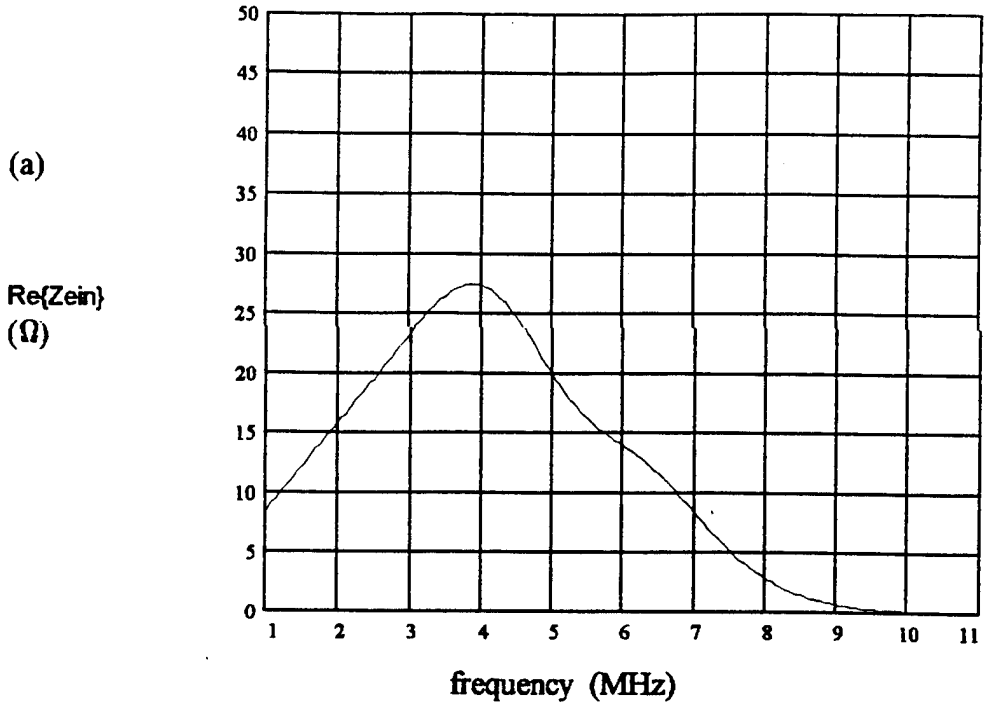

(b)

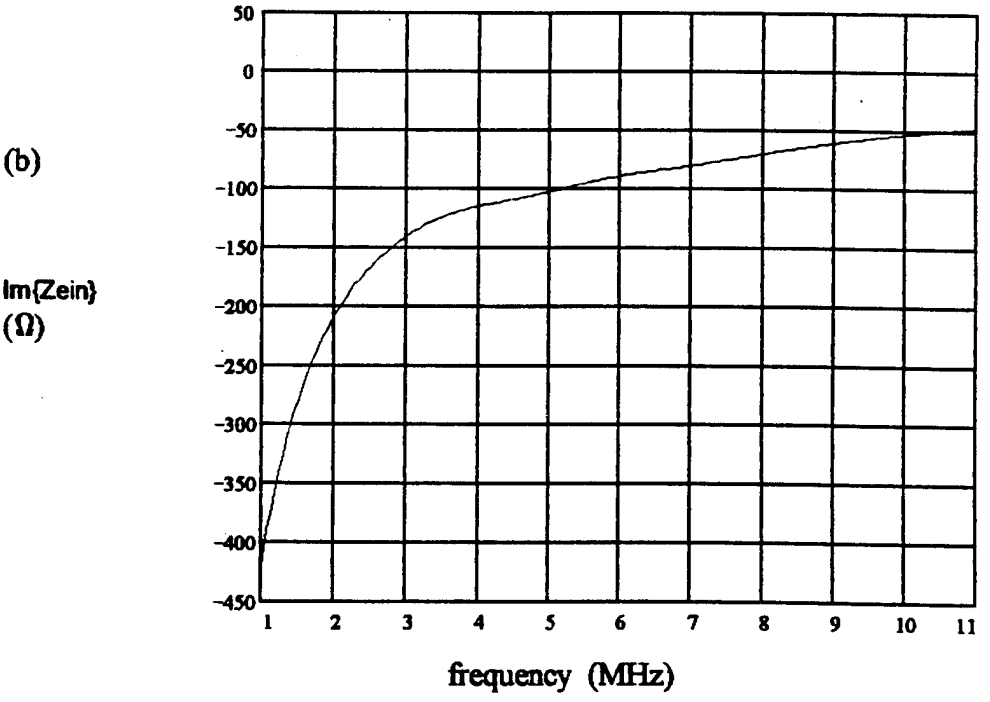

Figure 4.3 Modeled electrical input impedance for K85 transducer;
(a) real part; (b) imaginary part

(a)

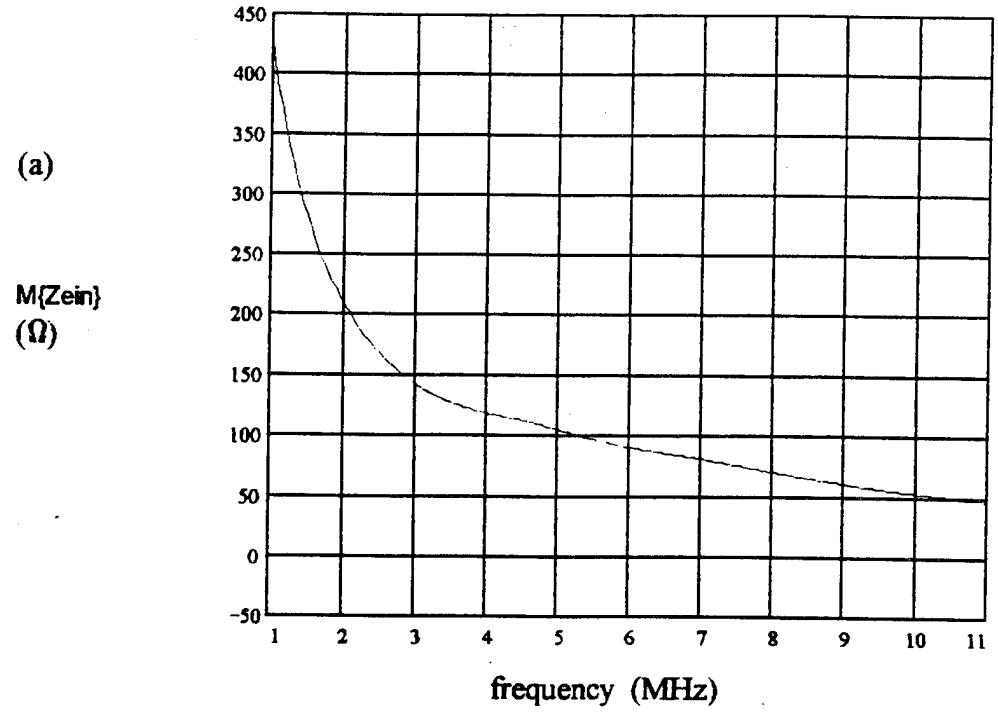

(b)

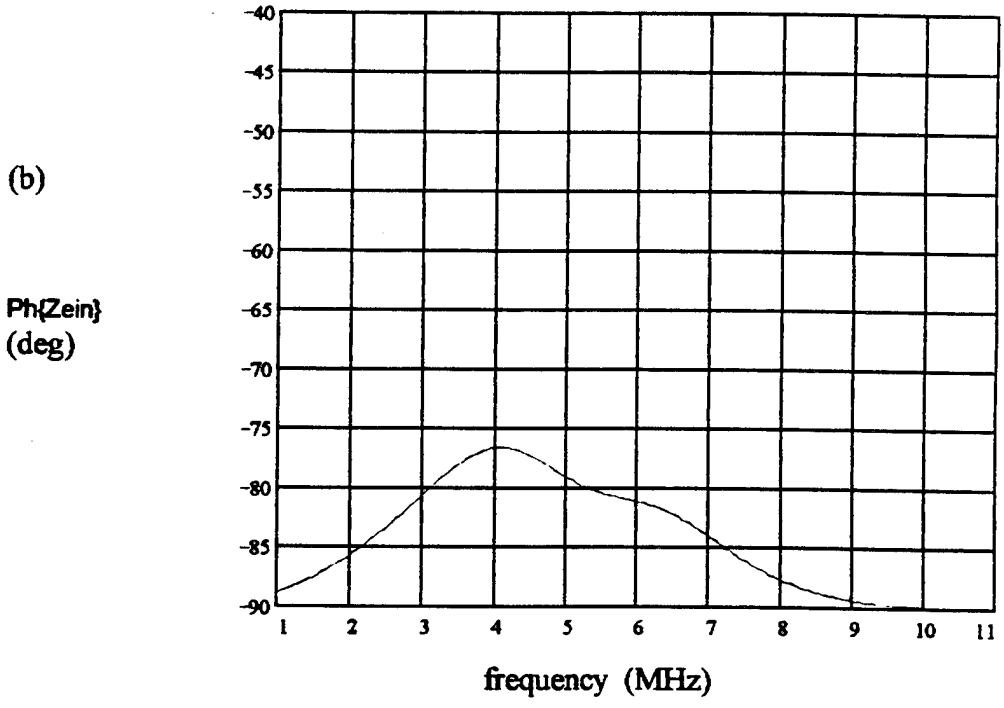

Figure 4.4 Modeled electrical input impedance for K85 transducer;
(a) magnitude; (b) phase

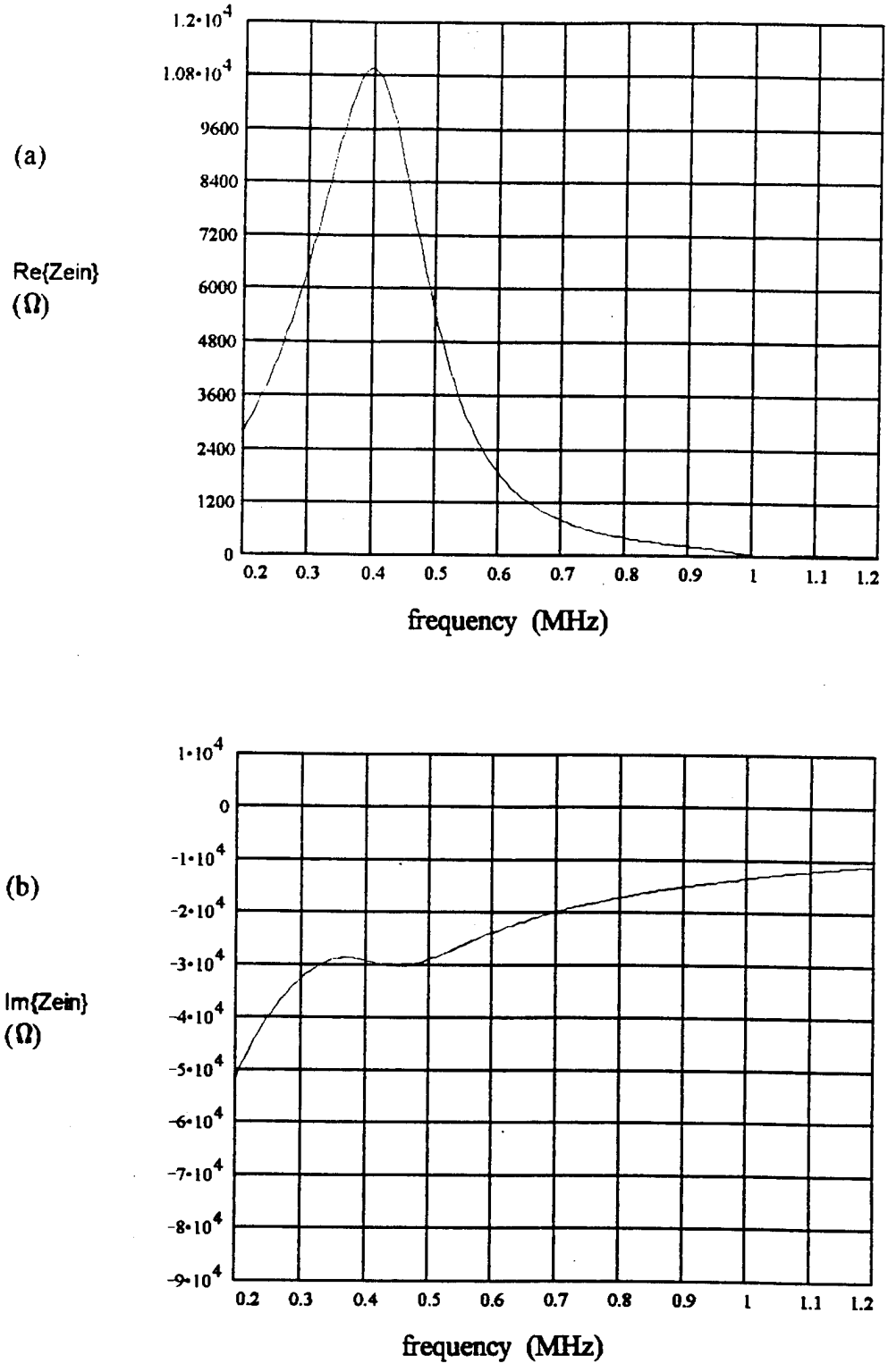

Figure 4.5 Modeled electrical input impedance for PVDF transducer; (a) real part; (b) imaginary part

(a)

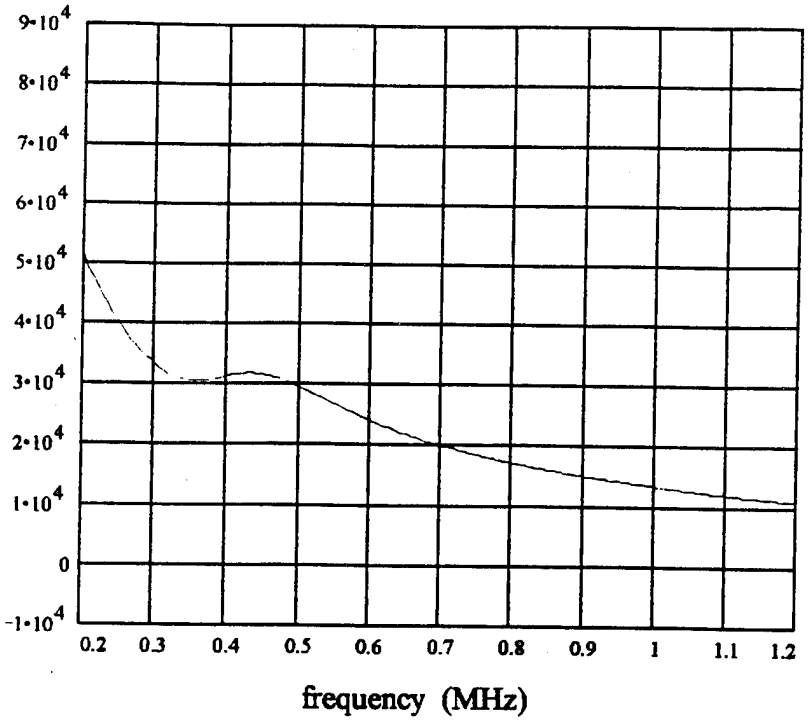

(b)

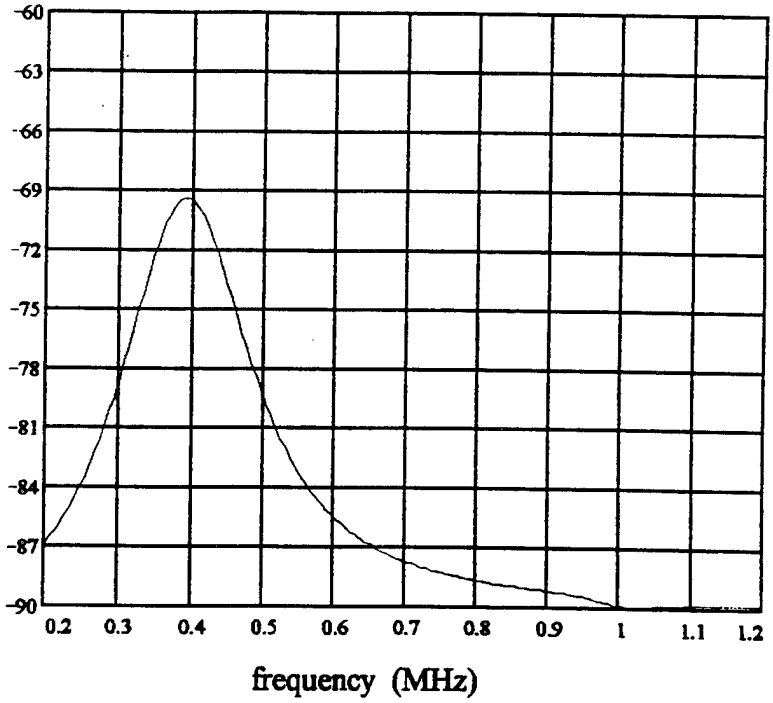

Figure 4.6 Modeled electrical input impedance for PVDF transducer;
(a) magnitude; (b) phase

along with the phase, shows a small dip and peak between 350 and 450kHz. The change in impedance, about 2kΩ, is small relative to the impedance value of 30kΩ. This is due to the losses within the piezoceramic material and to the loss to the water load. The higher impedance values seen in all of the curves are due to the very small value of the clamped capacitance, Co, since at low frequencies the impedance is inversely proportional to Co.

Thus all of the impedance curves show similar trends in their responses. The amount of damping of the transducer determines the effect of the mechanical resonance on the electrical input impedance. Less damped transducers, such as the PZT unit, show a more pronounced dip and peak in the magnitude curve than do highly damped units, such as the lead metaniobate unit, which shows a much smaller ripple. Also, it has been shown that the value of the clamped capacitance, Co, determines the general level of the impedance. Transducers with a very low value of Co, such as the PVDF unit, will operate at a much higher impedance level than transducers with higher values of Co. In extreme cases it may be necessary to use a matching transformer to couple the transducer to its associated electronics.

4.3 Simulated Transient Response

The transient response of a transducer is of primary importance in many NDT and medical imaging applications. A short ring down time is often necessary in applications where return pulses spaced closely in time must be clearly distinguishable. The same ring down time can be achieved with a greater number of cycles by increasing the operating frequency of the transducer. Sometimes, however, this is not an option due to the increased absorption of some load medium at higher frequencies. Therefore, it is important to be able to achieve the fastest ring down possible at any given frequency.

This section examines the transient response of each of the transducers when excited by an impulse whose duration is much shorter than the fundamental period of the transducer. In the frequency domain the input is broad band, containing roughly equal amplitude components at all frequencies of interest. The modeled voltage spike has an amplitude of 110V. The return echo detected by the receiver is the signal of interest. Typical pulser / receiver circuitry transmits the high voltage spike and receives the echo, which is amplified by 20 or 40dB. The receive probe can be the same as the transmit probe or can be a separate transducer. An attenuation factor, hereafter referred to as Attn, is used to reduce the amplitude of the signal for viewing on an oscilloscope. The amplified received signal is attenuated to a reference level of 600mV peak to peak. The attenuation necessary to scale the signal to this reference level is expressed in dB, i.e. Attn = 28dB. In order to examine the low level ring down, the response is also examined at an attenuation level 20dB less than that necessary to scale the signal to the reference level; for the above example that would be at Attn = 8dB. This is referred to as the -20dB ring down signal. For ease of comparison with measured responses, the program is designed to follow this procedure.

The transient response of the PZT5-A transducer is examined even though this is not of primary importance, since this transducer is designed to efficiently transfer energy from the electrical to the acoustical domain. As will be seen, however, the transient response can still give valuable insight into how well the transducer functions. A measure of the transducer efficiency can be seen from the amplitude of the received signal, expressed in terms of attenuation. A transducer with Attn = 58dB would be considered very efficient, while a transducer with Attn = 12dB would be considered inefficient.

The PZT5-A response is shown in Figure 4.7 at a level of both full scale and -20dB. The -20dB signal is essentially a blown up view of the lowest ten percent of the

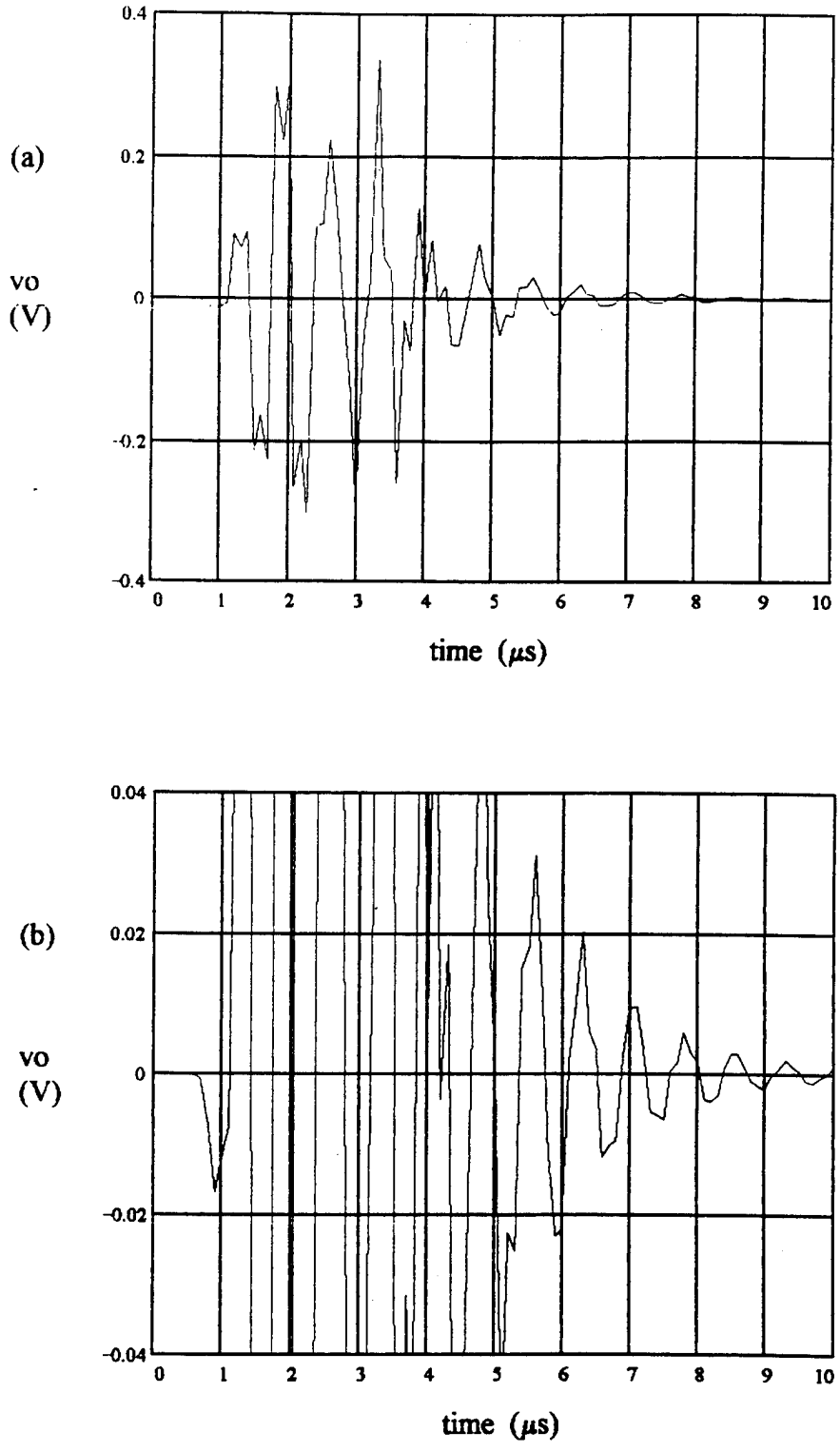

Figure 4.7 Modeled transient response of PZT5-A transducer, Attn. = 52dB, (a) full scale; (b) -20dB ringdown

voltage of the full scale signal. The modeled response can be seen to ring for several cycles after excitation. This is due to internal reflections between the piezoceramic and the matching layer and the air backing. The -20dB ring down time is the time between the first and last crossing of the -20dB signal with a reference voltage level which is 20dB lower than the peak to peak voltage level, 0.03V for all of the plots presented in this work. The -20dB ring down time for the PZT5-A transducer is 5.5μs. While this should not be considered a fast transient response, it does show a relatively good match between transducer and load. A poor match would show gradually decreasing amplitude over a longer time, indicating either a poor design or a construction anomaly, such as an air gap or bond layer between piezoceramic and matching layer. The efficiency is quite good, with A = 52dB. This is due in part to the reflections at the disk-air interface which constructively interfere at the disk-matching layer interface. Because of the impedance mismatch between the piezoceramic disk and the air backing, very little energy is transferred to the backing, increasing efficiency and also ring down time.

The transient response of the lead metaniobate transducer is shown in Figure 4.8. This shows a fast ring down with few extra cycles because this transducer is designed for high resolution. At the -20dB level, the signal can be seen to ring for only about 0.4μs; this would be the practical limit that two echoes would need to be spaced in time. With spacing less than 0.4μs, two pulses would not be differentiable. The match between the piezoceramic disk and the high impedance backing serves to absorb the energy incident at this interface, minimizing reflection and further ringing in time. This energy absorption also tends to decrease the efficiency. With A = 42dB, the probe is less efficient than the PZT probe; the reduced efficiency has been traded for increased resolution in time. A bond layer between disk and backing would increase the reflection at the interface between the piezoceramic disk and the high impedance backing. This would cause

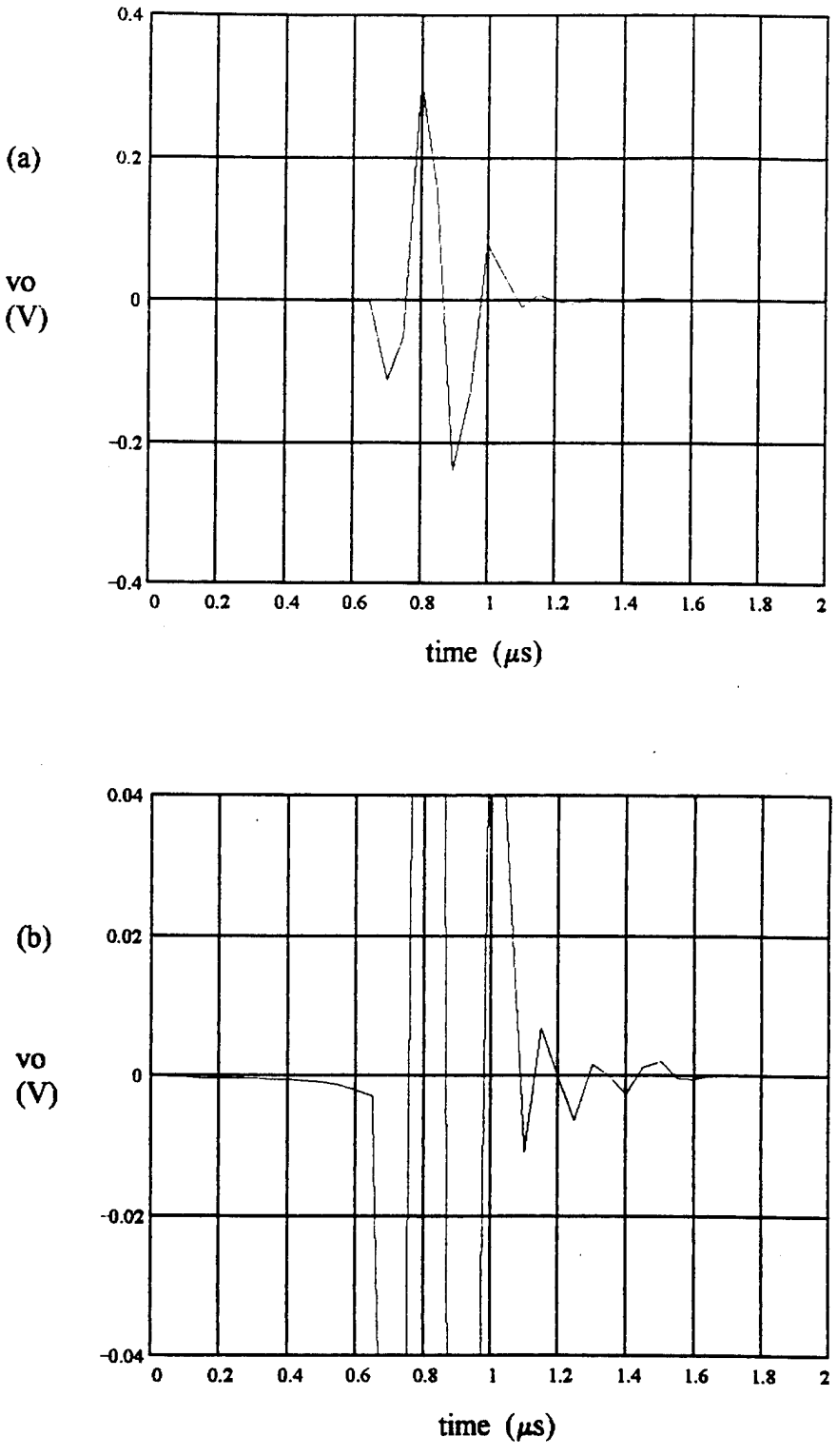

Figure 4.8 Modeled transient response of K85 transducer, Attn. = 42dB,
(a) full scale; (b) -20dB ringdown

additional cycles in the ring down, decreasing resolution. Effects such as this can easily be observed within the program by adjusting the appropriate parameters, making it useful not only for design of prototype probes but also for analysis of trouble within the production cycle.

The PVDF probe also exhibits few extra cycles, as shown in Figure 4.9. Its ring down is relatively fast for its low operating frequency of 500kHz, showing only two main cycles. The ringing that occurs late in time, however, is above the -20dB level, making the -20dB ring down time very long for this transducer. This is unexpected, since the close match between the impedance of the piezoceramic disk and the load medium should minimize reflection at this interface. The energy reflected at the piezoceramic disk / air backing interface should ideally be transmitted to the water load on the next cycle. The ringing in time should be small after the first few cycles, as the energy should be quickly transferred to the load. Overall the efficiency, with Attn = 6dB, is much lower than either the PZT or the lead metaniobate transducer; this is to be expected due to its relatively low stress constant, e_{33}. Use of a backing material whose impedance is close to that of the piezopolymer material would tend to decrease the ringing even further. The cost would be a further reduction in efficiency due to energy lost to the backing material.

The responses presented above are for ideal transducers; however, they are modeled after actual transducers. Actual transducers have matching layers which are not always $1/4\lambda$, backing materials which are not always homogeneous and of the right impedance, and bond layers which can significantly affect the response. The measurements presented in Chapter 5 are of imperfect transducers. Included with the measurements are additional modeled responses made by adjusting some of the parameters. Variations in the backing material, matching layer, and bond layers are purposefully made in order to examine their effect on the response. An attempt is made to adjust the parameters so that the modeled

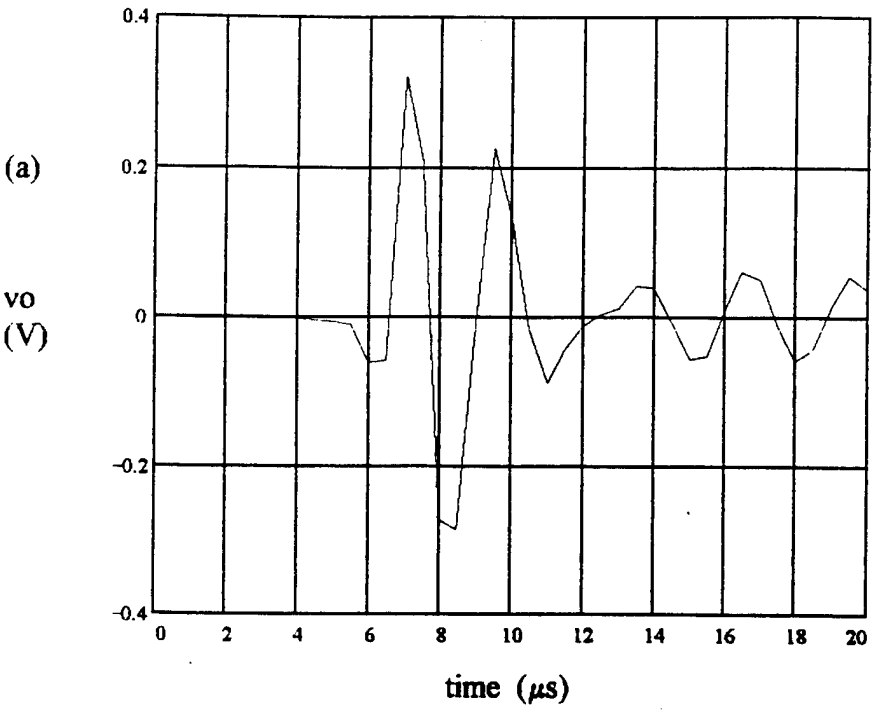

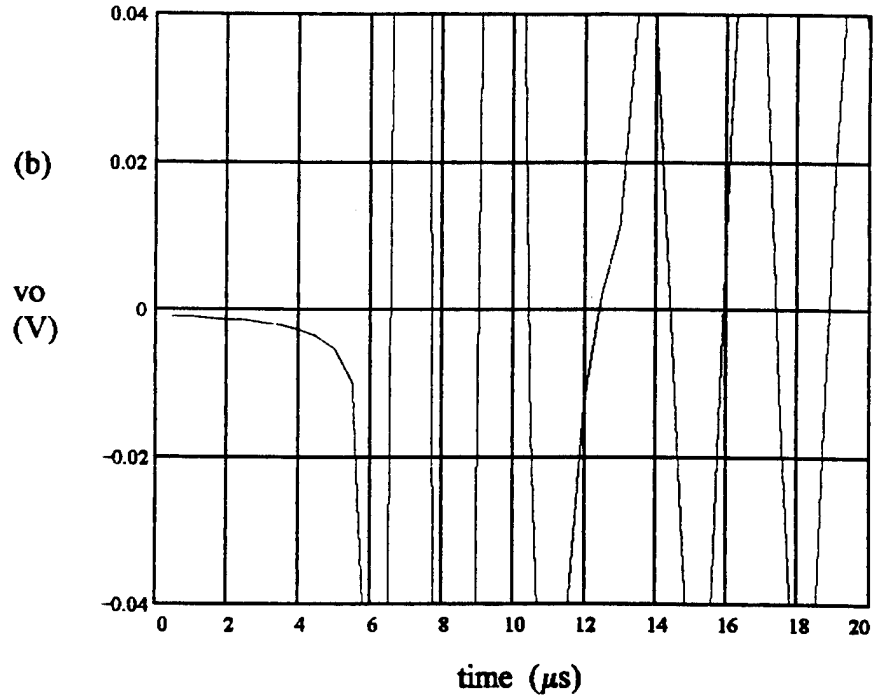

Figure 4.9 Modeled transient response of PVDF transducer, Attn. = 06dB,
(a) full scale; (b) -20dB ringdown

responses more closely match the measured responses. This is also useful for showing how the program can be used to adjust the balance between all of the different parameters in order to achieve the desired response, without building a single probe. It also shows how the program can be used to examine abnormalities in the response which are caused by imperfect bond layers, matching layers, and backing material.

Table 4.1 shows a summary of the modeled attenuation levels and ring down times presented above. Also included are the main parameters for each of the transducer configurations. It is included to facilitate comparison of each of the transducers.

Table 4.1 Summary of transducer model responses and input parameters

	PZT5-A	K85	PVDF	units
Attn	52	42	06	dB
-20dB ring down	5.5	0.5	N/A	μs
matching layer				
Za_m	3.8	3.8	N/A	Mrayl
t_m	16.6	4.9	N/A	mil
c_m	2.7	2.7	N/A	mm/μs
front bond layer				
Za_{bf}	3.8	3.8	33.0	Mrayl
t_{bf}	.005 μm	.005 μm	1.5 mil	
c_{bf}	2.7	2.7	3.7	mm/μs
piezoceramic				
Za_p	33.7	18.5	1.4	Mrayl
t1	0.053	0.012	0.022	in
d1	0.825	0.190	0.375	in
fo	1.6 MHz	5.4 MHz	750kHz	
rear bond layer				
Za_{bf}	3.8	3.8	33.0	Mrayl
t_{bf}	.005 μm	.005 μm	1.5 mil	
c_{bf}	2.7	2.7	3.7	mm/μs
backing material				
Z_b	415	14.5M	415	rayl

Chapter 5

MEASUREMENT AND COMPARISON OF TRANSDUCER RESPONSES

5.1 Introduction

This chapter presents measurements of the transducers modeled in Chapter 4, including the electrical input impedance and transient response. These measurements are compared with the modeled results. Also, adjustments to the model parameters are made to test possible construction variations which could improve or degrade the performance of the transducers. The validity of the model and its usefulness as an engineering tool are discussed.

5.2 Measurement of Electrical Input Impedance

The electrical input impedance is measured for each of the transducers modeled in Chapter 4. The measurement setup is shown in Figure 5.1. Each transducer is tested with its face submerged in water, i.e. with a water load. An absorptive pad is placed in the bottom of the container in order to reduce standing waves which can cause small ripples in the measured impedance.

At this point a note is in order about the plots of the measured impedance which are presented below, as they are plotted directly from the HP4194 impedance analyzer and those who are not familiar with this machine may have difficulty reading them. Each plot has two curves, either real and imaginary parts or magnitude and phase of Zein. The curves are labeled appropriately. The start and stop frequency for each is shown at the bottom right of the plot. As each plot has 10 divisions, the span between divisions is the

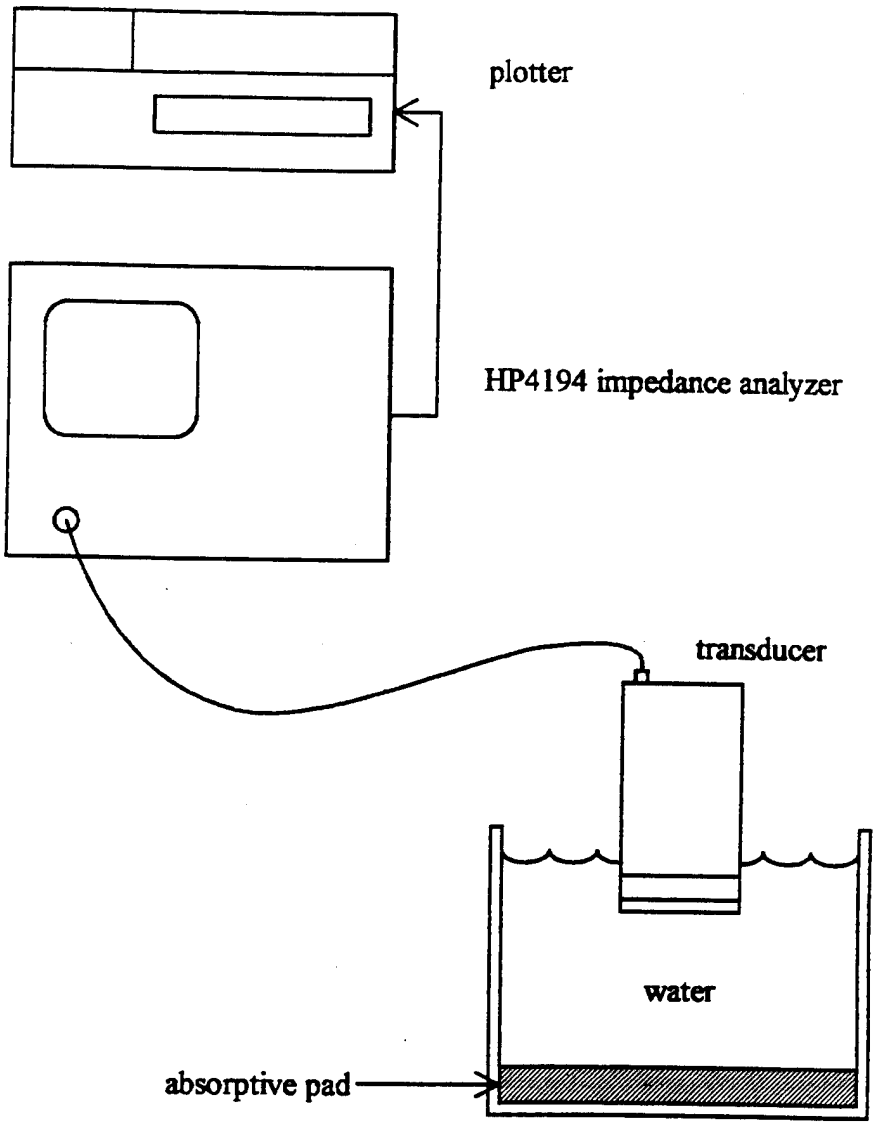

Figure 5.1 Impedance measurement test setup

start frequency minus the stop frequency divided by 10. The maximum value for each curve is shown at the top left of the plot. There are also 10 vertical divisions with the value between divisions for each curve shown at the bottom left of the plot. The upper right of the plot shows the value for each curve at the frequency marked by a circle on the curve. By following these guidelines the value of each curve at any frequency may be determined.

Figure 5.2 shows the real and imaginary parts of the impedance for the transducer built with PZT5-A. The real part is seen to peak at 1.7MHz with a value of 42Ω; at this frequency, the imaginary part has a value of -50Ω. The model of the ideal transducer predicted a peak of 44Ω at 1.6MHz, Figure 4.1; the predicted curve is also somewhat narrower than that observed. At 1.6MHz the predicted imaginary part is -40Ω. Also, it should be noted that the measured curves show a dip around 1.5MHz while the predicted curves are more symmetrical.

The measured magnitude and phase of Zein are shown in Figure 5.3. Similar to the measured real and imaginary parts, they also show a dip at 1.5MHz. At this frequency the impedance has a magnitude of 56Ω with a phase angle of -50 degrees. The modeled impedance of Figure 4.2 predicts a magnitude of 50Ω and a phase angle of -35 degrees. The measured values are close to the modeled values for an ideal transducer, with differences ranging from ten to twenty percent. It is desirable for all of the differences to be within or close to ten percent. The source of this difference is sought so that modifications to the transducer construction can be made within the program.

The difference between the measured impedance and the ideal modeled impedance provides clues as to what may be the cause. Since the resonance frequency of the measured transducer is slightly greater than predicted, it implies that perhaps the matching layer is thicker than a quarter wavelength. This would cause the match from piezoceramic

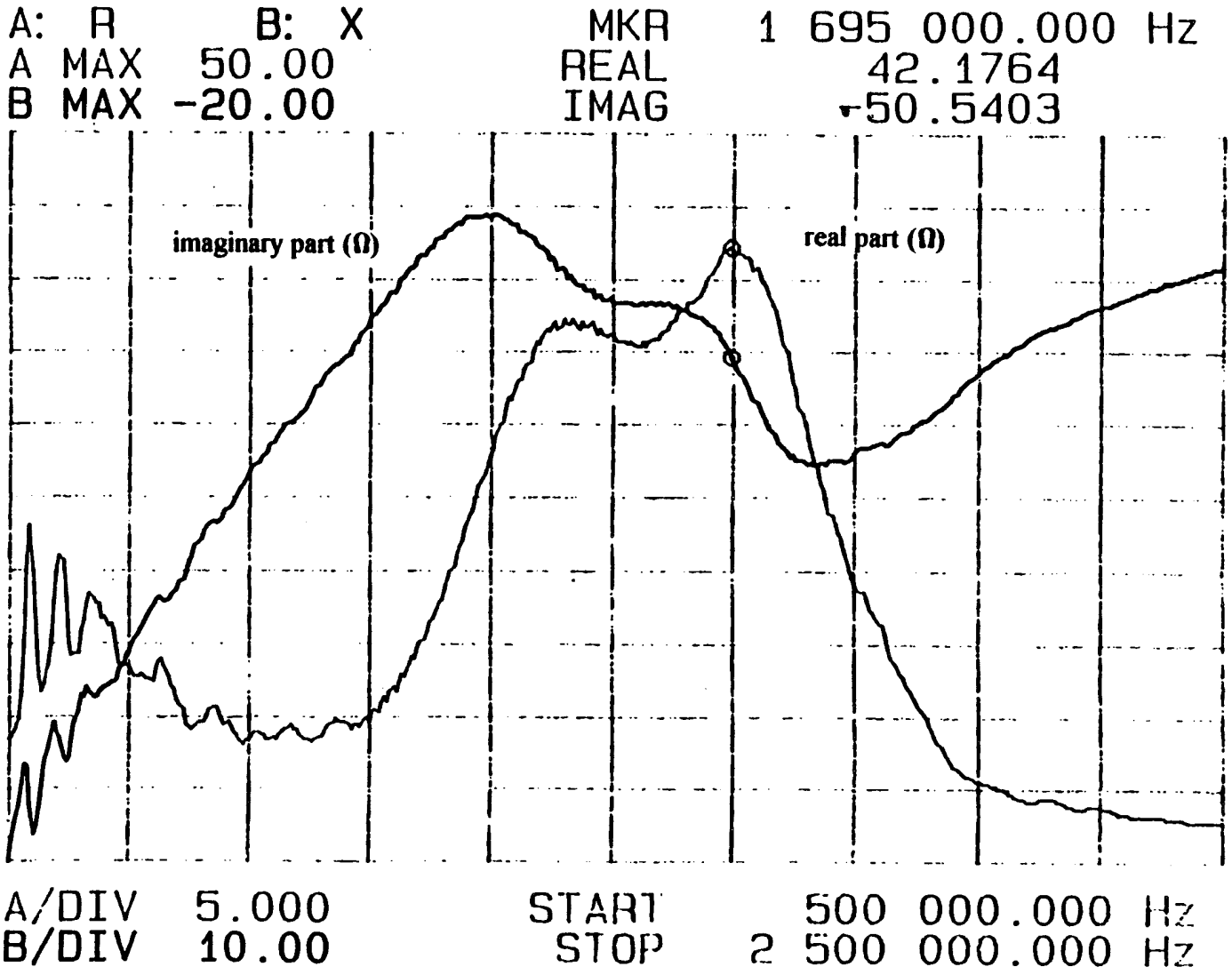

Figure 5.2 Measured real and imaginary part of Zein for PZT5-A transducer

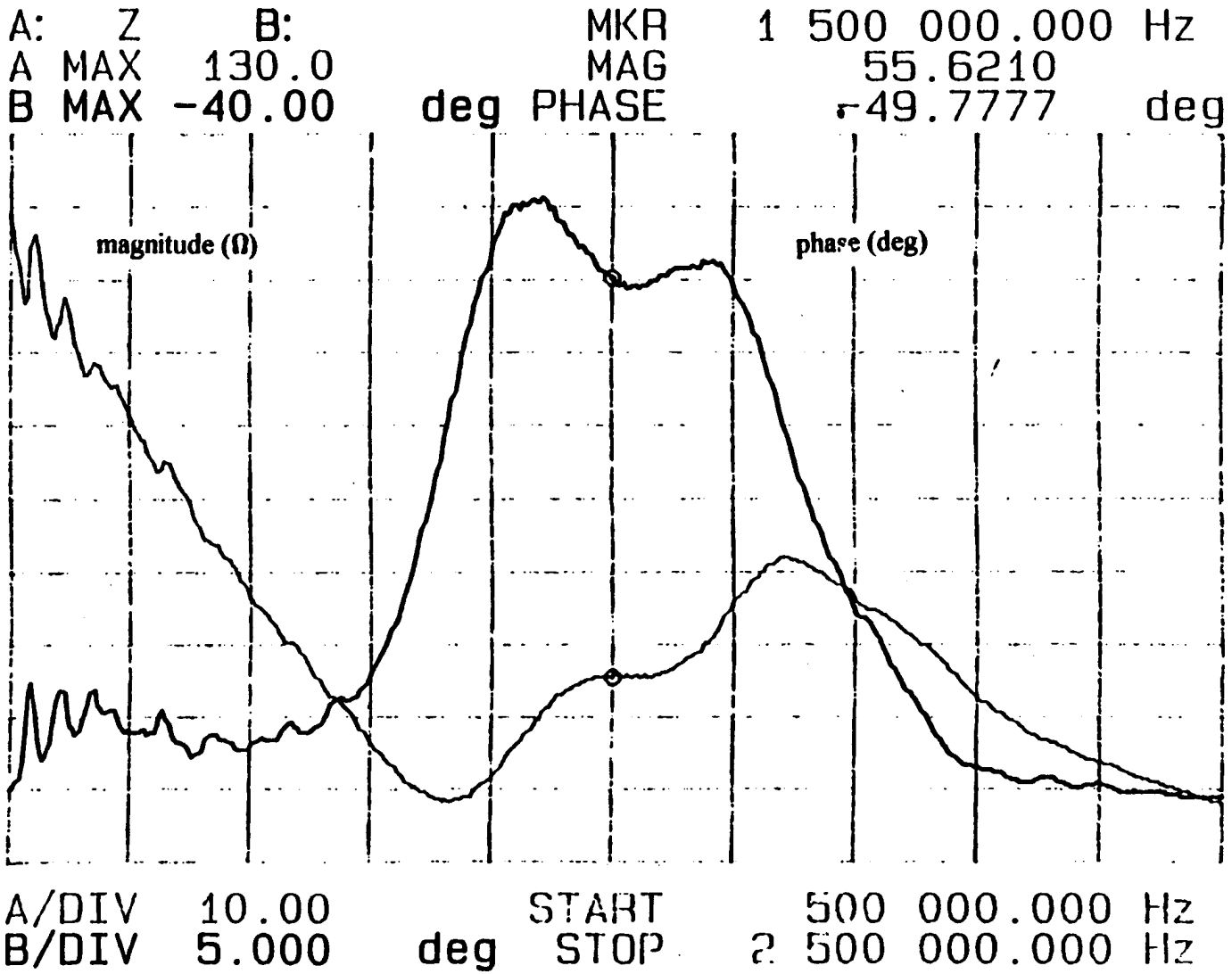

Figure 5.3 Measured magnitude and phase of Zein for PZT5-A transducer

disk to water load to be maximum at a frequency lower than the disk resonance frequency which would be the cause of the dip in the measured impedance. To test this theory, the model was adjusted so that the modeled matching layer is 10% too thick. The modeled real and imaginary parts of Zein under these circumstances are shown in Figure 5.4. It can be seen that, relative to the ideal modeled transducer of Figure 4.1, the resonance has indeed shifted to a higher frequency. The real part of Zein is again within 10% of the measured value at a resonance of just under 1.7MHz; the modeled imaginary part has a value of -50Ω, exactly the value measured at 1.7MHz. The magnitude of the adjusted modeled impedance, shown in Figure 5.5, has dropped to 43Ω at 1.5MHz, due to a dip in the curve. The phase has dropped to -48 degrees, more closely matching the measured value of -50 degrees. Table 5.1 summarizes the results for the measured and theoretical

Table 5.1 Impedance values for PZT5-A transducer variations

Matching layer	peak value of Re{Zein} (Ω)	frequency of peak Re{Zein} (MHz)	|Zein| @ 1.5MHz (Ω)
1/4λ	44.0	1.55	51.0
1/4λ + 10%	44.5	1.7	43.0
measured	42.2	1.7	55.6

cases. Also, the dip in the modeled impedance occurs at 1.5MHz for all four plots, exactly the frequency where the measured dips exist. This seems to verify that the matching layer is perhaps too thick, causing a shift and dip in the measured impedance. This also demonstrates how the program can be used to analyze what factors contribute to errors in the response of actual transducers. Variations in other parameters can easily be examined.

The measured real and imaginary parts of Zein for the lead metaniobate transducer are shown in Figure 5.6, as compared to the modeled results of Figure 4.3. The measured real

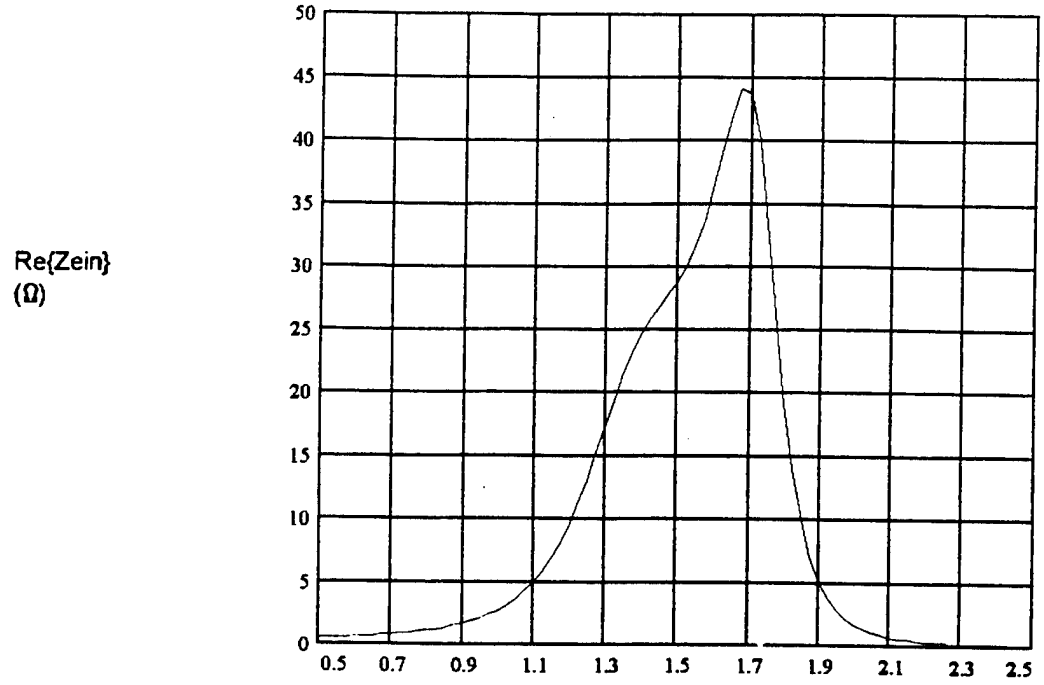

(a)

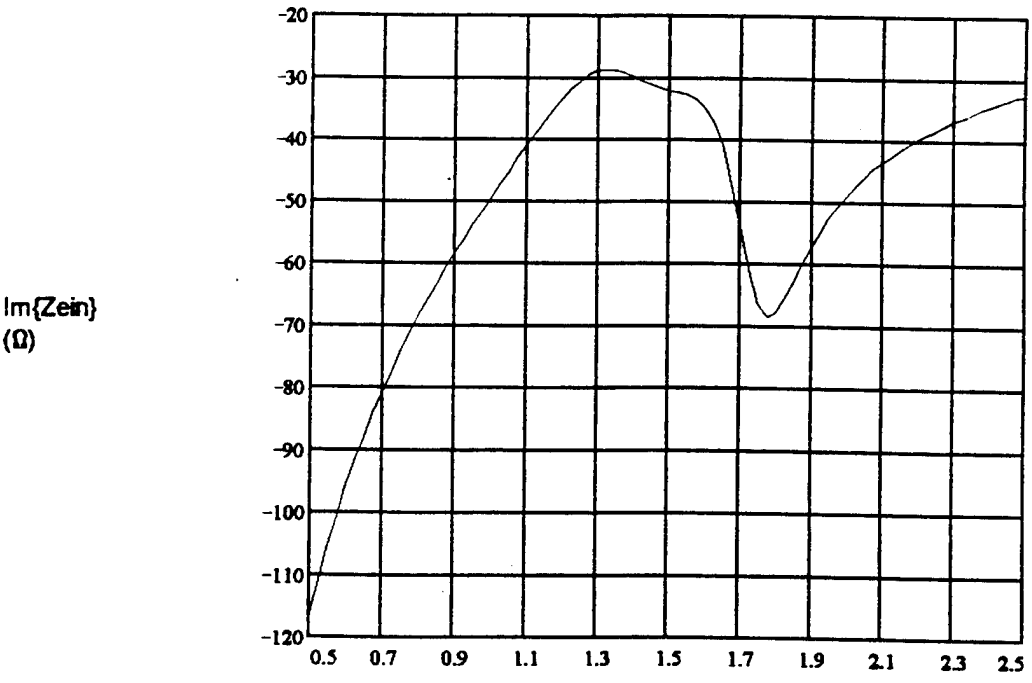

(b)

Figure 5.4 Modeled electrical input impedance for PZT5-A transducer with mathching layer 1/4λ + 10%; (a) real part; (b) imaginary part

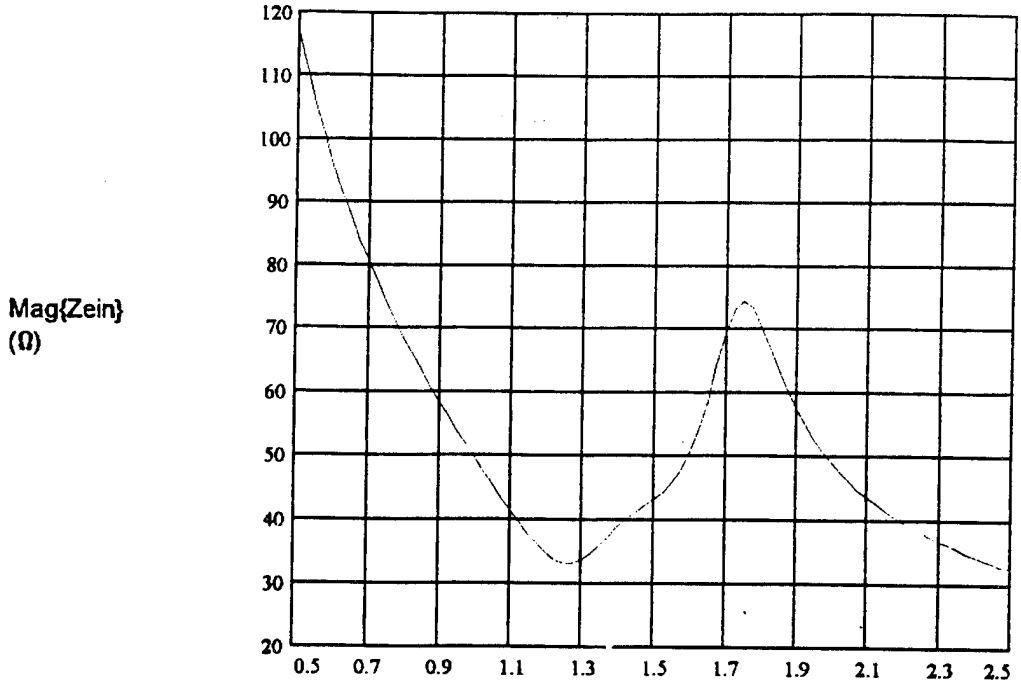

(a)

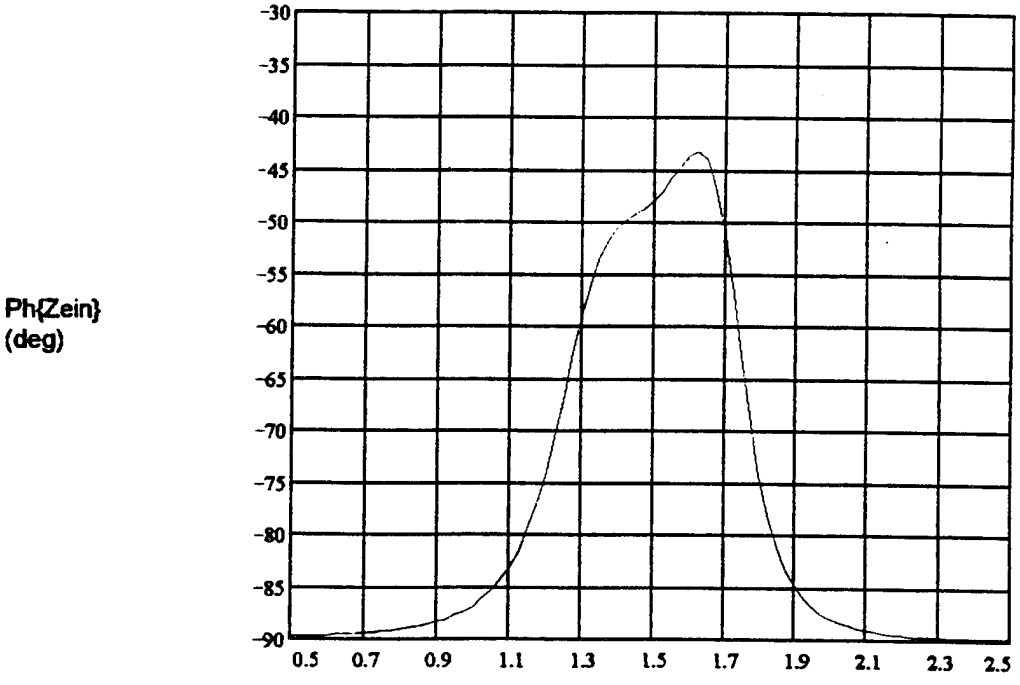

(b)

Figure 5.5 Modeled electrical input impedance for PZT5-A transducer with matching layer = 1/4λ + 10%; (a) magnitude; (b) phase

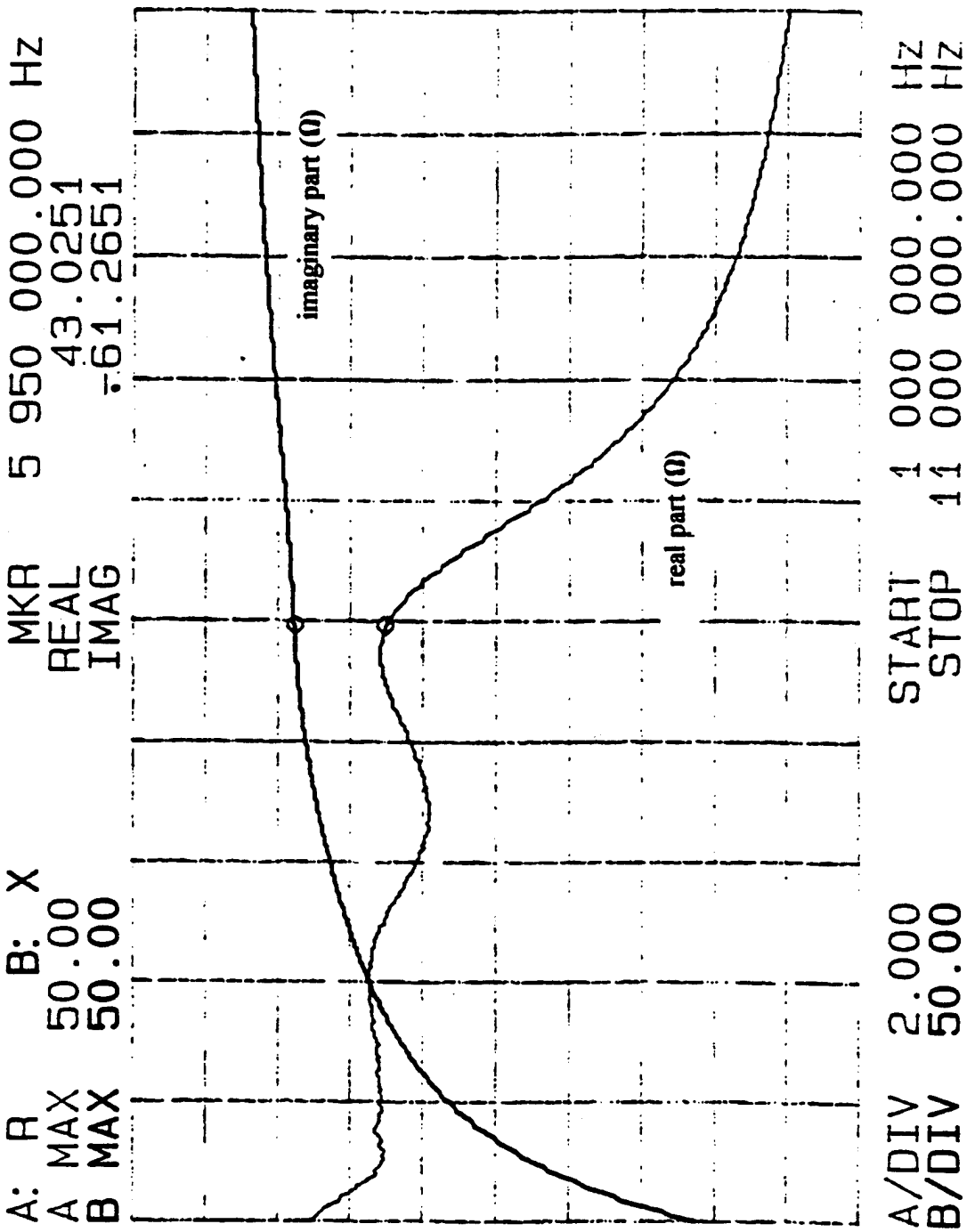

Figure 5.6 Measured real and imaginary part of Zein for K85 transducer

part is relatively flat below 6MHz, with a value of about 44Ω. This is higher than the modeled impedance, which peaked at 28Ω and decreases at low frequencies. It is expected that the real part would decrease below resonance, as was shown for the PZT transducer. It is not known what is causing the measured value to remain flat at low frequencies. The measured imaginary part curve is very similar in shape to the modeled curve, but the measured value of -61Ω at 6MHz is different by about 50% compared to the modeled value of -90Ω. It seems that the discrepancy is largest between 3.5 and 6.5MHz, where the effect of the mechanical resonance is greatest. The damping seems to affect the measured impedances more than the modeled impedance. It is possible that a loss mechanism existing in the actual transducers is missing in the model.

The measured magnitude curve, shown in Figure 5.7, agrees well with the modeled curve shown in Figure 4.4. At 6MHz the impedance magnitude measured 75Ω. The model predicted 85Ω, a difference of about 12%. The phase, however, is predicted to be much lower than what is measured; only at very low frequencies do the values agree. It is believed that this difference is caused by the low value which the model predicted for the real part; this causes the imaginary part to dominate the magnitude, resulting in a predicted phase angle closer to 90 degrees than measured.

A source for the difference between the measured and modeled responses has been tested. At high frequencies the inductance of the measuring leads sometimes causes strange results. To test this theory, a small series inductance of 0.5μH was placed in series with the modeled Zein. The resulting curves do not correspond any better than those without the additional inductance. Also, since the discrepancy also exists in the real part of the impedance at low frequencies, it is thought that lead inductance is not the problem and that the difference is caused by some other effect. This is where the inherent flexibility of implementing the program on Mathcad is of great value, since further modifications can

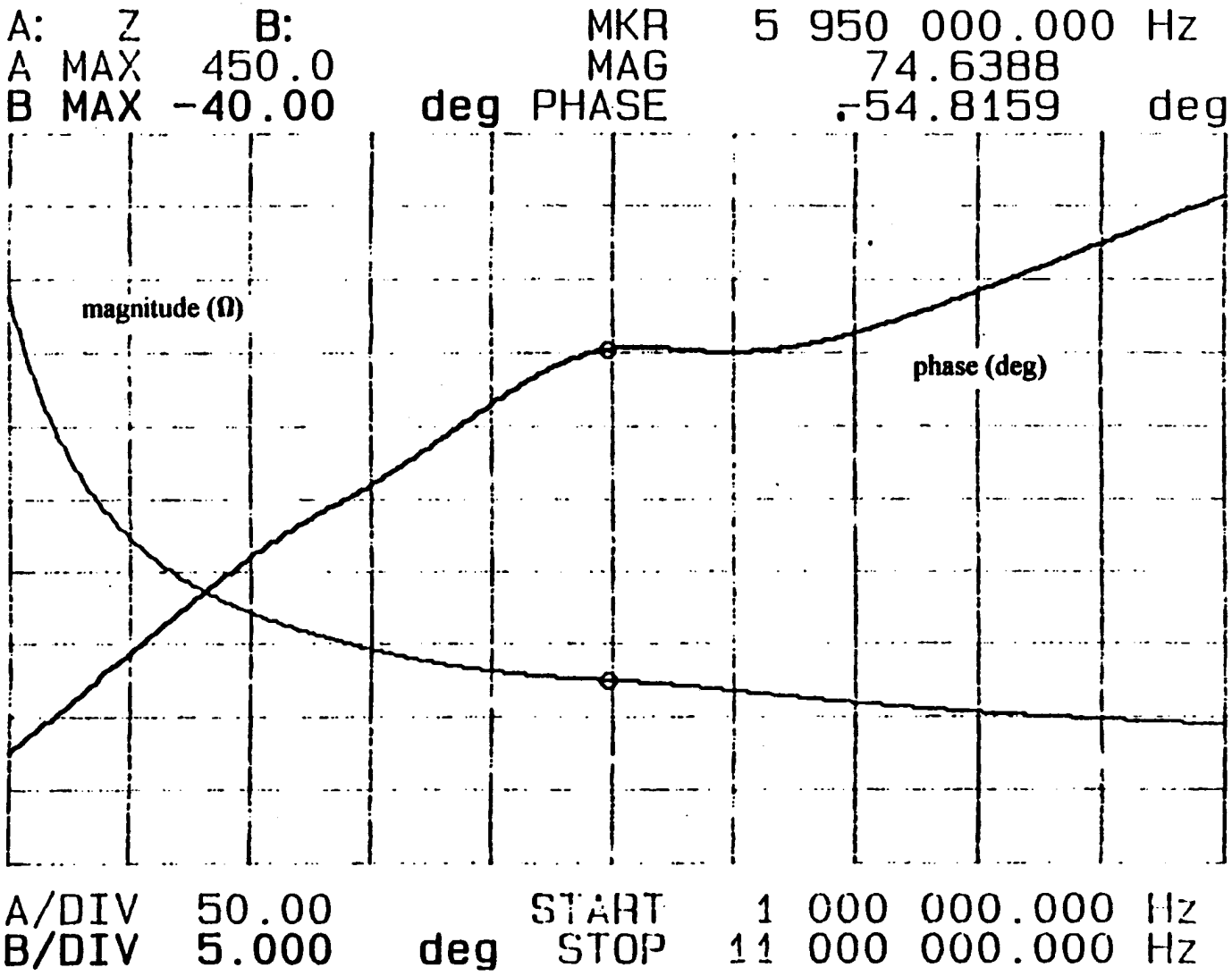

Figure 5.7 Measured magnitude and phase of Zein for K85 transducer

be easily made to the program which may help to isolate the cause of the difference. Even with the differences in the results, however, the agreement is sufficient to determine that the impedance of this design is close enough to the nominal 50Ω for all practical purposes.

Figure 5.8 shows the real and imaginary parts of Zein for the PVDF transducer. Unlike the modeled real part, Figure 4.5, the measurement shows no peaks or dips. The measured value of 3kΩ at 600kHz is not that far from the modeled value of 2kΩ; at lower frequencies, however, the error is much greater due to the peak in the modeled impedance. The measured imaginary part also shows no effects due to the resonance; in contrast, the modeled curve shows a peak and dip in the curve between 350 and 700kHz. The measured value of -19kΩ is close to the predicted value of -24kΩ, especially considering that the discrepancy is due to the peak in the response. The mechanical damping of the measured transducer at resonance seems to be greater than the damping of the modeled transducer.

The measured magnitude and phase of Zein, Figure 5.9, show a similar divergence from the modeled curves, as seen in Figure 4.6. Both measurements do not show any major resonance effects, while both predicted curves do. The measured magnitude of 20kΩ at 600kHz is close to the modeled value of 24kΩ; the discrepancy is again due to the lack of any measured resonance effects. The measured phase is flat, changing less than 5 degrees from 200kHz to 1.2MHz; the predicted phase changes almost 15 degrees over the same range. It should be noted that all of the measured impedances for the PVDF transducer are over 1kΩ due to the low value of Co, as discussed in Chapter 4. The degree of accuracy of the model is good enough to show that to use this transducer with standard NDT equipment a matching transformer would likely be required.

A plot of the real and imaginary parts of Zein for the PVDF transducer with an air load on the front face is shown in Figure 5.10. The effect of the air load is to increase the

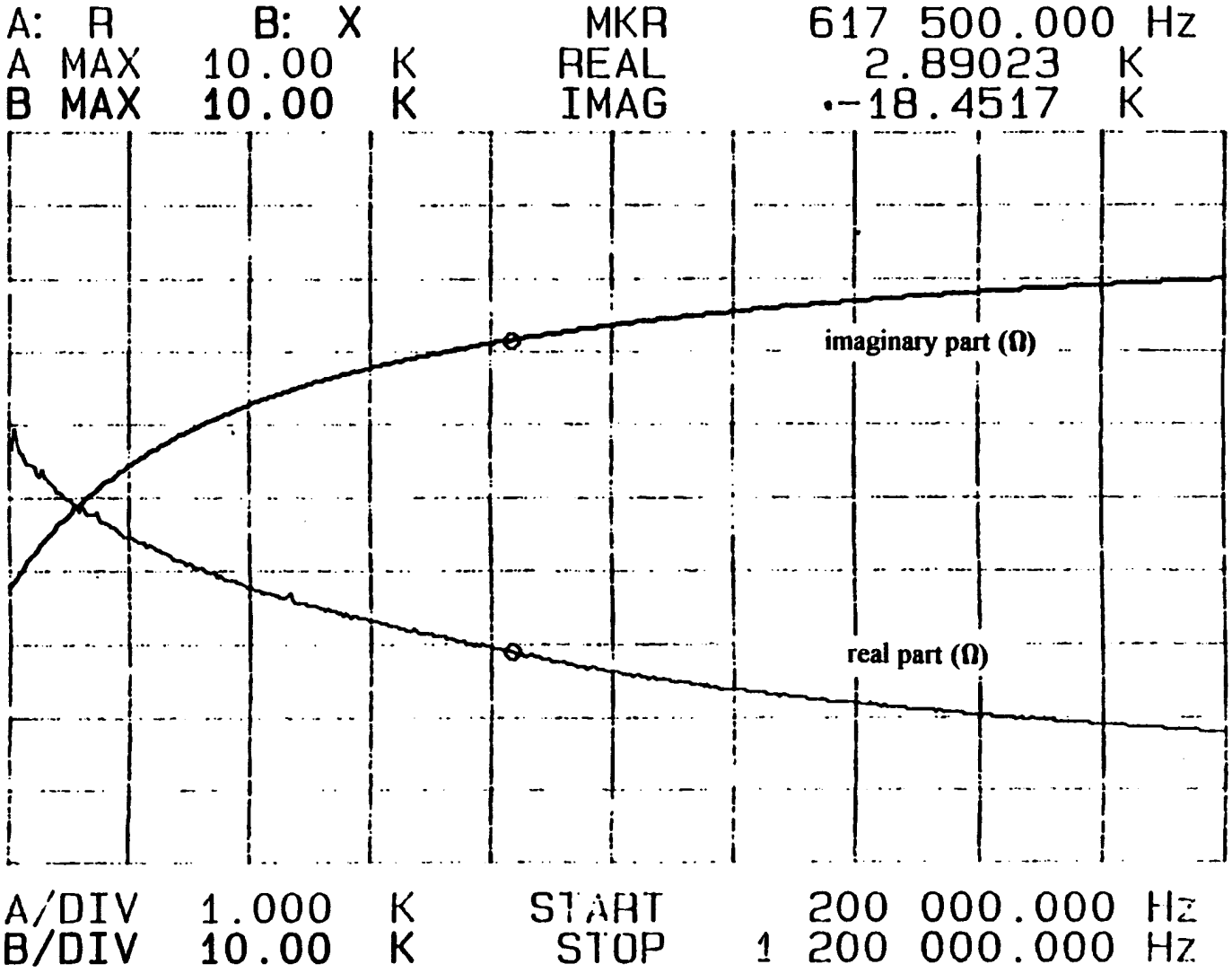

Figure 5.8 Measured real and imaginary part of Zein for PVDF transducer

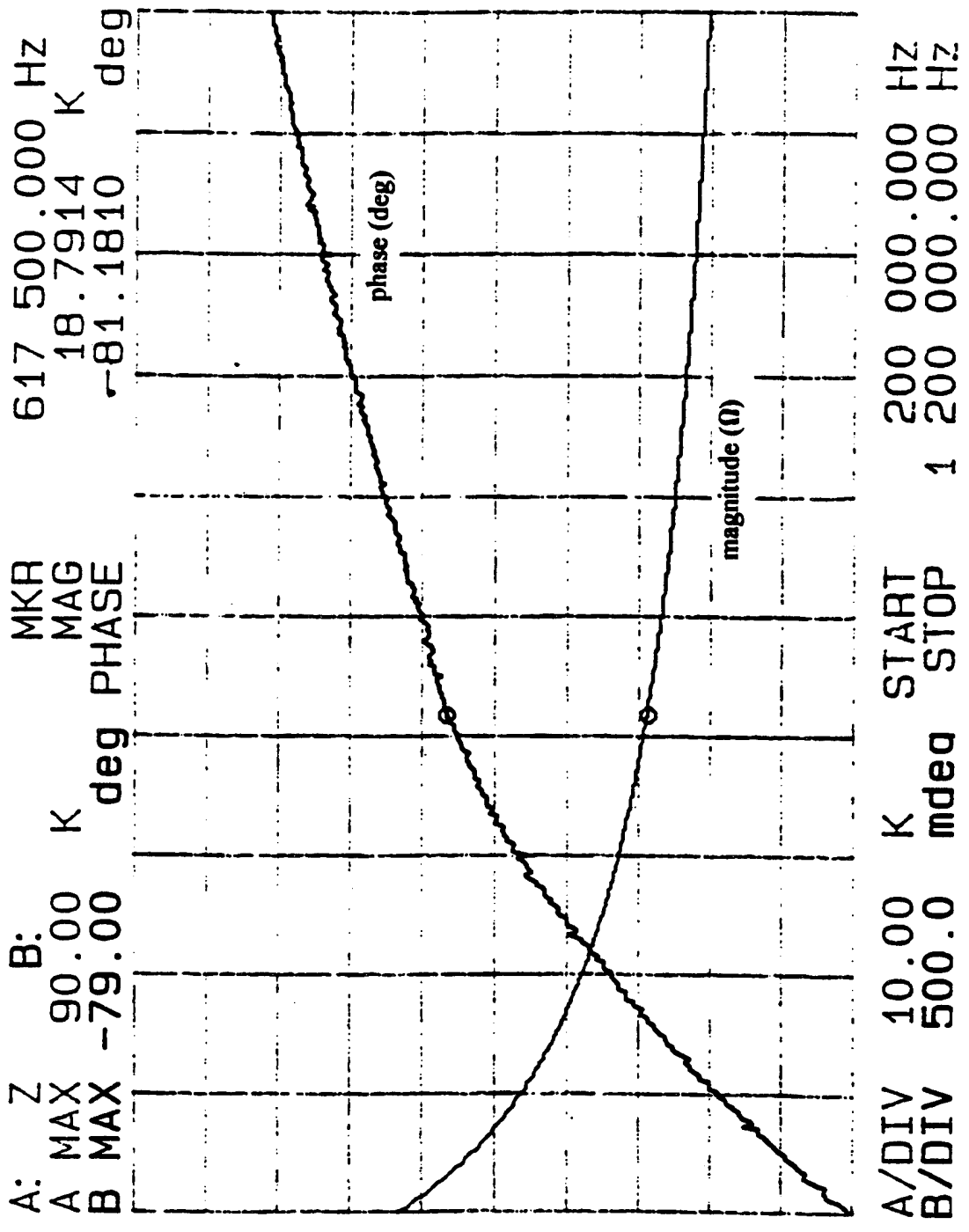

Figure 5.9 Measured magnitude and phase of Zein for PVDF transducer

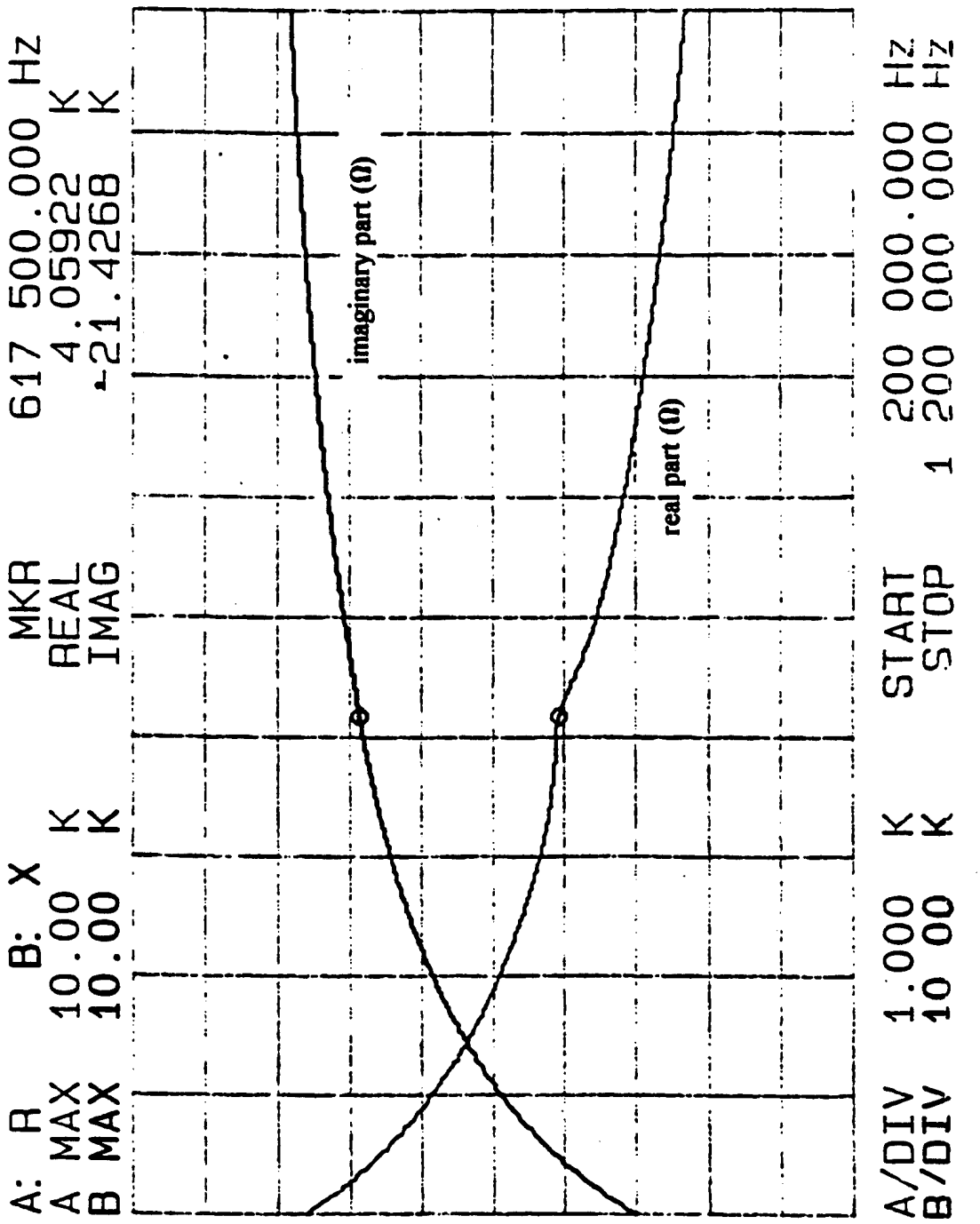

Figure 5.10 Measured real and imaginary part of Zein for PVDF transducer with air load

Q of the transducer by eliminating the loss mechanism from disk to water, as there is an impedance mismatch between the PVDF and the air load. The result is a bump at about 600kHz in the real part curve. A similar effect is seen in Figure 5.11 where the phase response has a bump at 600kHz. While these plots still do not agree with the modeled plots of Figures 4.5 and 4.6, the fact that a resonance is measured can be an indicator that a particular parameter needs to be adjusted in the model.

Overall the measured impedance curves agree reasonably well with those predicted by the models. The agreement is particularly good for the low loss PZT probe, where it was shown that the matching layer is about 10% too thick. While the other measurements did not show the same degree of accuracy, the results seem adequate enough to determine if the operating impedance is at an acceptable level. The measured impedance can also be used to determine how damped the resonance of the transducer is. For both of the highly damped probes, the model predicts less damping than what is observed. For the PZT probe, the amount of damping is accurately presented. It is possible that the model cannot accurately predict the effect of the loss mechanisms on the impedance, leading to a small difference between measured and predicted responses. This could be due in part to the lack of any modeled loss in the piezoelectric materials themselves. The loss factor is both temperature and frequency dependent, making it difficult to model. The internal loss is greatest for the PVDF material, followed by the lead metaniobate and then the PZT material. The correlation between the magnitude of the neglected loss factor and the difference between the modeled and measured impedances agrees in this respect, suggesting that this missing factor may be a cause for part of the difference.

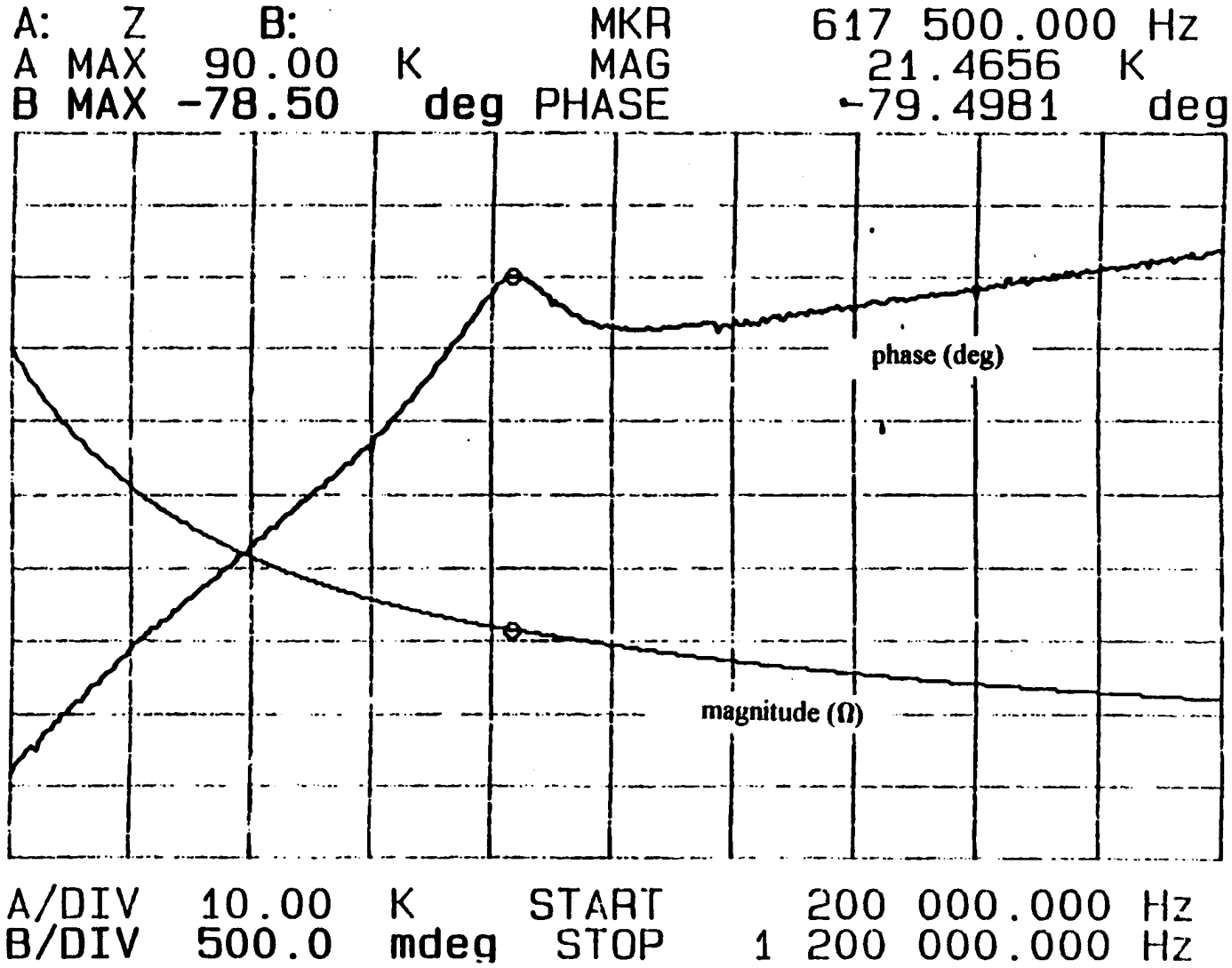

Figure 5.11 Measured magnitude and phase of Zein for PVDF transducer with air load

5.3 Measurement of the Transient Response

The transient response is measured for each transducer using the setup shown in Figure 5.12. The transducer is mounted so as to allow adjustment in order to orient the face perpendicular to the flat reflective plate. The plots are scaled to a reference level of 600mV, with the attenuation level noted. The low level ring down of the signal is examined with the attenuation level 20dB less. This is the same procedure as followed for the modeled plots. The model assumes that the medium is lossless and that all energy incident on the plate is reflected back to the transducer. Scattering and absorption are thus neglected. With careful orientation, close spacing between the transducer and the reflector, and clear water, these are good approximations to the actual measurement conditions used to test the transducers.

At this point a word is in order about the measured transient response plots presented below, as they are plotted directly from the screen of the digital oscilloscope. The important parameters are the time per division on the horizontal axis and the volts per division on the vertical axis. These can be found to the right of the plot under the label Channel 1. The volts per division is the same for each plot and is equal to 0.1V. The chosen time per division is dependent on the operating frequency of the transducer.

The measured transient response of the PZT5-A transducer is shown full scale in Figure 5.13; this can be compared to the modeled response of Figure 4.7. The measured efficiency of this transducer, with A = 48dB, is slightly less than the 52dB predicted by the model. Many factors could account for this. The piezoceramic stress constant could be slightly less than predicted, or other parameters could be in error. Energy reflected from the plate at angles off perpendicular, which does not return to the receive transducer, and absorption by the water probably account for a part of the loss. The shape of the

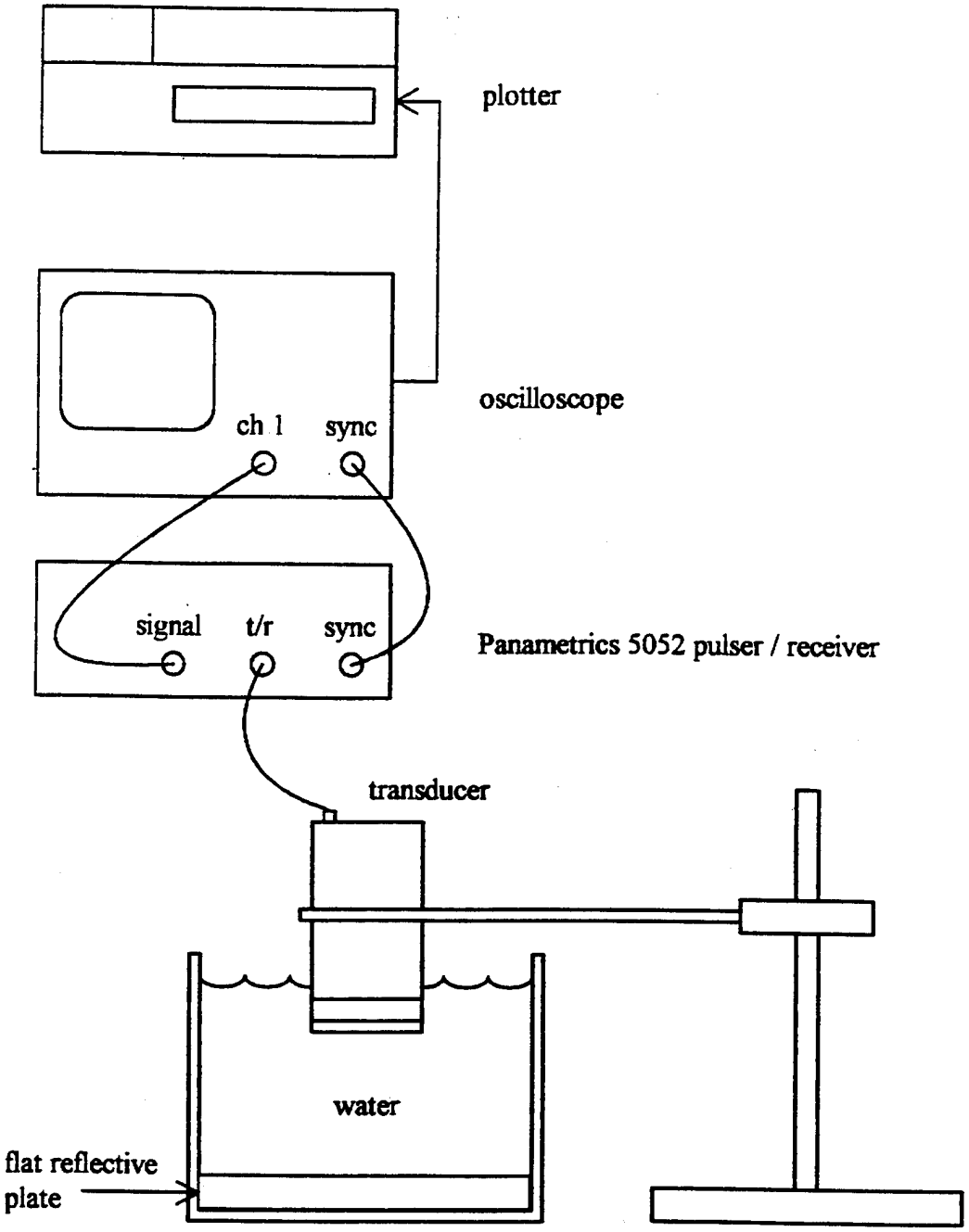

Figure 5.12 Test setup for transient response measurements

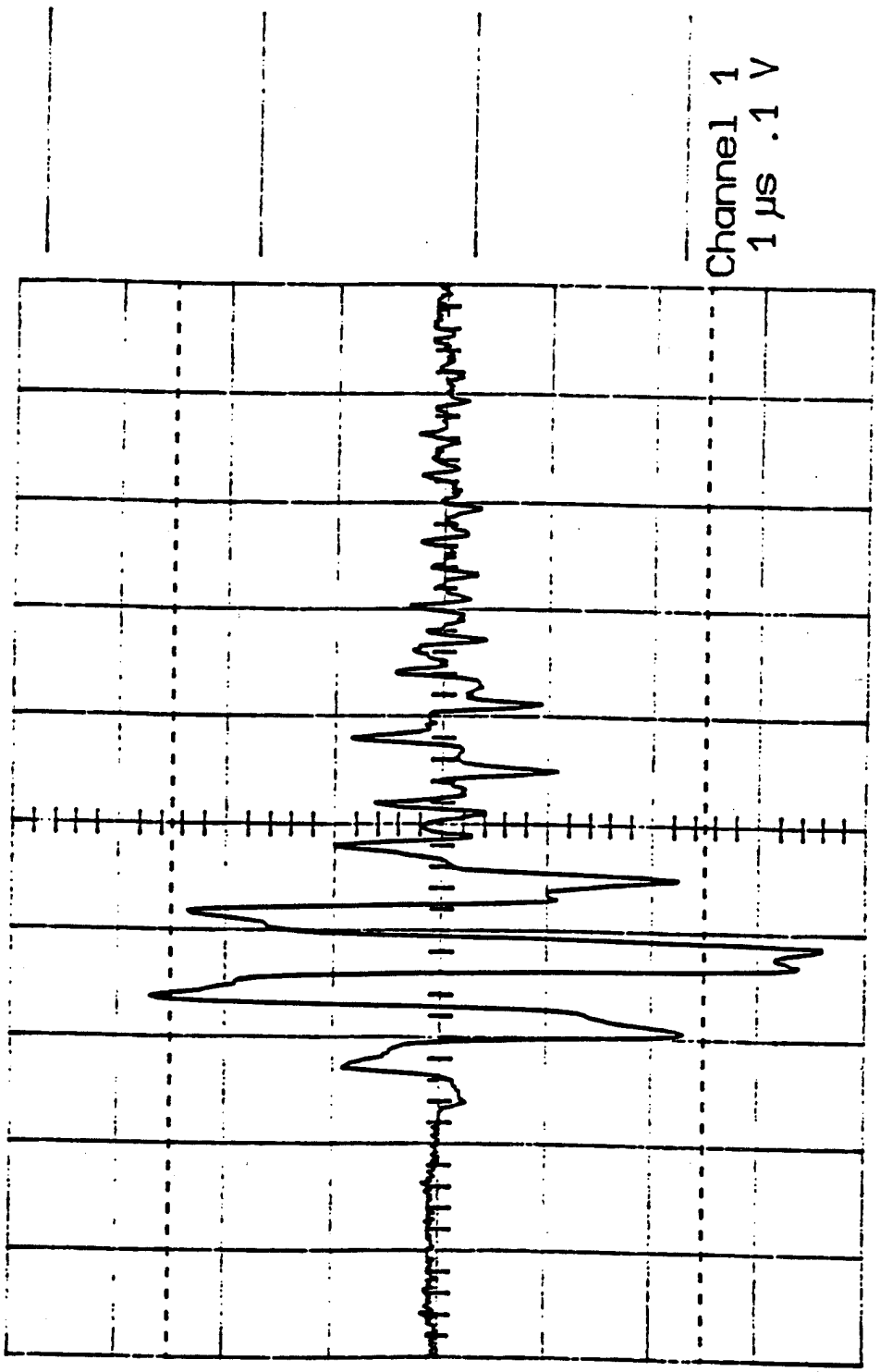

Figure 5.13 Measured transient response of PZT5-A transducer, Attn = 48dB, full scale response

measured transient response, however, is very similar to that modeled; the measured response has just one less cycle, indicating larger damping than predicted.

The signal measured at -20dB, shown in Figure 5.14, is also very similar to that predicted by the model, both with equal pulse widths of about 6μs. Both measurements show the effect of higher harmonics on the response, causing a higher frequency ringing to be superimposed on the cycles of the fundamental. To test whether the irregularities are actually due to higher harmonics, the probe was measured while tilted a few degrees off perpendicular. This was done to reduce the amplitude of the higher harmonics, since the increased directivity at these higher frequencies should lessen their effect on the response when the probe is tilted. The result, shown in Figure 5.15, is a marked decrease in high frequency interference. The amplitude of the signal is the same, with A = 48dB. The same effect could be achieved with the computer by filtering the harmonics.

The modeled transient response is examined for the case of the matching layer which is 10% thicker than a quarter wavelength, as suggested from the comparison between the modeled and measured impedance; this is shown in Figure 5.16. The response is similar to the modeled case with a quarter wavelength, but the higher amplitude of the third cycle causes the attenuation for the thick layer case to be slightly greater. The thicker layer case also shows a greater amount of ringing after the main cycles ring down, largely due to higher order modes. This can be seen clearly in the -20dB ring down response where the pulse width has increased to 8.5μs. These higher order modes are usually not as evident in actual measurements. The transient responses for the modeled and measured cases are summarized in table 5.2.

The measured transient response for the K85 transducer is shown full scale in Figure 5.17 and the modeled response in Figure 4.8. The measured efficiency, with A = 38dB, is about 37% less than the model prediction of 42dB. With one and a half major cycles, the

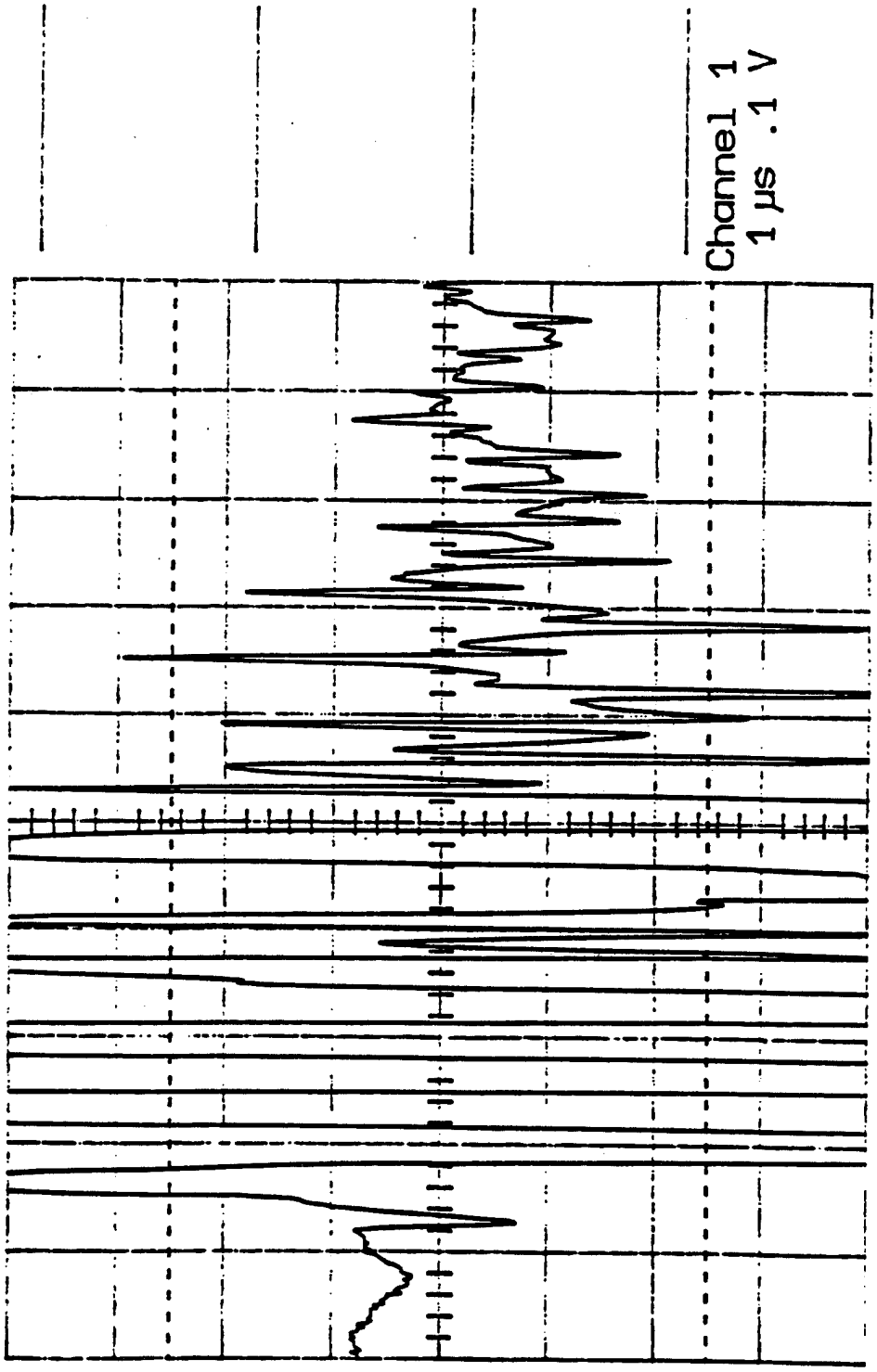

Figure 5.14 Measured transient response of PZT5-A transducer, Attn = 28dB, -20dB ring down response

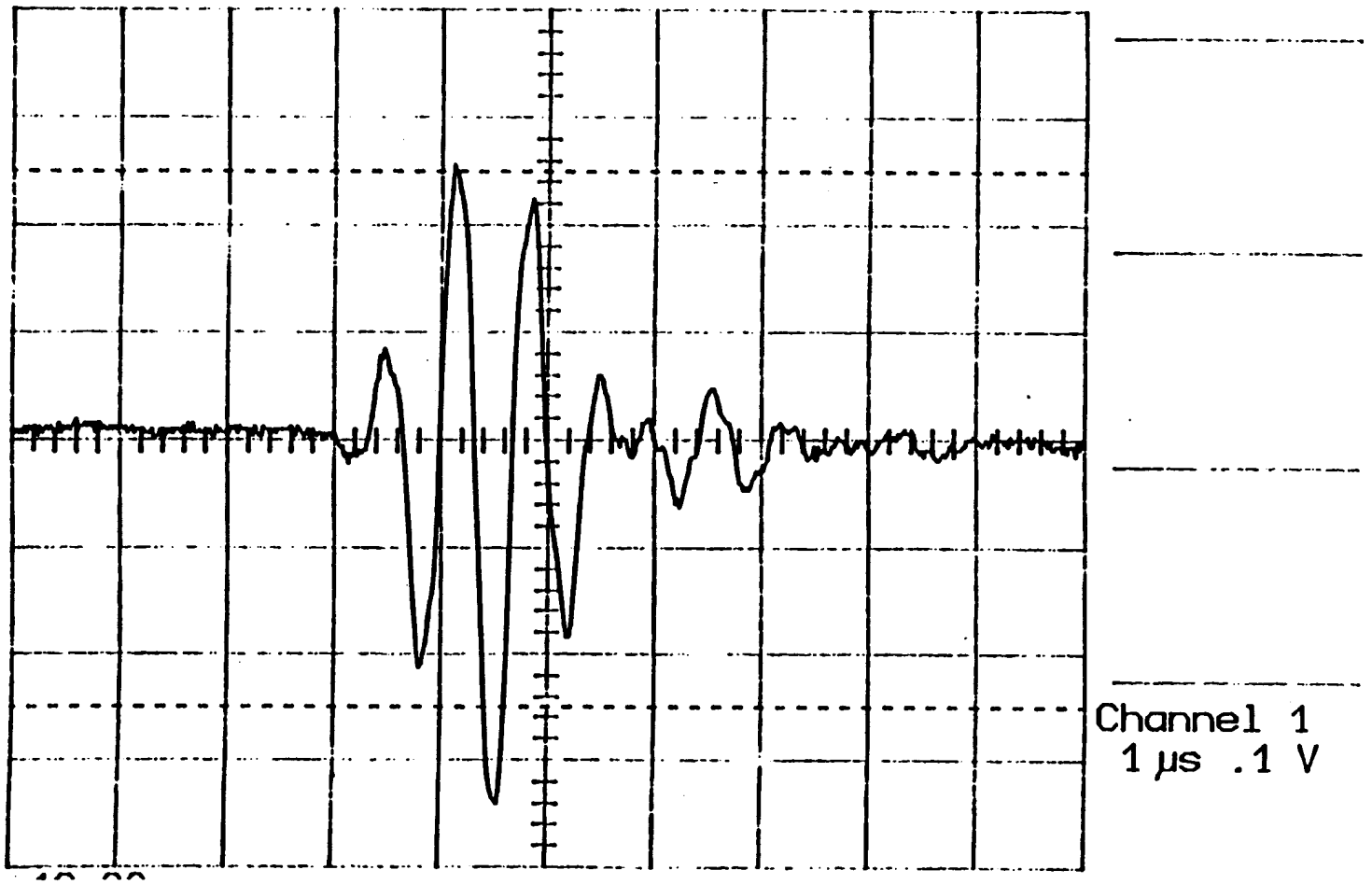

Figure 5.15 Measured transient response of PZT5-A transducer, Attn = 48dB, full scale response, probe tilted a few degrees

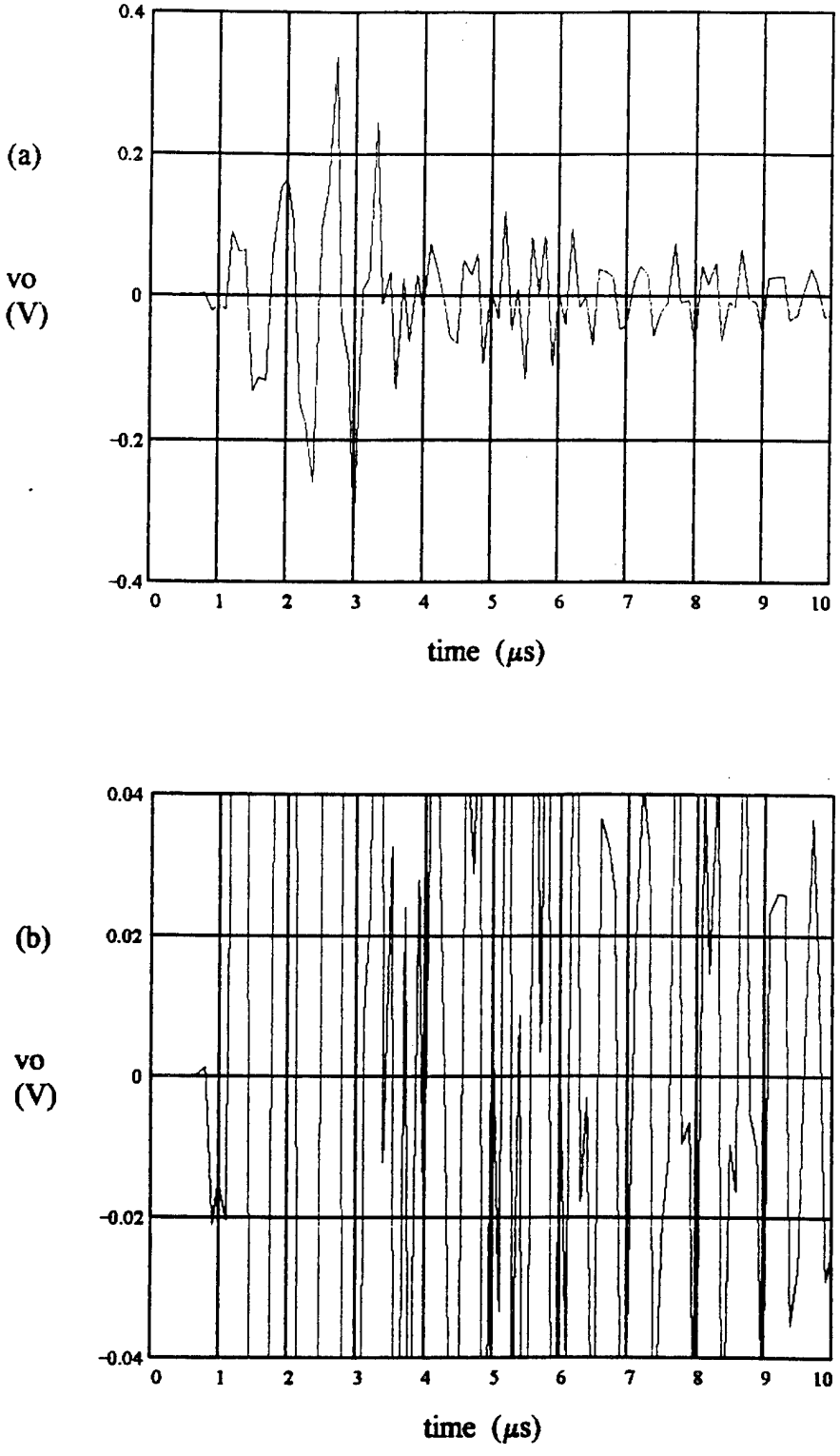

Figure 5.16 Modeled transient response of PZT5-A transducerwith matching layer = 1/4λ + 10%; Attn. = 54dB, (a) full scale; (b) -20dB ringdown

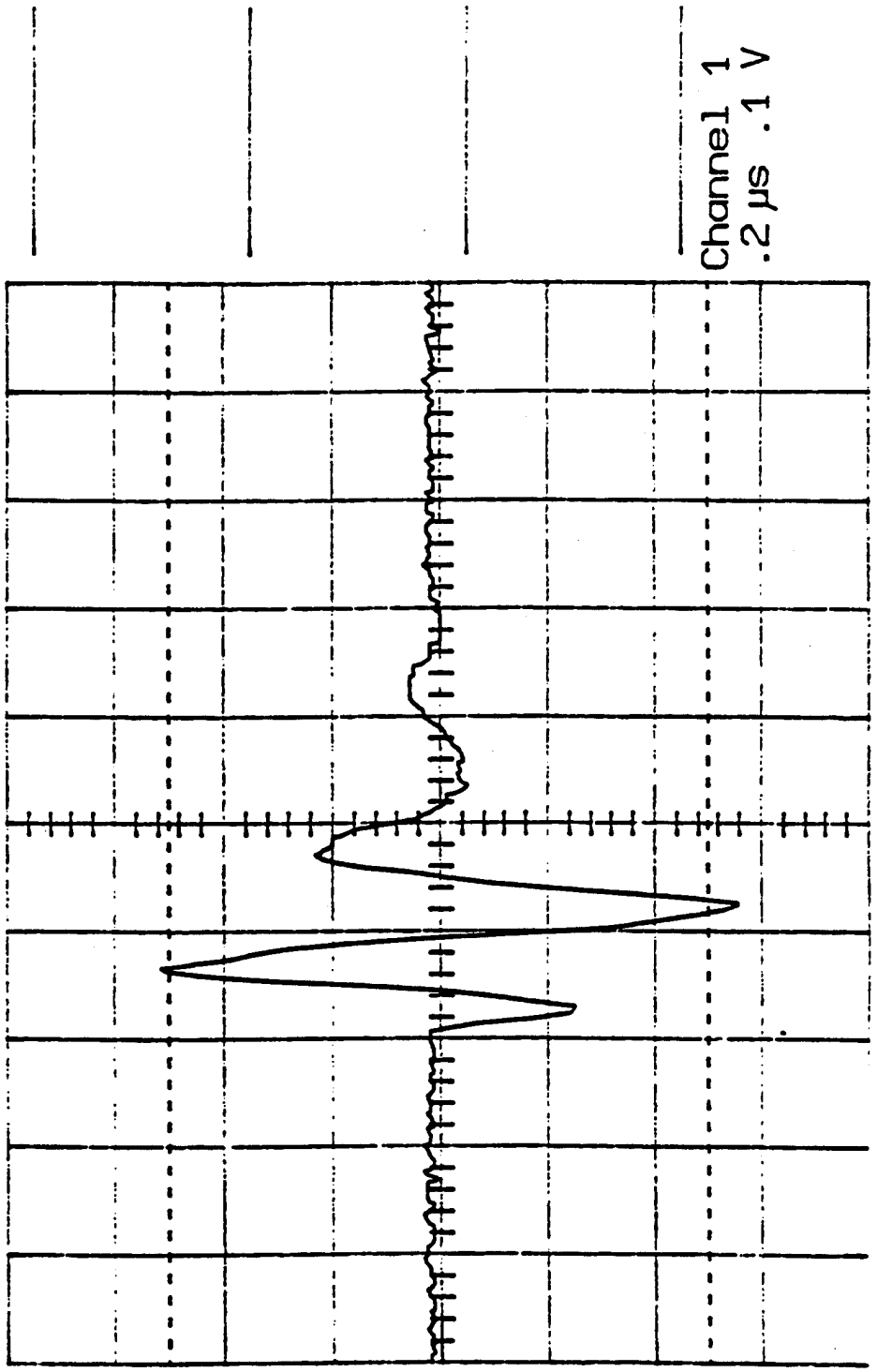

Figure 5.17 Measured transient response of K85 transducer, Attn = 38dB, full scale response

Table 5.2 Attenuation and ring down times for PZT5-A transducer variations

rear bond layer t_{br} (μm)	matching layer t_m (μm)	backing material Za_b (rayl)	Attn. (dB)	-20dB pulse width (μs)
0.005	1/4λ	415	52	4.5
0.005	1/4λ + 10%	415	54	8.5
measured	N/A	415	48	5.4

measured waveform is very close to the modeled response. Ringing after the second cycle is measured to be just slightly more than predicted by the model. This can be seen more clearly in the -20dB ring down plot shown in Figure 5.18. If the last negative pulse could be eliminated, the ring down could be improved to be close to 0.4μs. This could be required in applications where the highest possible resolution is required.

The thickness of the modeled matching layer is increased to 10% thicker than a quarter wavelength and the transient response examined, as shown in Figure 5.19. The effect is to lower the overall amplitude of the signal to A = 40dB while increasing the amplitude of the second cycle slightly. This causes the pulse width to increase to 0.5μs, as seen in the -20dB ring down response. The modeled response with the thicker matching layer does more closely match the measured response, suggesting that the transducer may have a slightly thick matching layer.

To examine how the ring down of the transducer is affected by changes in the backing impedance and bond layer thickness, these parameters are adjusted in the model. A rear bond layer of thickness 0.005μm, unrealistically thin, is used in the original model. A new thickness of 12.5μm, about 0.5mils, was modeled and is presented in Figure 5.20. The effect is to maintain the same attenuation level as the ideal model, A = 42dB, while greatly

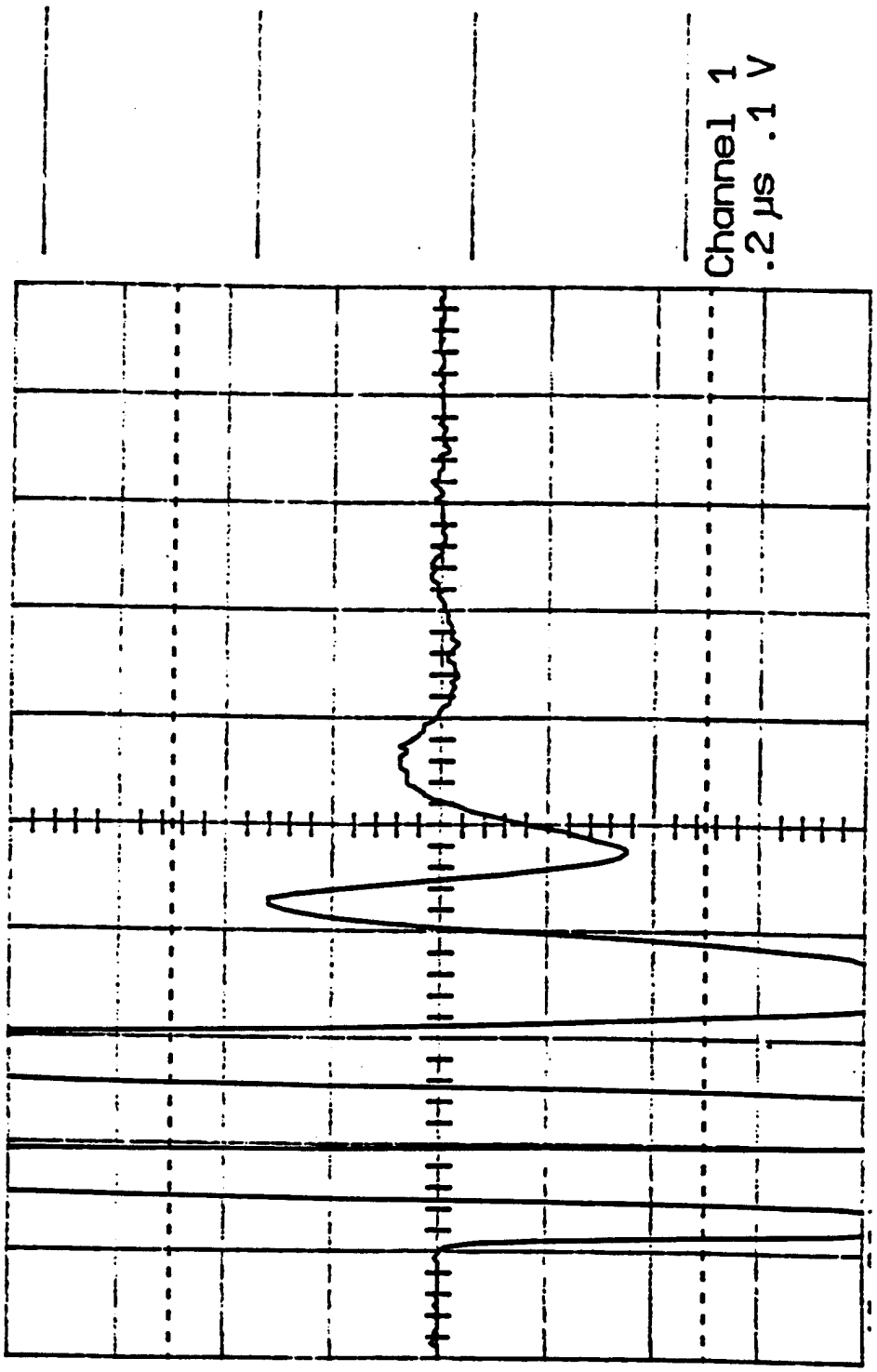

Figure 5.18 Measured transient response of K85 transducer, Attn = 18dB, -20dB ring down response

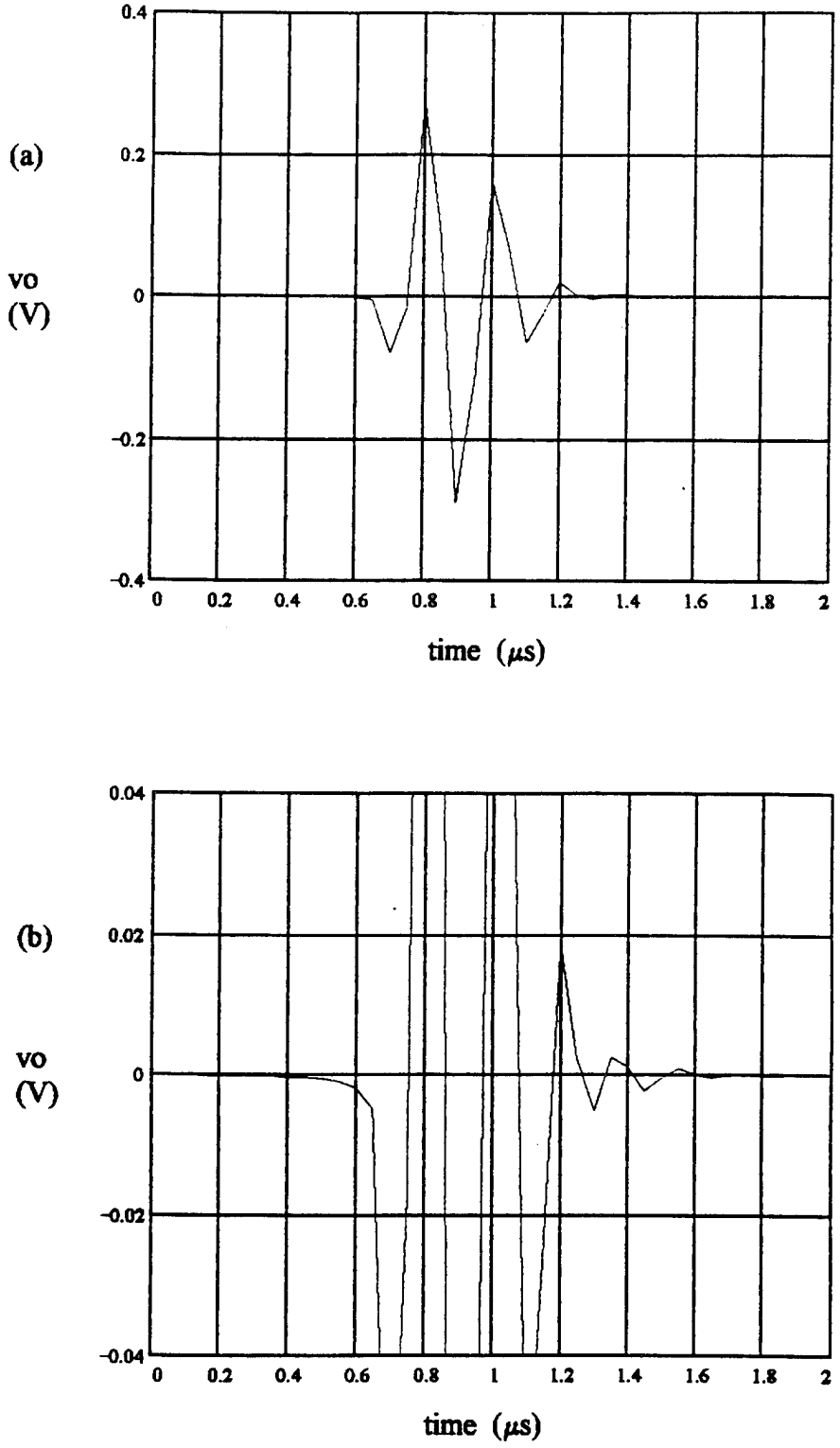

Figure 5.19 Modeled transient response of K85 transducer with matching layer = 1/4λ + 10%; Attn. = 40dB, (a) full scale; (b) -20dB ringdown

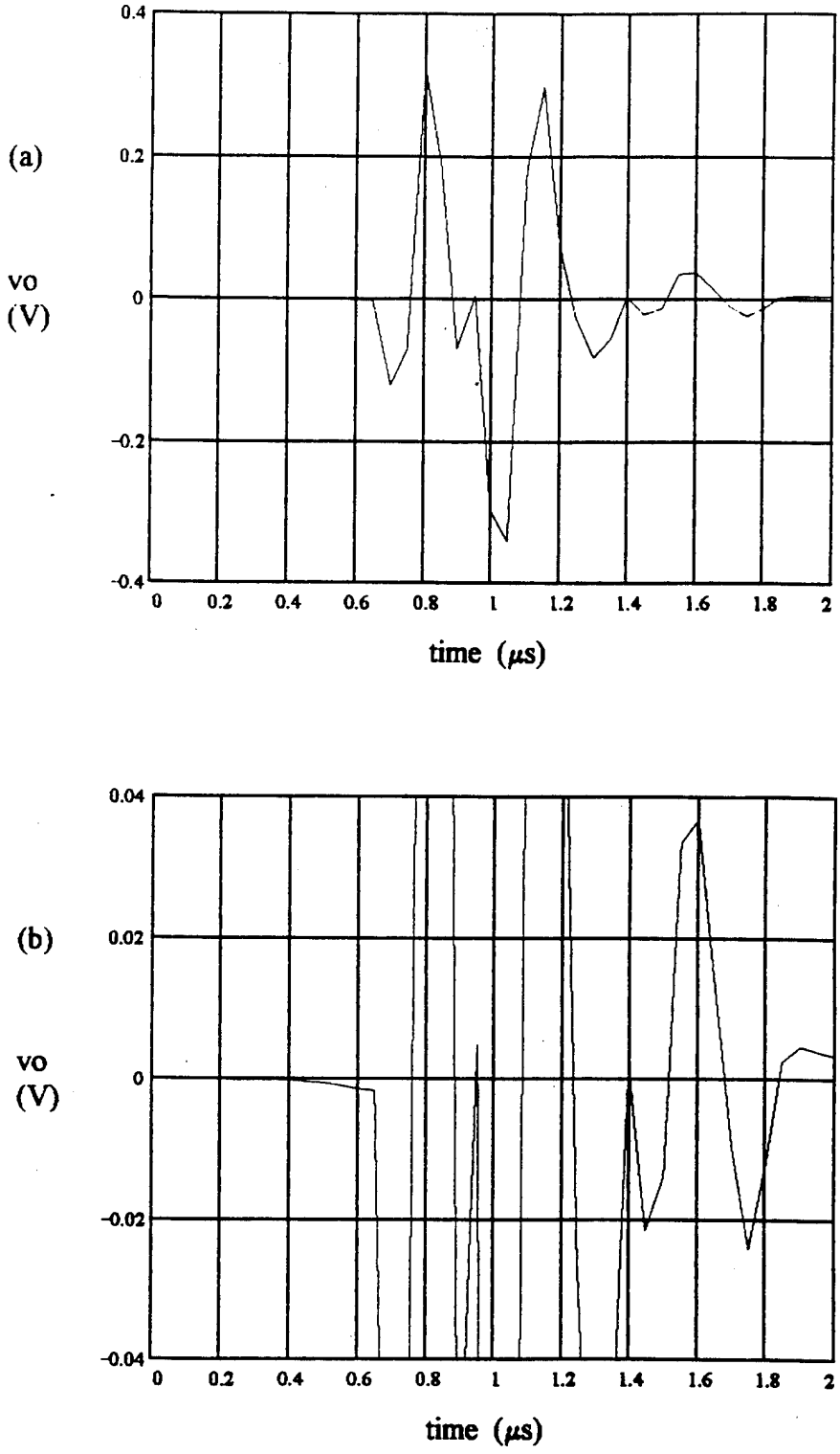

Figure 5.20 Modeled transient response of K85 transducer, rear bond layer = 12.5μm; Attn. = 42dB, (a) full scale; (b) -20dB ringdown

increasing the amplitude of the second cycle and the subsequent ringing further in time. This is due to the decreased absorption by the backing owing to a larger reflection at the interface. This is especially evident in the -20dB signal, where several extra cycles are evident. The pulse width has increased considerably to 8.5μs. It is evident that a bond layer between the backing and piezoceramic should be minimized, if possible. If a group of manufactured probes were to all show such a response, the model could pinpoint that the cause is a bond layer problem between the ceramic and the backing.

In order to improve the performance of the probe, the backing impedance was increased. The best ring down time was achieved for a transducer with a backing impedance of 17.5Mrayl, slightly lower than the impedance of the piezoceramic disk. The transient response is shown in Figure 5.21. The ring down has been improved considerably over the previous examples, with a pulse width of 0.3μs. In certain high resolution applications, this type of response may be necessary. Making a backing which is lossy enough to dissipate the absorbed wave and whose impedance is 17.5Mrayl, however, may not be practical. In this case the program can be used to optimize the materials which are available in order to achieve the best practical response.

The transient responses for the variations on the lead metaniobate transducer are summarized in Table 5.3 which shows the attenuation level and the -20dB ring down time for each case.

The transient response of the PVDF transducer is shown in Figure 5.22. The setup is the same as for the other probes accept that an additional 40dB of gain was required, due to the extremely low measured signal level. This is also why a -20dB ring down is not shown, as that level is near the noise floor. With two major cycles, the measured response looks very similar to the one predicted by the model. The extremely low signal level may be an effect of the mismatch between the connecting cable impedance, 50Ω, and the

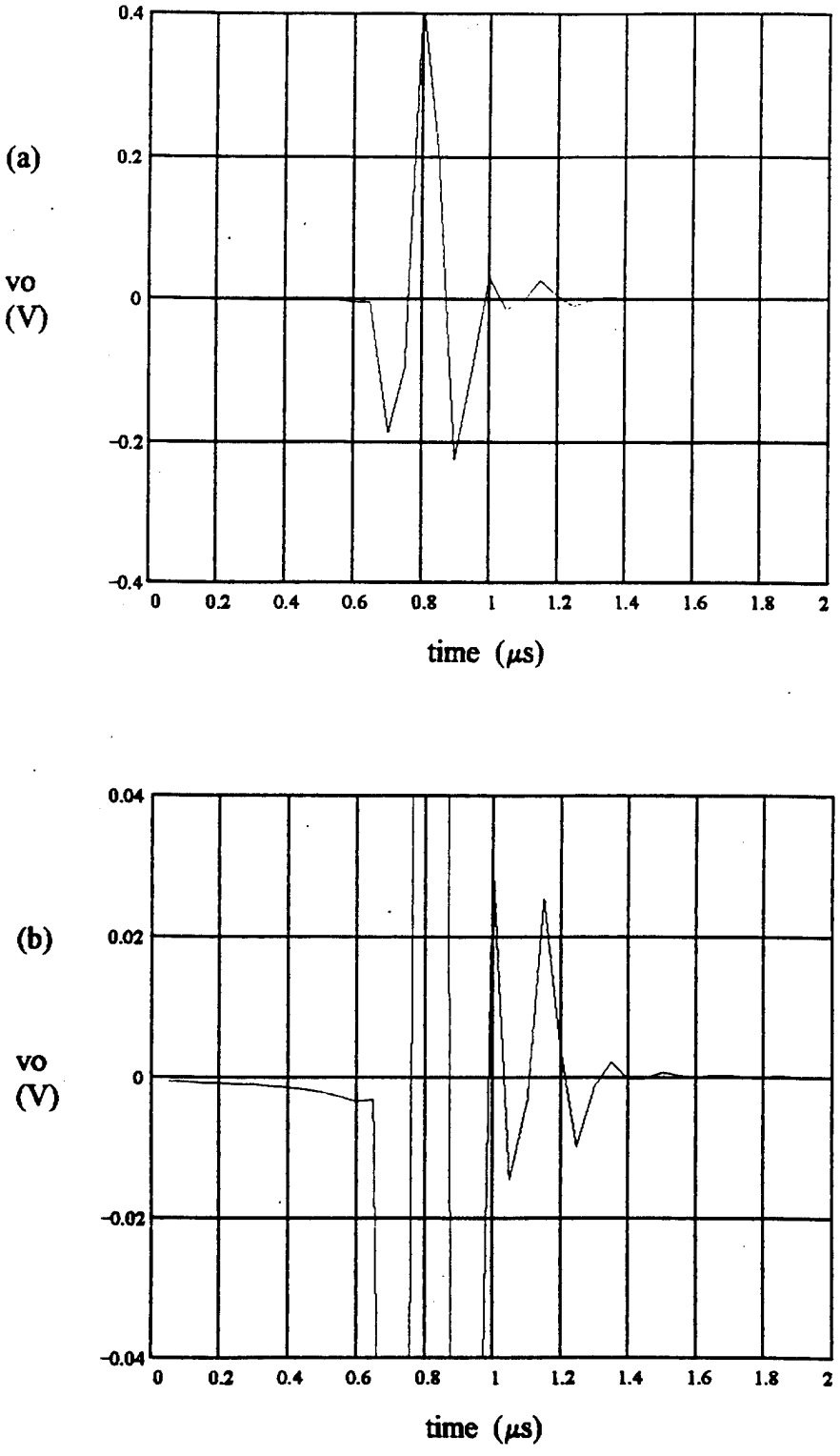

Figure 5.21 Modeled transient response of K85 transducer with Zab = 17.5Mrayl, Attn. = 38dB, (a) full scale; (b) -20dB ringdown

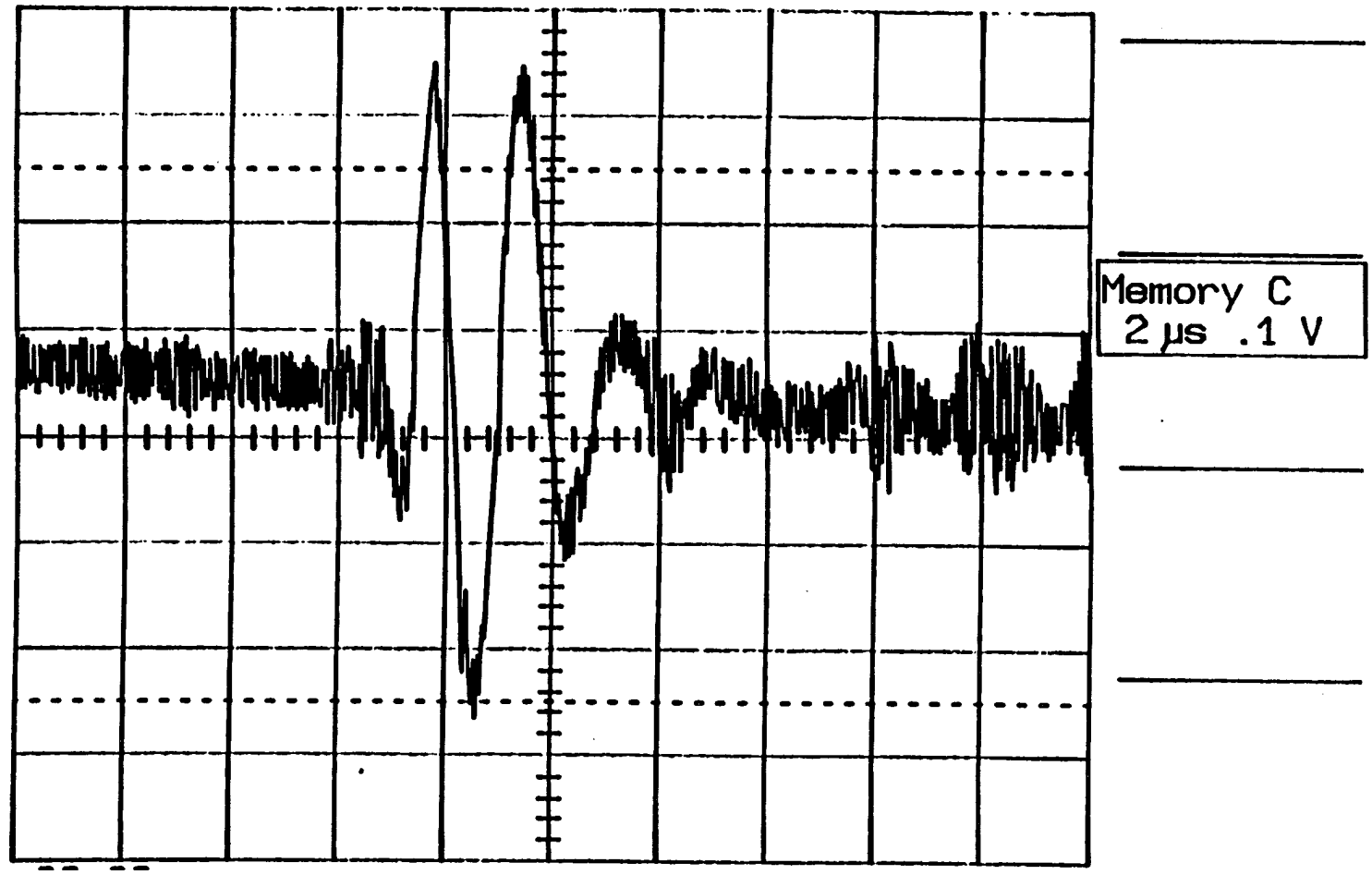

Figure 5.22 Measured transient response of PVDF transducer, Attn = 8dB, gain = 80dB, full scale response

Table 5.3 Attenuation and ring down times for lead metaniobate transducer variations

rear bond layer t_{br} (μm)	matching layer t_m (μm)	backing material Za_b (Mrayl)	Attn. (dB)	-20dB pulse width (μs)
0.005	1/4λ	14.5	42	0.40
0.005	1/4λ + 10%	14.5	40	0.50
0.005	1/4λ	17.5	38	0.30
12.5	1/4λ	14.5	38	1.10
measured probe	$\approx$1/4λ + 10%	$\approx$14.5	38	0.55

operating impedance of the transducer, over 10kΩ. The model could be modified to include the effects of cable mismatches on the responses. With a signal level this low, however, it is unlikely that even a matching transformer would enable this transducer to be efficient enough for most imaging applications. Only in situations where its unique physical parameters are of considerable worth would this material be chosen over a more typical piezoceramic. The fact that the model is able to predict the response of a material in such contrast to more typical piezoceramics is a testament to its usefulness and versatility as a design and development tool.

In summary, the transient response measurements are all reasonably close to those predicted by the model, both in signal level and in ring down characteristics. The measured response of the PZT probe showed one less cycle than the predicted response. The measured ring down for the lead metaniobate probe showed a small amount of additional ringing. An adjustment to the model showed that this is likely due to the thickness of the matching layer. Further adjustments to the model showed how a thicker bond layer would deteriorate the response, and how an increase in the impedance of the backing material could improve the ring down by minimizing the reflection at the interface

between disk and backing. The usefulness of the program for analyzing new materials is demonstrated by the close agreement between the measured and modeled responses for the PVDF probe. The efficiency of this probe, however, was shown to be so low as to limit its usefulness to only very specialized applications.

Chapter 6

CONCLUSIONS AND RECOMMENDATIONS

6.1 Conclusions

This work presents a model that has been developed to aid in the design of ultrasonic piezoelectric transducers. The model is based on the Mason model for a piezoelectric resonator operating in the longitudinal or thickness mode. The model also includes provisions for a backing material and a matching layer, as well as bond layers between the piezoceramic and the backing material and the matching layer. A sub-model is developed for each of these parts. A detailed description of each of the elements which form the model is presented. The limitations and approximations used for each part are discussed. The complete equivalent circuit is shown, as the mechanical terminals of each sub-model are connected.

An analysis of the complete equivalent circuit is presented in order to simulate the electrical input impedance under loaded conditions. The simulated input impedance is used to predict the force produced on the face of the transmitting probe. This force is then applied to the face of the receive probe and the resulting output voltage is determined. Thus the complete transfer function from a water loaded transmitting probe to an electrically loaded receiving probe is derived. A complete derivation shows how the analysis is implemented in software.

A separate section is included to show how the parameters which specify the transducer are converted to the elements which form the equivalent circuit. The physical constants for the piezoceramic material are chosen from a table of common types. Physical constants for the other materials are entered separately. The constants and dimensions

for each of the materials are then used to calculate the values for each of the elements of the equivalent circuit. For example, the acoustical impedance of the backing material is scaled by area to calculate the mechanical impedance used in the equivalent circuit. The program allows for some flexibility in entering parameters; for example, if entering the matching layer thickness is more convenient than entering the frequency where it is a quarter wave, then the program can be easily changed to accommodate this.

Parameter values are then presented for three different transducers: a PZT probe designed to efficiently transfer energy from electrical to acoustical domains; a lead metaniobate probe with a fast ring down to facilitate high resolution imaging; and a PVDF probe included as a contrast to more traditional probes. The major parameters which affect the impedance and transient response are discussed for each transducer. For the PZT probe it is the air backing and the matching layer which contribute most heavily to its higher efficiency and longer ring down. The lead metaniobate probe is most affected by the high impedance backing designed to absorb and dissipate the rear traveling energy, improving ring down at the expense of efficiency. The impedance match between the piezoelectric material and the water load for the PVDF probe enables it to be built without a matching layer.

Responses are predicted for each of the transducer configurations. The electrical input impedance is shown for water-loaded probes. The effect of the mechanical resonance on the response is explained. With only a small amount of damping from the match between piezoceramic and water through the matching layer, the PZT probe exhibits the most resonance effects. The lead metaniobate probe is highly damped due to the high impedance backing; it therefore has smaller resonance effects. The PVDF probe also shows a well controlled resonance, due to the excellent match between the piezoceramic disk and the water load. The low static capacitance of this probe causes its

impedance level to be much higher than the other designs.

The transient response to a short duration pulse is also predicted for each of the probes. The PZT probe is shown to have a more efficient response and a longer ring down time, again due to its low damping. The ring down of the lead metaniobate probe is faster, due again to the absorption of the backing. The efficiency is reduced relative to the PZT probe. The efficiency of the PVDF probe is very low, due to its very low piezoelectric stress constant, e_{33}. Even the low level ring down is poor due to extended ringing in time.

Measurements of the actual transducers which the probes are modeled after are also presented. The measured electrical input impedance of the PZT probe agrees well with the predicted response, except for a discontinuity around resonance. An adjustment to the model shows that the actual matching layer is about 10% too thick. This demonstrates how the program can be used to isolate the cause of irregularities in the response. The measured impedance of the lead metaniobate probe is close to what the model predicts; the model predicted a slightly greater effect from the resonance. The measured PVDF impedance is also similar, but again the model predicts a slightly greater effect from the resonance than what was observed.

The measured transient response for the PZT probe agrees well, having one less major cycle but a similar low level ring down. The lead metaniobate probe measurements also agree well, both having short ring down times. However, the addition of a 6μm bond layer to the modeled probe makes the agreement even better. A 25μm bond layer makes the predicted response slightly worse than measured. In order to improve the performance of the probe, the model is adjusted so that the backing impedance is closer to the piezoceramic impedance. The low level ring down is shown to be improved for this case. This again shows how the program can be used to isolate the cause for a poorer than

expected response and to show what parameters need modification in order to improve the response. The measured transient response of the PVDF probe is very similar in shape to the modeled response, but the measured signal level is much lower. This may be due to the mismatch between the transducer operating impedance and the impedance of the connecting cable.

6.2 Recommendations for Future Work

A practical, computer based method of analyzing ultrasonic piezoelectric transducers has been presented. The computer program is able to generate a predicted electrical input impedance and a simulated transient response for a pair of matched probes or a single probe used as a pulser and receiver. Transducers suitable for a variety of applications have been demonstrated, including high resolution probes suitable for medical imaging or NDT applications and high efficiency probes suitable for ultrasonic cleaning.

The assumptions and approximations assumed in deriving the model do cause some limitations on the responses obtainable. Adjustments or extensions to the model could expand the number of cases which could be analyzed. It would be straightforward, for example, to enable the program to accurately model a load medium, the loss of which is high and varies with frequency. An additional filtering element between the transmitter and receiver could be used to account for the additional losses. Diffraction effects could be handled with a similar approach. This would enable the program to predict the benefits or drawbacks of focusing of the beam.

The program could also be modified so that the transmit probe has different properties than the receive probe. This would allow an additional degree of freedom to meet the system response specifications. The addition of electrical tuning elements to the

probes would also provide a very useful way to modify the response of the system, adjusting both the electrical input impedance and the impulse response.

Since many ultrasound applications use arrays of transducers instead of a single element, the program could be used as the basis for an expanded design tool which could predict the response of a complete array of transducers where the amplitude and phase of the signal used to drive each element is variable. A program of this complexity would take much more computing power than the single element version presented in this work.

REFERENCES

[1] P. N. T. Wells, *Biomedical Ultrasonics*, Academic Press, London (1977).

[2] H. E. Karrer and A. M. Dickey, "Ultrasound Imaging, an Overview," *Hewlet Packard Journal*, Vol 34, Oct. (1983).

[3] P. C. Pedersen and H. S. Ozcan, "Ultrasound Properties of Lung Tissue and Their Measurement," *Ultrasound in Med & Biol*, Vol 12 (6), 483-499 (1986).

[4] J. Krautkramer, H. Krautkramer, *Ultrasonic Testing of Materials*, 2nd ed., Springer-Verlag, New York (1977).

[5] K. H. Beck, "Ultrasonic Transducer Focusing for Inspection of Cylindrical Material," *Materials Evaluation*, Vol 49, 875-882 (1991).

[6] K. K. Shung, M. B. Smith and B. Tsui, *Principles of Medical Imaging*, Academic Press, San Diego, CA (1992).

[7] D.W.Fitting and L. Adler, *Ultrasonic Spectral Analysis for Nondestructive Evaluation*, Plenum Press, New York (1981).

[8] A. F. Brown, "Material Testing by Ultrasonic Spectroscopy," *Ultrasonics*, Vol 11, 202 (1973).

[9] A. F. Brown and J. P. Weight, "Generation and Reception of Wideband Ultrasound," *Ultrasonics*, Vol 12, 161-167 (1974).

[10] M. G. Silk, *Ultrasonic Transducers for Nondestructive Testing*, Adam Hilger, Bristol (1984).

[11] W. P. Mason, "Properties of Transducer Materials" in *American Institute of Physics Handbook*, edited by D. E. Gray, McGraw Hill, New York (1957).

[12] K. Krimholtz, D. A. Leedom and G. L. Matthaei, "New Equivalent Circuits for Elementary Piezoelectric Transducers," *Electr. Lett., Vol.* 6, 398-399 (1970).

[13] G. Kossoff, "The Effects of Backing and Matching on the Performance of Piezoelectric Ceramic Transducers," *IEEE Trans. on Sonics and Ultrasonics*, Vol. SU13(1), 20-31 (1966).

[14] H. W. Persson and C. H. Hertz, "Acoustic Impedance Matching of Medical Ultrasound Transducers," *Ultrasonics*, Vol 23, 83-89 (1985).

[15] D. Fox and J. F. Donnelley, "Simplified Method for Determining Piezoelectric Constants for Thickness Mode Transducers," *J. Acoust. Soc. Am.* 65(4), Nov., 1261-1265 (1978).

[16] H. A. Wolf, *Transient Response Optomization of Piezoelectric Disk Transducers by Time Domain Techniques*, Ph.D. Thesis, The Pennsylvania State University, 1979.

[17] C. S. Desilets, J. D. Fraser and G. S. Kino, "The Design of Efficient Broad-Band Piezoelectric Transducers," *IEEE Trans. on Sonics and Ultrasonics, Vol.* SU25(3), 115-125 (1978).

[18] M. G. Silk, "Prediction of the Effects of some Constructional Variables on the Performance of Ultrasonic Transducers," *Ultrasonics*, Vol 21, 27-33 (1983).

[19] D. A. L. Collie and M. A. Player, "Extended Computer Method for Predicting the Transient Response of Ultrasonic NDT Probes," *Ultrasonics*, Vol 27, 141-149 (1989).

[20] "TEA-Transducer Element Analysis," NRL / USRD, WECO, Cleveland.

[21] J. F. Lindberg, "TRN," NUWC, New London.

[22] G. Kileman, "PiezoCAD," Sonic Concepts, Woodinville, WA.

[23] D. F. McCammon, *The Design of Piezoelectric Transducers Using Goal Programming*, M.S. Thesis, The Pennsylvania State University, 1979.

[24] R. A. Sigelman and A. Caprihan, "Design Method for Ultrasound Transducers Using Experimental Data and Computers," *J. Acoust. Soc. Am.*, Vol 62, 1491-1501 (1977).

[25] E. A. Gerber, "A Review of Methods for Measuring Constants for Piezoelectric Vibrators," *Proc. IRE*, Vol 41, 1103-1112 (1953).

[26] A. V. Oppenheim and R. W. Schafer, *Discrete Time Signal Processing*, Prentice-Hall, Englewood Cliffs (1989).

[27] "Kezite Material Compositions and Specifications," Keramos, Inc. (1992).

[28] D. A. Berlincourt, D. R. Curran, and H. Jaffe, *Piezoelectric and Piezomagnetic Materials in Physical Acoustics*, (W. P. Mason, ed.), Academic Press, New York (1964).

[29] "Kynar Piezo Film - Technical Manual," Pennwalt Corp.

[30] R. H. Tracrell, "Properties of PVDF," Ratheon Research Div., Lexington, MA.